The Hashemite Kingdom of Jordan
Scientific Research Support Fund
The Hashemite University

JJEES

Jordan Journal of Earth and Environmental Sciences

Volume (9) Number (2)

JJEES is an International Peer-Reviewed Research Journal

ISSN 1995-6681 jjees.hu.edu.jo August 2018

Jordan Journal of Earth and Environmental Sciences (JJEES)

JJEES is an International Peer-Reviewed Research Journal, Issued by Deanship of Scientific Research, The Hashemite University, in corporation with, the Jordanian Scientific Research Support Fund, the Ministry of Higher Education and Scientific Research.

Editorial Board:

The International Advisory Board:

Editorial Board Support Team:

Submission address:

Manuscripts should be submitted electronically to the following e-mail:

jjees@hu.edu.jo

For more information and previous issues:

www.jjees.hu.edu.jo

Hashemite Kingdom of Jordan

Scientific Research Support Fund

Hashemite University

Jordan Journal of Earth and Environmental Sciences

JJEES

An International Peer-Reviewed Scientific Journal

Financed by the Scientific Research Support Fund

Volume 9 Number (2)

http:// jjees.hu.edu.jo/

ISSN 1995-6681

المجلة الأردنية لعلوم الأرض والبيئة
Jordan Journal of Earth and Environmental Sciences (JJEES)
http://jjees.hu.edu.jo

Hashemite University

Deanship of Scientific Research

TRANSFER OF COPYRIGHT AGREEMENT

Journal publishers and authors share a common interest in the protection of copyright: authors principally because they want their creative works to be protected from plagiarism and other unlawful uses, publishers because they need to protect their work and investment in the production, marketing and distribution of the published version of the article. In order to do so effectively, publishers request a formal written transfer of copyright from the author(s) for each article published. Publishers and authors are also concerned that the integrity of the official record of publication of an article (once refereed and published) be maintained, and in order to protect that reference value and validation process, we ask that authors recognize that distribution (including through the Internet/WWW or other on-line means) of the authoritative version of the article as published is best administered by the Publisher.

To avoid any delay in the publication of your article, please read the terms of this agreement, sign in the space provided and return the complete form to us at the address below as quickly as possible.

Article entitled:----------

Corresponding author: ----------

To be published in the journal: Jordan Journal of Earth & Environmental Sciences (JJEES)

I hereby assign to the Hashemite University the copyright in the manuscript identified above and any supplemental tables, illustrations or other information submitted therewith (the "article") in all forms and media (whether now known or hereafter developed), throughout the world, in all languages, for the full term of copyright and all extensions and renewals thereof, effective when and if the article is accepted for publication. This transfer includes the right to adapt the presentation of the article for use in conjunction with computer systems and programs, including reproduction or publication in machine-readable form and incorporation in electronic retrieval systems.
Authors retain or are hereby granted (without the need to obtain further permission) rights to use the article for traditional scholarship communications, for teaching, and for distribution within their institution.

☐ **I am the sole author of the manuscript**

☐ **I am signing on behalf of all co-authors of the manuscript**

☐ **The article is a 'work made for hire' and I am signing as an authorized representative of the employing company/institution**

Please mark one or more of the above boxes (as appropriate) and then sign and date the document in black ink.

Signed:_____ **Name printed:** _____

Title and Company (if employer representative) : _____

Date: _____

Data Protection: By submitting this form you are consenting that the personal information provided herein may be used by the Hashemite University and its affiliated institutions worldwide to contact you concerning the publishing of your article.

Please return the completed and signed original of this form by mail or fax, or a scanned copy of the signed original by e-mail, retaining a copy for your files, to:

Deanship of Scientific Research
The Hashemite University P.O. Box 150458, P.C.13115, Zarqa, Jordan
Tel.: 00962 53903333/ Ext. 4235
Fax: 00962 53826823
E-mail: jjees@hu.edu.jo

Subscription

Jordan Journal of Earth & Environmental Sciences (ISSN 1995-6681)
An International Peer- Reviewed Research Journal
Published by the Deanship of Scientific Research - The Hashemite University

Name:	الاســـــــــــم:
Specialty:.....	التخصـــــــــص:
Address:.....	العنـــــــــوان:
P.O. Box:.....	صنـــدوق البريـــــد:
City & Postal Code:	المدينة: الرمز البريدي:
Country:.....	الـــــــــــدولة:
Phone:.....	رقـــم الهاتـــــف:
Fax No:.....	رقـــم الفاكـــــس:
E-mail:.....	البريـــد الإلكترونـــي:
Method of payment:	طريقـــــة الدفـــع:
Amount Enclosed:.....	المبلـــغ المرفـــق:
Signature:.....	التوقيـــــــــع:

Cheques should be paid to Deanship of Research - The Hashemite University

I would like to subscribe to the Journal:

For

- ☐ One year
- ☐ Two years
- ☐ Three years

One year Subscription Rates

	Inside Jordan	Outside Jordan
Individuals	10JD	70$
Students	5JD	35$
Institutions	20JD	90$

Correspondence

Subscriptions and sales:

Professor Fayez Ahmad
Deanship of Scientific Research
The Hashemite University P.O. Box 150458, P.C.13115, Zarqa, Jordan
Tel.: 00962 53903333/ Ext. 4235
Fax: 00962 53826823
E-mail: jjees@hu.edu.jo

JJEES
Jordan Journal of Earth and Environmental Sciences

JJEES
Jordan Journal of Earth and Environmental Sciences

Volume 9, (Number 2), August, 2018
ISSN 1995-6681
Pages 75 - 80

Assessment of PM10 concentration and its prediction using meteorological parameters in the air of Isfahan, Iran

Masoud Masoudi* [1] and Soraya Gerami [2]

Associate Professor of Department of Natural Resources and Environmental Engineering, Shiraz University, Iran.
Department of Natural Resources and Environmental Engineering, Shiraz University, Iran.

Received June 2017; Accepted July 2018

Abstract

In the present study, air quality analyses for particulate matters (PM_{10}) were conducted in the Iranian city of Isfahan. The measurements were taken in three different locations to prepare average data in the city. The average concentrations were calculated for every twenty-four hours, each month and each season in the city of Isfahan. Results showed that the highest concentration of PM_{10} occurs generally in the morning, while the least concentration was observed in the evening. Monthly concentrations of PM_{10} showed the highest value being in July, while the least value was found in August. The seasonal concentrations showed that the least amounts were found in winter and the highest amounts in spring. Relations between the air pollutant and some meteorological parameters were calculated statistically using the daily average data. The wind data (velocity, direction), temperature, evaporation, and rainfall are considered as independent variables. The relationships between concentration of the pollutants and the meteorological parameters are expressed by multiple linear regression equations for both annual and seasonal conditions using SPSS software. The RMSE test showed that among different prediction models, the stepwise model is the best option.

Keywords: PM_{10}, Air pollution, Meteorological Parameters, Regression model, Isfahan.

1. Introduction

Air sustains life, but the air we breathe is not pure. It contains a lot of pollutants and most of these pollutants are toxic (Sharma, 2001). While developed countries have been making progress over the last century, air quality has been getting much worse especially in developing countries where air pollution exceeds all health standards. For example, in Lahore and Xian (china), dust is ten times higher than health standards (Sharma, 2001).

Particulate Matter (PM) is one of the seven conventional (criteria) pollutants including SO_2, CO, particulates, hydrocarbons, nitrogen oxides, O_3 and lead (Cunningham and Cunningham, 2002). These pollutants produce the highest volume of pollution in the air and pose the most serious threats for human health and welfare (Haque and singh, 2017; Masoudi et al., 2017). Concentration of these pollutants, especially in cities, has been regulated by Clean Air Act since 1970 in the USA (Cunningham and Cunningham, 2002). Particulate pollutants may be classified according to their nature and size into the following constituents: smoke, mist, spray, fumes, soot, and dust; the latter being the main part of PM. Dust is composed of fine solid particulates ranging in size from 1 to 100 micron (Masoudi et al., 2016).

The presence of pollutants in the atmosphere, causes a lot of problems, thus the study of pollutant' behavior becomes necessary (Asrari et al., 2007). The health risks of PM depend upon the size. Some of the main problems include: their toxicity, lung damages (e.g. silicosis, black lung disease), mutagenic and carcinogenic effects, Irritation (eye, nose and throat) and heart damage (Lung not as efficient, heart must work harder to get oxygen) (Masoudi et al., 2016).

The status of pollutants' concentrations and the effects of meteorological and atmospheric parameters on these pollutants compose the base for the following studies: Ho and Lin (1994) studied semi-statistical models for evaluating the NO_x concentration by considering source emissions and meteorological effects. The street level of NO_x and SPM in Hong Kong has been studied by Lam et al. (1997). In another study, the relationship between monitored air pollutants and meteorological factors, such as wind speed, relative humidity ratio and temperature was statistically analyzed using SPSS. According to the results obtained through the multiple linear regression analysis, in some months there was a moderate and weak relationship between air pollutants such as the PM level and the meteorological factors in Trabzon city (Cuhadaroglu and Demirci, 1997).

Mandal (2000) has shown the progressive decrease of air pollution from west to east in Kolkata. Statistical modeling of ambient air pollutants in Delhi has been studied by Chelani, et al. (2001). Abdul-Wahab and Al-Alawi (2002) developed a neural network model to predict the tropospheric (surface or ground) ozone concentrations as a function of meteorological conditions and various air quality parameters. The results of this study showed that the artificial neural network (ANN) is

* Corresponding author. e-mail: masoudi@shirazu.ac.ir

a promising method for air pollution modeling. The observed behavior of pollution concentrations to the prevailing meteorological conditions has been studied over the period from June 13 to September 2, 1994, for the Metropolitan Area of Sao Paulo (Sánchez-Ccoyllo and Andrade, 2002). Results show low concentrations associated with intense ventilation, precipitation and high relative humidity. While high values of concentrations prevailed due to weak ventilation, absence of precipitation and low relative humidity for some pollutants. Also for predicting CO, Sabah et al. (2003) used a statistical model.

Elminir (2005) confirmed the dependence of air pollutants on meteorology over Cairo in Egypt. The results state that wind direction was found to have an influence not only on pollutant concentrations but also on the correlation between pollutants. As expected, the pollutants associated with traffic were at the highest ambient concentration levels when wind speed was low. At higher wind speeds, dust and sand from the surrounding desert were entrained by the wind, thus contributing to ambient particulate matter levels. It was also found that the highest average concentrations of NO_2 and O_3 occurred at humidity being ≤ 40 % which is indicative of strong vertical mixing. For CO, SO_2 and PM_{10} the highest average concentrations occurred at humidity being above 80 %.

In another research, data on the concentrations of seven air pollutants (CH_4, NMHC, CO, CO_2, NO, NO_2 and SO_2) and the meteorological variables (wind speed and direction, air temperature, relative humidity and solar radiation) were used to predict the concentration of ozone in the atmosphere using both multiple linear and principal component regression methods (Abdul-Wahab et al., 2005). Results showed that while high temperature and high solar energy tended to increase the day time ozone concentrations, the pollutants NO and SO_2 being emitted to the atmosphere were being depleted. However, the model did not predict the night time ozone concentrations as precisely as it did for the day time. Asrari et al. (2007) studied the effect of meteorological factors for predicting CO. Also, variations in the concentration of CO at different times have been shown in this study.

Dundar et al. (2013) determined some heavy metal contents in PM_1 and PM_{10} by AAS analysis. Sample solutions were FAAS-analyzed for Cd, Cr, Cu, Fe, Mn, Ni, Pb and Zn elemental contents. The highest values were found for Zn and Fe, respectively.

Li et al. (2014) presented the spatial and temporal variation of Air Pollution Index (API), and examined the relationships between API and meteorological factors during 2001–2011 in Guangzhou, China. Correlations were found between API and a variety of meteorological factors. Temperature, relative humidity, precipitation and wind speed were negatively correlated with API, while diurnal temperature range and atmospheric pressure were positively correlated with API in the annual condition. Yoo et al. (2014) mentioned that all of the pollutants showed significant negative correlations between their concentrations and rain intensity due to washout or convection. The relative effect of the precipitation on the air pollutant concentrations is estimated as: $PM_{10} > SO_2 > NO_2 > CO > O_3$, indicating that PM_{10} was most effectively cleaned by rainfall.

Ozelkan et al. (2015) determined PM_{10} data using multispectral satellite images' reflectance values in Izmir, Turkey. The results showed that the B5/B7 and B7/B5 ratio values of Landsat 5TM were more correlated and appropriate than other band ratios to determine PM_{10}.

Wang et al. (2015) studied air quality in Chongqing, the largest mountainous city in China. A statistical analysis of SO_2, PM_{10} and NO_2 concentrations was conducted from 2002 to 2012. The analysis of Pearson correlation indicated that the concentrations of SO_2, PM_{10} and NO_2 were positively correlated with atmospheric pressure, but were negatively correlated with temperature and wind speed. The analysis of Multi-Pollutant Index (MPI) showed that air quality in Chongqing was serious.

Statistical modeling of PM_{10} in Tehran was studied by (Masoudi et al., 2016). According to the results obtained through multiple linear regression analysis of the seasonal and annual conditions, there were significant relationships between PM_{10} levels and the meteorological factors in this city. Such results between other pollutants and meteorological factors in other Iranian cities were observed such as O_3 in Ahvaz (Masoudi et al., 2014), SO_2 in Ahvaz (Masoudi et al., 2017a), NO_2 in Tehran (Masoudi et al., 2017b) and CO in Shiraz (Masoudi et al., 2017c).

The present study exhibits diurnal, monthly and seasonal variations in the concentration of PM_{10} and also a statistical model that is able to predict amount of PM_{10}. This is based on multiple linear and nonlinear regression techniques. Multiple Regression estimates the coefficients of the linear and nonlinear equations involving one or more independent variables that best predict the value of the dependent variable (PM_{10} amount in this study). So, a large statistical and graphical software package (SPSS, Software Package of Social Sciences, V. 20) as one of the best known statistical packages has been used (Kinnear, 2002).

2. Materials And Methods

2.1. Study Area

The research area, Isfahan, capital of Isfahan Province, is the biggest city in the central part of Iran (Fig. 1) located around 32° 38' N and 51º 40' E and the elevation is about 1590 m above the mean sea level. It has a semi-arid climate with four distinct seasons. Its residential population was about 1,834,000 in 2011. Isfahan is built on the banks of the Zayandeh-rud River. There is heavy traffic in the city as well as many factories and industrial sites around the city. Because of these problems, Isfahan is considered as one of the most polluted cities in Iran particularly in terms of PM_{10} (Mansouri and Hamidian, 2013). Hence, it was necessary to carry out an ambient air quality analysis in the city of Isfahan.

Also, high amounts of PM_{10} have been observed more over the recent years in the western and southern parts of Iran. The main source of this pollution is the arid lands of Iran's western neighboring countries especially Iraq. Following the wars of USA with Iraq, the number of the critical zones for the detachment of soil particles through wind erosion processes increased because of the mismanagement and negligence in taking remedial measures and conservation actions against wind erosion. This was more evident at the end of spring

and summer seasons with the precipitation being very low, and the wind speed and evaporation being high,which left the soil very dry allowing for wind erosion and carrying soil suspended particles to long distances.

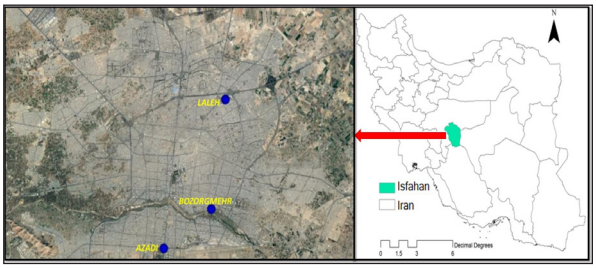

Figure 1. Position of Isfahan in Iran and its air pollution measurement stations.

2.2. Data and Methodology

Three available sampling stations in the city, namely: Azadi, Bozorg-mehr and Laleh belonging to the Iranian Department of Environment were selected to represent different traffic loads and activities (Fig. 1).

The sampling was performed every thirty minutes daily for each pollutant during all months of 2010 and 2011 in the three stations. the samples were recorded in the stations and were then transferred to the Department of Environment in Isfahan. Among the measured data in the three stations, PM_{10} was chosen and the data were taken from the Department of Environment in Isfahan. Averages were then calculated for every hour, monthly and seasonally for the three stations by Excel. Finally, the averages of data at the three stations were used to show the air pollution situation as diurnal, monthly and seasonal graphs of the concentration of PM_{10} in the city. Two models of devices namely, Ecotec and Enviro–Tech, have been used for measuring air pollution in the stations.

Studying the correlation between PM_{10} and metrological parameters in the synoptic station of the city was the next step. The metrological parameters studied include: temperature (min, max), rain, wind direction, wind speed and evaporation extracted from the Meteorological Organization of the country (Iran).

In the next step, the daily average data at the three stations in 2011 were considered as dependent variables in the statistical analysis, while daily data of the meteorological parameters during this year were selected as independent variables in SPSS (V. 20). The linear regression equation showed that the concentration of PM_{10} depends on the kind of meteorological parameters, and gives an idea about the levels of this relation. The relationship between the dependent variables and each independent variable should be linear because linear regression equation is simpler and closer to reality (Masoudi et al., 2016).

The model for predicting PM_{10} was determined using two multiple regression modeling procedures of 'enter method' and 'stepwise method'. In 'enter method', all the independent variables selected were added to a single regression model. In the 'stepwise method' which is better, all the variables can be entered or removed from the model depending on significance. Therefore, only those variables which have more influence on the dependent variable are observed in a regression model.

3. Results and Discussion

In Figs. 2, 3 and 4, the diurnal, monthly and seasonal variations in the concentration of PM_{10} have been presented based on average over the two years of 2010 and 2011. As shown in fig. 2, the high concentration of PM_{10} occurs in the morning, while the least concentration occurs in the evening. The main cause of high PM_{10} during this time is likely to be the morning rush hours. The monthly concentration of PM_{10} showed the highest values in July and the least amounts occurred in August (Fig. 3). Seasonal concentration (Fig.4) shows the highest values being in spring (April to June), and the least amounts were in winter (January to March). These results are almost in good agreement with other results obtained in other cities such as Shiraz (Ordibeheshti and Rajai poor, 2014) and Ahvaz (Asadifard, 2013), but differ somewhat with the results of Tehran city (Masoudi et al., 2016).

Precipitation is low and evaporation is high during these times especially at the end of spring and the beginning of summer, therefore, the soil would be very dry allowing for wind erosion and carrying soil suspended particles over long distances. The origin and source of most of the particle matters during this period are the dry lands of a western neighboring country especially the critical zones in the country of Iraq (Fig. 5 and 6) (Masoudi et al., 2016).

Unfortunately, all graphs showed that the concentrations of the PM_{10} are greater than the Primary Standards of PM_{10} (50 $\mu g/m^3$) recommended by the National Ambient Air Quality Standards (NAAQS) of USA and Iran, respectively to protect human health. Increase in PM can have different consequences and health problems. This pollution can cause and increase a number of related illnesses such as cancer and lung damaging (Kelly and Fussell, 2015; Liu et al., 2018). Unfortunately such health problems have been recorded by Health offices in the region over the recent years. Currently Ahvaz, a big city in the south western part of Iran is introduced as the worst polluted city in the world according to a survey in 2011 carried out by the World Health Organization because of the high concentration of dust during the year (Guinness World Records, 2013).

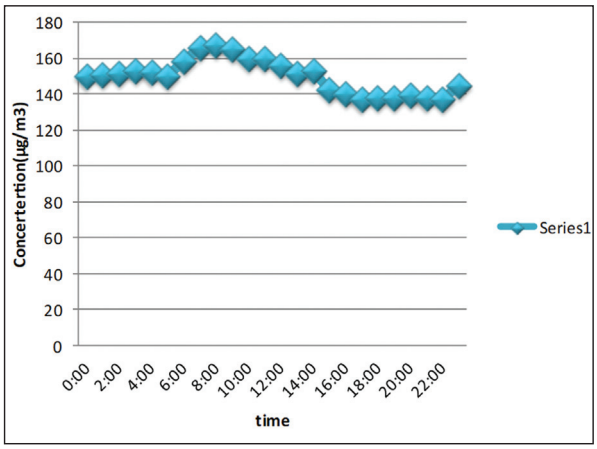

Figure 2. Diurnal variation of PM10 concentration in Isfahan (average of 2010 and 2011).

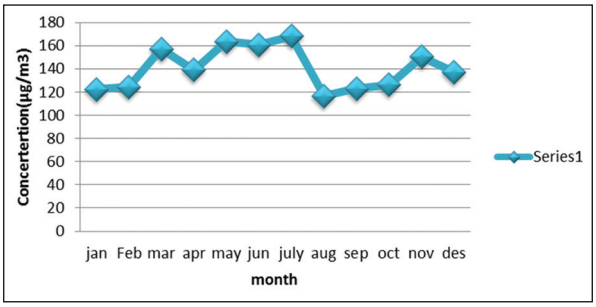

Figure 3. Monthly variation of PM10 concentration in Isfahan (average of 2010 and 2011).

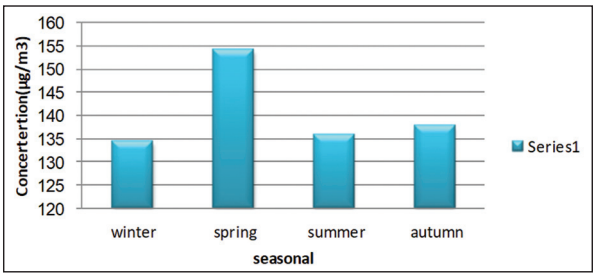

Figure 4. Seasonal variation of PM10 concentration in Isfahan (average of 2010 and 2011).

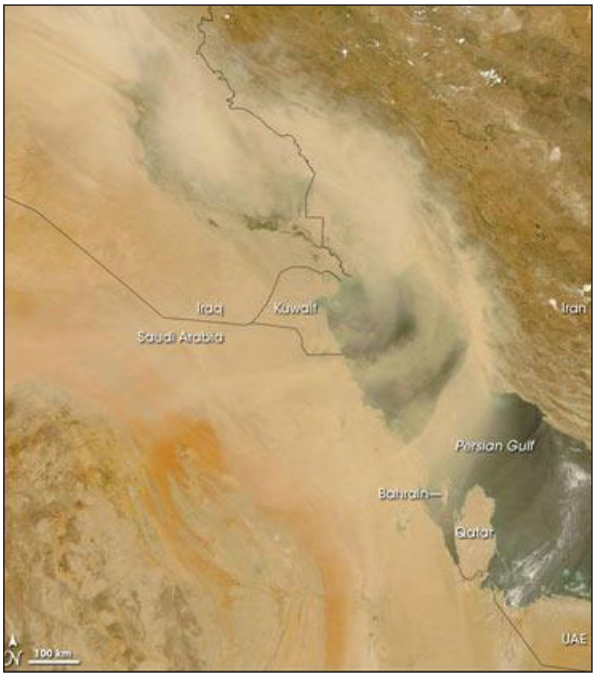

Figure 5. A satellite image showing that the origin and source of most of the dust pollution carried by wind in Iran are the dry lands of western neighboring countries especially the country of Iraq.

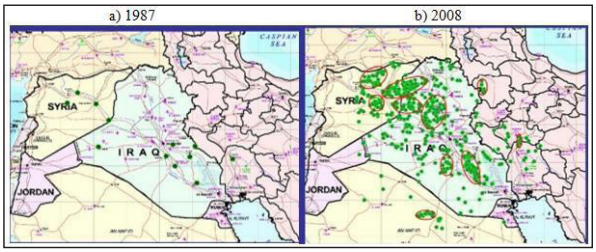

Figure 6. Two maps of western neighboring countries of Iran showing the increasing number of critical points for the detachment of soil particles during wind erosion processes especially in Iraq over the recent years.

Table 1 shows the relationships between PM_{10} and other air pollutants. For example the concentration of PM shows negative correlation with O_3, NO_2, NOx, while it shows positive correlation with CO and SO_2. These results are almost in good agreement with other results of PM_{10} assessment in other Iranian cities of Shiraz (Ordibeheshti and Rajai poor, 2014) and Ahvaz (Asadifard, 2013), but are not in agreement with the results of Tehran city (Masoudi et al., 2016). Correlation coefficients significant at the 0.05 level are identified with a single asterisk (significant), and those significant at 0.01 level are identified with two asterisks (highly significant).

Table 1. Correlation between air pollutants and PM_{10}.

	NO_2	NOx	O_3	SO_2	CO
Pearson Correlation	-.409**	-.172**	-.334**	.083	.235**
Sig. (2-tailed)	.000	.001	.000	.123	.000
N	344	344	344	344	344

Table (2) regarding the analysis of variance shows that both regressions of 'enter' and 'stepwise' methods for the annual condition are highly significant indicating a significant relation between the different variables.

Analysis of variance (a)

Table 2. Tables of analysis of variance for both regressions of 'enter' (a) and 'stepwise' (b) methods for annual condition.

Model	Sum of Squares	df	Mean Square	F	Sig.
Regression	443535.225	5	88707.045	37.111**	.000
Residual	807918.904	338	2390.293		
Total	1251454.129	343			

Predictors: (Constant), Rain, Wind direction (max), Wind speed (max), Temperature (max), Temperature (min), Evaporation
Dependent Variable: PM_{10}

Analysis of variance (b)

Model	Sum of Squares	df	Mean Square	F	Sig.
Regression	437622.996	3	145874.332	60.943**	.000
Residual	813831.133	340	2393.621		
Total	1251454.129	343			

Predictors: (Constant), Rain, Wind $Speed_{(mean)}$), temperature
Dependent Variable: PM_{10}

In the following tables (3) the coefficients of PM_{10} pollution model and regression lines for both enter and stepwise methods in annual condition are presented. Regression coefficients, standard errors, standardized coefficient beta, t values, and two-tailed significance level of t have been shown in the Tables.

Table 3. Coefficients of PM pollution model and regression lines for both enter (a) and stepwise (b) methods for annual condition.

Coefficients (a)

Model	Unstandardized Coefficients		Standardized Coefficients	t	Sig.
	B	Std. Error	Beta		
(Constant)	114.802	14.720		7.799	.000
Temperature (max)	3.183	.913	.497	3.485**	.001
Temperature (min)	-.005	1.103	-.001	-.004	.997
Rain	-4.452	1.502	-.142	-2.963**	.003
Wind direction	-.041	.026	-.075	-1.566	.118
Wind speed(mean)	-4.342	.949	-.224	-4.576**	.000

Dependent Variable: PM

Coefficients (b)

Model	Unstandardized Coefficients		Standardized Coefficients	t	Sig.
	B	Std. Error	Beta		
(Constant)	109.063	8.746		12.470	.000
Temperature (max)	3.260	.294	.509	11.094**	.000
Wind speed (mean)	-4.898	.868	-.253	-5.642**	.000
Rain	-4.391	1.431	-.140	-3.068**	.002

Dependent Variable: PM

The linear regression equations show that the PM_{10} pollution depends on the meteorological parameters, and also gives an idea about the levels of relations. The linear model equations after using the 'enter method' and the 'stepwise method' for annual condition are:

- *PM_{10} amount ($\mu g/m^3$) using the 'enter method' for annual condition = 114.802 + (-.005) $Temperature_{(min)}$ + (3.183) $Temperature_{(max)}$ + (-4.452) Rain + (-.041) Wind $direction_{(max)}$ + (-4.342) Wind $speed_{(max)}$ R= 0.595 (significant at 0.001)*
- *PM_{10} amount ($\mu g/m^3$) using the 'stepwise method' for annual condition = 109.063 + (-4.391) Rain+ (-4.898) Wind $speed_{(mean)}$ + (3.260)Temperature(max) R= 0.591 (significant at 0.001)*

Results of the linear regression model show that when wind speed and rain have reverse effect on the concentration of PM_{10}, i.e., when these parameters increase, the concentration of PM_{10} decreases. On the other hand, when temperature (max) increases, the concentration of PM_{10} significantly increases (Table 3b). Other meteorological parameters show different effects on PM_{10} amounts; however, these results are not significant. For example, wind direction has reverse effects on the concentration of PM_{10} (Table 3a). These results are almost in good agreement with other results regarding PM_{10} measurements in other Iranian cities like Ahvaz (Asadifard, 2014), Shiraz (Ordibeheshti and Rajai poor, 2014) and Tehran (Behzadi and Sakhaei, 2014) and other regions (Li et al., 2014; Yoo et al., 2014). Actually some of these events happen in real conditions. Increase in the rainfall and wind speed usually decrease most of air pollutants (Asrari et al., 2007).

The values and significance of R (multiple correlation coefficient) in both equations show the capability of these to predict PM_{10} amount. The amount of Adjusted R^2 in both equations is almost 0.35 showing that different parameters can calculate almost 35 % variability of PM_{10}. This result indicates that to predict most air pollutants such as PM_{10}, the natural and anthropogenic sources of their production such as consumption of fossil fuel and wind erosion processes must be taken into consideration. On the other hand, R in the enter method (0.595) is equal to that in the stepwise method (0.591), showing no difference. Therefore, the second equation based on the stepwise method can be used to predict PM_{10} in the city instead of using the first equation which needs more data. On the other hand, no difference between the two R values indicates that the excluded variables in second equation have less effects on measuring PM_{10} in the city.

Beta in Table 3 shows the independent variables (meteorological parameters) which have more effects on the dependent variable (PM_{10}). The beta in the both Tables (4) shows a highly significant effect of some variables such as rain, temperature(max) and wind speed compared to other meteorological parameters for measuring PM_{10} which is close to the results of Asadifard (2013), Ordibeheshti and Rajai poor (2014), Masoudi et al. (2014) and Behzadi and Sakhaei (2014). Parameter Sig (P-value) from Table (4) shows the degree of relation between PM_{10} and meteorological parameters. For example, Table (4a) shows that wind speed has a higher effect on PM_{10} than wind direction.

On the other hand, in Table (4), the linear regression equations of PM_{10} amount are presented for both enter and stepwise methods in different seasonal conditions. Almost all of the models are significant. Stepwise methods show those meteorological parameters which are most important during these seasons for estimating the pollution. Among the models, spring models have the highest R compared to the R of other seasonal models. R in autumn and spring models are higher than in annual models, also indicating that relations between the pollutant and meteorological parameters are stronger than the whole year during these seasons. These results differ somewhat with other results regarding PM_{10} assessment in other Iranian cities of Ahvaz (Asadifard, 2013) and Shiraz (Ordibeheshti and Rajai poor, 2014), but they are consistent with the results of Tehran (Behzadi and Sakhaei, 2014).

Table 4. PM_{10} amount ($\mu g/m^3$) using two methods of enter and stepwise for different seasonal condition.

Season	enter method	R	stepwise method	R
Spring	= -22.475+(7.115) Tmax + (.030) Tmin + (-1.387) WSmax + (-.065) WDmax+ (-.459) R + (0.364) E	.763 (significant at 0.01)	=- 54.660 + (7.373) Tmax	.751 (significant at 0.01)
Summer	= 330.725 + (-9.519) Tmax + (11.942) Tmin + (-5.851) WSmax + (.039) WDmax + (-88.934) R + (1.317) E	.472 (significant at 0.05)	= 90.577 + (5.584) Tmin	.292 (significant at 0.05)
Autumn	= 74.404 + (5.548) Tmax + (1.038) Tmin+ (.351) WSmax + (-.052) WDmax + (-3.431) R + (-6.012) E	.693 (significant at 0.01)	= 65.239 + (4.861) Tmax	.649 (significant at 0.01)
Winter	= 134.112 + (3.209) Tmax + (-3.901) Tmin + + (-3.487) WSmax + (-.084) WDmax + (-6.138) R	.616 (significant at 0.01)	= 171.403 + (-8.077) R + (-5.444) WSmax	.566 (significant at 0.01)

Note: Tmax =Temperature (max), Tmin=Temperature (min), WSmax =Wind speed (max), WDmax =Wind direction (max), R=Rainfall, E=Evaporation

To test which annual model is better to use, RMSE (Root Mean Square of Error) is calculated for different linear models of enter and stepwise. Predicted amounts using the different annual models for 24 days during 2012 are calculated and compared with observed data during those days using RMSE equation:

$$RMSE = \sqrt{\frac{\sum_{i=1}^{n}(O_{obs} - O_{pre})^2}{n}}$$

O_{obs}: observed PM_{10} value O_{pre}: predicted PM_{10} value using model

The values of RMSE in both linear models of enter (42.771) and stepwise (41.978) show the capability of the stepwise model in predicting PM amount compared to the enter model. This result which is the same as the results of Asadifard (2013), Ordibeheshti and Rajai poor (2014), Masoudi et al. (2014) and Behzadi and Sakhaei (2014) indicates that to predict most air pollutants such as PM_{10}, one may take into consideration only the linear models of stepwise which need less data and an easier calculation than the enter model.

In conclusion it can be said that Isfahan is one of the polluted cities in Iran. Hence, a need was felt to carry out an ambient air quality analysis in the city. Results showed that there were significant relationships between PM_{10} and some meteorological parameters. Based on these relations, different multiple linear regression equations for PM_{10} for annual and seasonal conditions were prepared. Results showed that among the different prediction models, the stepwise model was the best option. Also, different variations in concentration during the day, months, and seasons were observed. These results agree to Asadifard (2013), Ordibeheshti and Rajai poor (2014) and (Masoudi et al., 2016). So, in regard to the pollution situation of the study area, further research must be carried out. Also, According to the obtained model, if the conditions of this present study do not change, life in the study area will be impossible in the future years owing to the increasing proportion of pollutants. Therefore, as far as possible, some strategies such as the reduction in the number of imported vehicles and the proportion of distance traveled by vehicles etc. and dust consolidation in the source areas can be applied to achieve pollution reduction.

References

[1] Abdul-Wahab, S.A., and Al-Alawi, S.M. (2002). Assessment and prediction of tropospheric ozone concentration levels using artificial neural networks. Environmental Modelling & Software 17(3): 219–228.

[2] Abdul-Wahab, S.A., Bakheit, C. S., and Al-Alawi, S.M. (2005). Principal component and multiple regression analysis in modelling of ground-level ozone and factors affecting its concentrations. Environmental Modelling & Software 20 (10): 1263–1271.

[3] Asadifard, E. (2013). Study of Air Pollution and its relationship with meteorological parameters in Ahvaz city. Project of B.Sc. degree in Shiraz University.

[4] Asrari, E., Sen, P.N., and Masoudi, M.(2007). Status of carbon mono oxide in Tehran City- Iran. Pollution Research 26 (4): 531-535.

[5] Behzadi, F., and Sakhaei, M.(2014). Study of Air Pollution and its relationship with meteorological parameters in Tehran city. Project of B.Sc. degree in Shiraz University.

[6] Chelani, A.B., Gajghate, D.G., Tamhane, S.M. Hasanet, M.Z. (2001). Statistical modeling of ambient airpollutants in Delhi. Water, Air and Soil Pollution 1326: 315-331.

[7] Cuhadaroglu, B. and Demirci, E. (1997). Influence of some meteorological factors on air pollution in Trabzon city. Energy and Buildings 25 (3) : 179–184.

[8] Cunningham, W.P., and Cunningham, M.A. (2002). Principles of Environmental Science inquiry and applications. MxGraw Hill Company.

[9] Dundar, M.S., Altundag, H., Yilmazcan, O., Kaygaldurak, S. (2013). Determination of some heavy metal contents in PM1 and PM10 airborne particulate matters by AAS analysis. Fresenius Environmental Bulletin , 22: 3179–3183.

[10] Elminir, H.K. (2005). Dependence of urban air pollutants on meteorology. Science of the Total Environment, 350: 225–237.

[11] Guinness World Records (2013). Page 036 (Hardcover edition). ISBN 9781904994879.

[12] Haque, M.S., and Singh, R.B. (2017). Air Pollution and Human Health in Kolkata, India: A Case Study. Climate 2017, 5, 77; doi:10.3390/cli5040077. 1-16.

[13] Ho, L.C., and Lin, W.Y. (1994). Semi-statistical model for evaluating the effects of source emissions and meteorological effects on daily average NOx concentrations in South Taiwan. Atmospheric Environment 37: 2051-2059.

[14] Kelly, F., and Fussell, J. (2015). Air pollution and public health: emerging hazards and improved understanding of risk. Environ Geochem Health. 2015; 37(4): 631–649.

[15] Kinnear, P.R. (2002) SPSS for windows made simple release 10. Psychology press.

[16] Lam, G.C.K., Leong, D.Y.C. (1997). Street level concentration of NOX and suspended particulate matter in Hong Kong. Atmospheric Environment 93: 1-11.

[17] Li, L., Qian, J., Ou, C.Q., Zhou, Y.X., Guo, C., and Guo, Y. (2014). Spatial and temporal analysis of Air Pollution Index and its timescale-dependent relationship with meteorological factors in Guangzhou, China, 2001–2011. Environmental Pollution 190: 75-81.

[18] Liu, H.Y., Dunea, D., Iordache, S., and Pohoata, A. (2018). A Review of Airborne Particulate Matter Effects on Young Children's Respiratory Symptoms and Diseases. Atmosphere 2018, 9, 150; doi:10.3390/atmos9040150. 1-18.

[19] Mandal, S. (2000). Progressive decrease of air pollution level from west to east at Calcutta', Indian Journal of Environmental Protection 20: 6-10.

[20] Mansouri, B., and Hamidian, A. (2013). Assessment of the Air Quality of Isfahan City, Iran, Using Selected Air Quality Parameters. Iranian Journal of Toxicology. 7(21): 842-848.

[21] Masoudi M., Asadifard E., Rastegar M. (2014). Status and prediction of ozone as an air pollutant in Ahvaz City, Iran. Caspian Journal of Environmental Sciences. 12: 215-224.

[22] Masoudi, M., Sakhaei, M., Behzadi, F. and Jokar, P. (2016). Status Of PM10 as an air pollutant and its prediction using meteorological parameters in Tehran, Iran. Fresenius Environmental Bulletin. 25 (6): 2008-2017.

[23] Masoudi, M., Asadifard, E., Rastegar, M. and Shirvani, A. (2017a). Status and prediction of sulfur dioxide as an air pollutant in the city of Ahvaz, Iran. Pollution, 3(2): 201-211

[24] Masoudi, M., Behzadi, F., Sakhaei, M. (2017b). Concentration of NO_2 in the Air over Tehran, Iran. Russian Meteorology and Hydrology, 42: 728–730.

[25] Masoudi M., Rajaipoor N., Ordibeheshti F. (2017c). Status and prediction of CO as an air pollutant in Shiraz, Iran. Fresenius Environmental Bulletin. 26: 3697-3704.

[26] Ordibeheshti, F. and Rajai poor, N. (2014). Study of Air Pollution and its relationship with meteorological parameters in Tehran city. Project of B.Sc. degree in Shiraz University.

[27] Ozelkan E., Karaman M., Mostamandy S., Uça Avcı Z.D., Toros, H. (2015). Derivation of PM10 Levels Using OBRA on Landsat-5TM Images: A Case Study in Izmir, Turkey. Fresenius Environmental Bulletin, 24(4b): 1585-1596.

[28] Sabah, A., Al-Rubiei, R., and Al-Shamsi, A. (2003). A statistical model for predicting carbon monoxide levels. International Journal of Environment and Pollution 19: 209-224.

[29] Sánchez-Ccoyllo, O.R. and Andrade, M.F. (2002) The influence of meteorological conditions on the behavior of pollutants concentrations in São Paulo, Brazil. Environmental Pollution, 116 (2): 257–263.

[30] Sharma, B.K. (2001). An Introduction to environmental pollution. Krishna prakashan media (p) ltd.

[31] Wang; S.M., Yu; H., Song; L., Xie; Y. and Zhu, Q. (2015). Air quality in a mountainous city: A case study in Chongqing, China. Fresenius environmental bulletin, 24 (9), 2699-2706.

[32] Yoo, J.M., Lee, Y.R., Kim, D., Jeong, M.J., Stockwell, W.R., Kundu, P.K., Oh, S.M., Shin, D.B., and Lee, S.J. (2014). New indices for wet scavenging of air pollutants (O_3, CO, O_2, SO_2, and PM10) by summertime rain. Atmospheric Environment, 82: 226-237.

JJEES
Jordan Journal of Earth and Environmental Sciences

Volume 9, (Number 2), August, 2018
ISSN 1995-6681
Pages 81 - 88

Physical and Technical Characteristics of Jarash Clay deposits from Northern Jordan

Talal Mohammad Al-Momani[1] and "Mohammed-Ezz-Aldien" Ibrahim Dwairi[1]

Department of Earth and Environmental Sciences, Faculty of Science, Yarmouk University, Irbid – Jordan.

Received 18 December, 2017; 6 June, 2018

Abstract

Detailed analysis of the physical and technical characteristics of Jarash clay deposits in northern Jordan reveals the strong potentiality of those deposits from the industrial point of view. The results of this study show the usefulness of those deposits in various industrial sectors, with emphasis on the possible usefulness of the clay in pottery, ceramic tiles, and brick-making industries. One hundred and two samples were collected from seven different outcrops for the physical and technical analysis. The results of physical properties after attrition and wet sieving obtained in this study include: whiteness, bulk density, oil absorption, and specific gravity. Whiteness ranges from (25.4% to 54.9%) with an average value of (40.1%). Bulk density ranges from (0.86 to 1.22 g/cm^3) with an average value of (0.99 g/cm^3). Oil absorption ranges from (23.25 to 46.5 ml/100gm) with an average value of (33.1 ml/100gm). Specific gravity ranges from (2.02 to 2.7) with an average value of (2.24). the grain size analyses for the bulk samples range from sandy clay to clayey sand on the Shepard sediment classification ternary diagram. The technical characterization resulting after attrition and wet sieving have also been examined. The plastic limit ranges from (15.9 to 26.3%) with an average value of (10.74%), liquid limit ranges from (34.2 to 71.5%) with an average value of (48.18%), and plasticity index ranges from (18.3 to 45.2%) with an average value of (19.74%).

According to the physical, chemical, technical properties, clay identification and the clay workability chart of Jarash clay deposits after attrition and wet sieving, it can be said that Jarash clay deposits are suitable for pottery, ceramic tiles, and the brick-making industries.

Keywords: Clay, Kaoline, specific gravity, oil absorption, bulk density, liquid limit, plastic limit, grain size, Jordan.

1. Introduction

Clay minerals are of high importance in the mineral industries. Kaolin group encompasses different hydrosilicates minerals, i.e., kaolinite, dickite, nacrite and halloysite with kaolinite being the most common (Murray, 1988; Murray, 1999; Murray, 2007). For many industrial applications, kaolin must be refined and processed from the crude state to enhance its whiteness, purity, and other important commercial characteristics. The impurities in kaolin including quartz, micas, illite, montmorillonite, goethite, hematite, pyrite, anatase, rutile, ilmenite, tourmaline, zircon and other heavy minerals can be removed by wet processing (Murray, 1999).

Clay minerals represent about 16 % of the total volume of the sedimentary rocks of the earth's solid surface. Deposits of less than two microns of the grain diameter are termed clay. As a rock, clay usually consists of a mixture of clay minerals and other rock debris of varying composition (Khoury 2002; Khoury et al., 2008).

Kaolinite [$Al_2Si_2O_5(OH)_4$] is the most interesting phyllosilicate clay mineral. It is widely employed as raw material in ceramics, paper filling and coating, refractory, fiberglass, cement, rubber and plastics, paint, catalyst, pharmaceutics and agriculture (Aras, et al., 2007; Diko et al., 2011; Diko et al., 2016; Ediz, et al., 2015; Ekosse, 2010; Murray, 2007). The main uses of kaolinite are in paper filling and coating (45 %), refractories and ceramics (31 %), fiberglass (6%), cement (6 %), rubber and plastic (5 %), paint (3 %), and other industries (4 %) (Baba et al., 2015).

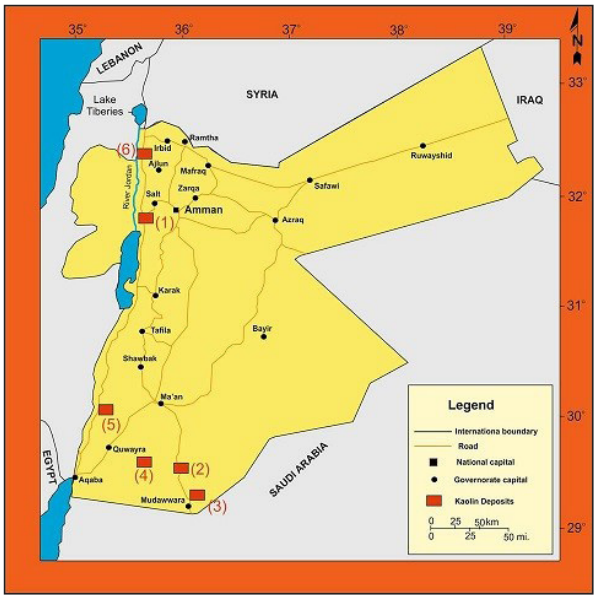

Figure 1. Occurrences of Kaolin clay deposits in Jordan (modified after Yasin and Ghannam, 2006).

* Corresponding author. e-mail: talalmom@yu.edu.jo

Kaolin deposits occur in different localities in Jordan. Figure (1) shows the occurrences of different localities of kaolin clay deposits in Jordan. These deposits are distributed throughout Jordan in the north (e.g. Jarash area), central (e.g. Mahis area) and in the south (e.g. Batn El-Ghoul, Al Mudawwara, Ghor Kabid, Jabel Umm Saham, and Dubaydib areas). The current research paper focuses on Jarash clay deposits located in northern Jordan. Figure (2) shows the geological map of the study area.

2. Geological Setting of the Study Area

The study area is located thirty-eight km to the south of Irbid city and around forty-five km to the north of Amman city. The coordination are 32˚ 12′ 00″ N – 32˚ 14′ 00″ N and 35˚ 51′ 50″ E – 35˚ 53′ 25″ E. Figure (2) shows a geological map of the study area. The geology of the study area was studied by several researchers (Amireh, 1996; Amireh and Abed, 1999; Ahmad et al., 2012; Abu Hamad et al., 2016). The sandstone of the study area belongs to the lower Cretaceous Sandstone (Aptain-Albian age) which consists of clastic sedimentary rocks including sandstone with intercalation of claystone where the sandstone dominates over the claystone. It also contains conglomerates, siltstone, and three inter-bedded carbonates sequences (Amireh, 1996).

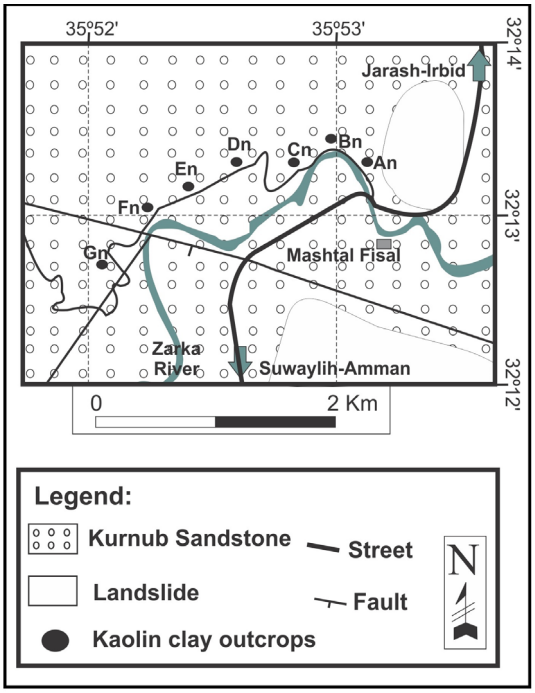

Figure 2. Geological map of the study area (Modified from Sawariah and Barjous, 1993; Royal Jordanian Geographic Center, 2003).

3. Materials And Methods

3.1. Field Work and Sampling

Field works were performed during summer of 2015 focusing on Jarash clay deposits. One hundred and two samples were collected from seven different outcrops abbreviated as (An, Bn, Cn, Dn, En, Fn and Gn). The samples were chosen from Jarash clay deposits, using the channel sampling methods. Table (1) shows the coordinates and description of these outcrops and the elevations of the selective outcrop.

Table 1. Coordination of the seven outcrops in the study area and there elevation above the sea level.

Outcrop	N	E	Elevation in meter	Description
An	32˚13′ 20″	35˚53′05″	225	Clay, vary-colored, light grey to light brown, medium to fine grained, soft to hard, red intercalation.
Bn	32˚13′ 33″	35˚52′ 55″	231	Clay, light grey- with brown, medium to fine grained, soft.
Cn	32˚13′ 23″	35˚52′ 45″	229	Clay, vary-colored, light grey - yellowish brown, medium to fine grained, soft to slightly hard.
Dn	32˚13′ 26″	35˚32′ 35″	239	Clay, vary-colored, mainly grey, fine to medium grained, soft.
En	32˚13′ 10″	35˚52′ 25″	244	Clay, light grey to brown and yellow, medium to fine grained, soft to hard.
Fn	32˚13′ 06″	35˚52′ 12″	274	Clay, light grey to yellow, medium to fine grained, slightly hard.
Gn	32˚12′ 50″	35˚52′ 05″	323	Clay, light brownish grey to yellow, medium to fine grained, soft to slightly hard.

3.2. Laboratory Works

Size reduction, grain size analysis, whiteness, specific gravity, oil absorption, bulk density, plastic limit (PL), liquid limit (LL), and plasticity index tests were carried out on one hundred and two representative samples after performing the attrition scrubbing test and wet sieving using the 63µm mish.

3.3. Size Reduction, Attrition Scrubbing and Wet Sieving

The size reduction is one of the most important processes used during sample preparation. The attrition scrubbing can be referred to as the first step of the wet sieving. The purpose of this process was to reduce the coarse size of the sample into finer size by the disintegration and separation of the fine particles by water (Preston and Tatarzyn, 2013; Sandgren et al., 2015). Laboratory attrition scrubber model (IKA-Werk TR-50) was used in this study. The wet sieving was done according to the method of British Geological Survey Laboratories for kaolin (Bloodworth et al., 1993). Sieves that were used in the wet sieving process included the size fractions 2 mm, 1 mm, 0.500 mm, 0.250 mm, 0.125 mm, and 0.063 mm.

The grain size analysis and wet sieving was used to: 1- Determine the percentage of the sand, silt, and clay available in the sample, 2- Separate the fine particles from the coarse particles, 3- Eliminate the major impurities (Sandgren et al., 2015; Bloodworth et al., 1993).

The whiteness is an indicator of the purity of the sample. Sixty five representative samples from Jarash clay including

twenty seven samples before attrition scrubbing and wet sieving and, and thirty eight samples after attrition scrubbing and wet sieving (<63µm) were analyzed using (KETT Electric Laboratory Whiteness test C130 instrument) at the laboratories of Ministry of Energy and Mineral Resources.

Specific gravity was carried out for the samples based on standard methods of ASTM D 854-00. Oil absorption is one of the most important factors used in testing the materials for different industrial application and industries. The tests of oil absorption were done according to the BS 3483: part B7: British Standard method for testing of pigments paint. Representative samples from Jarash clay after attrition and wet sieving were chosen and examined at Earth and Environmental Sciences Department in Yarmouk University. The bulk density is defined as the mass of many particles of the material divided by the total volume. Representatives samples were chosen for the density test.

The liquid limit (LL) is arbitrarily defined as the water content. The plastic limit (PL) means that the lowest water content at which the soil samples stay plastic. The plastic index is the difference between the liquid limit (LL) and the plastic limit (LL). Fourteen bulk representative samples were selected from Jarash clay which included seven samples before attrition scrubbing and wet sieving and seven samples after attrition scrubbing and wet sieving. All applied using the methods of (ASTM D 4318).

4. Results and Discussion

4.1. Results of Physical and Technical Characteristics

Physical characteristics include whiteness, specific gravity, oil absorption, bulk density, and grain size distribution, while the technical characteristics include plastic limit, liquid limit and plasticity index which are both presented and discussed in this section.

The degree of whiteness which refers to the purity of clay is an important factor in the industrial evaluation of kaolin products. Whiteness values before wet sieving and attrition differ from whiteness values after wet sieving and attrition (Table 2). Whiteness values before wet sieving and attrition range between 24.90 and 50.02 % with an average value of 33.61 % and standard deviation of 6.09 %. On the other hand, whiteness values after attrition and wet sieving ranges from 25.4 to 54.9 % with an average value of 40.1 % and a standard deviation value of 6.61 %. Whiteness values after attrition and wet sieving for the fraction (<63 µm) has increased dramatically to 40.1 % compared to 33.61 % before attrition and wet sieving.

Table 2. Results of the physical characteristics of the representative samples of Jarash clay

Physical Characteristics	Min.	Max.	Average	Standard deviation
Whiteness before attrition and wet sieving (%)	24.90	50.20	33.61	6.09
Whiteness after attrition and wet sieving (%)	25.40	54.9	40.10	6.61
Specific gravity after attrition and wet sieving	2.02	2.70	2.24	0.14
Oil absorption after attrition and wet sieving(ml /100 g)	23.25	46.50	33.10	5.68
Bulk density after attrition and wet sieving (g/cm^3)	0.86	1.22	0.99	0.056

4.2. Technical Characteristics

The results of liquid limit (LL), plastic limit (PL), and plasticity index (PI) before and after attrition and wet sieving for the seven bulk representative samples are shown in Table (3).

Liquid limit before attrition and wet sieving ranges from 26.3 and 49.0 % with a mean of 31.89 %, while liquid limit after attrition and wet sieving shows different values that range from 34.2 and 71.5 % with a mean of 48.18 % (Table 3). When the plastic limit was examined, the results before attrition and wet sieving ranged from 13.9 and 23.5 % with a mean of 16.40 %, while after attrition and wet sieving the plastic limit ranged from 15.9 and 26.3 % with a mean of 10.74 %. In addition, plasticity index before attrition and wet sieving were around 10.1 and 25.5 % with a mean of 15.49 % in time the plasticity index after attrition and wet sieving were around 18.3 and 45.2 % with a mean of 19.74 %. The different values of standard deviation for liquid limit (LL), plastic limit (PL), and plasticity index (PI) in table (3) are related to the grain size variations in the samples. The percentage of the silt and clay size (<63 µm) (Table 4), and the contents of kaolinite and plastic kaolin (Figure 4 and Figure 6) for the representative samples of Jarash clay before and after the attrition and wet sieving are presented.

Table 3. Results of technical characteristics of the representative bulk samples of Jarash clay.

Technical Characteristics	Min.	Max.	Average	Standard deviation
Liquid limit before attrition and wet sieving	26.3	49.0	31.89	7.88
Liquid limit after attrition and wet sieving	34.2	71.5	48.18	13.74
Plastic limit before attrition and wet sieving	13.9	23.5	16.40	3.29
Plastic limit after attrition and wet sieving	15.9	26.3	10.74	3.34
Plasticity Index before attrition and wet sieving	10.1	25.5	15.49	5.23
Plasticity Index after attrition and wet sieving	18.3	45.2	19.74	10.50

Seven representative samples from Jarash clay were examined for their Atterberg limits before attrition and wet sieving, and then those samples examined for their Atterberg limits after attrition and wet sieving. Figures (3 and 4) show the results which were graphically used as an identification chart for clay and clay workability chart. The bulk samples before wet sieving and attrition are plotted graphically in the region of the kaolinite (Figure 4). According to the clay workability sheet (Bain and Highly, 1978), the following bulk samples (Cn, Dn, En, and Gn) fall within the region of the optimum molding properties; the bulk samples (An, Bn and Fn) fall within the acceptable molding properties (Figure 3).

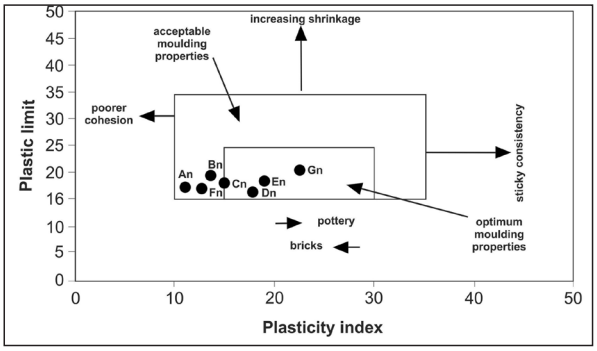

Figure 3. Clay workability chart of the samples before wet sieving and attrition [The standard figure modified after (Bain and Highly, 1978)].

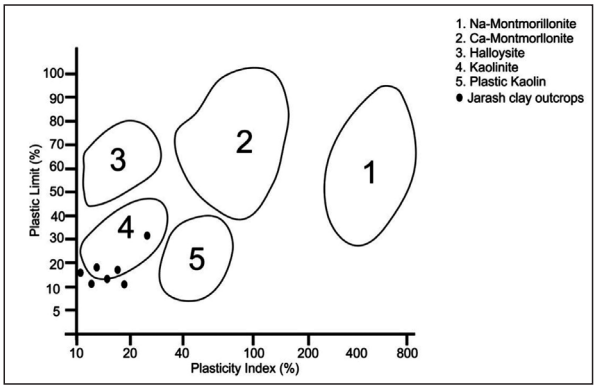

Figure 4. Clay identification of the bulk samples before wet sieving and attrition for Jarash clay [The standard figure modified after (Bain, 1971)].

For those samples where Atterberg limits were measured after attrition and wet sieving (<63µm), figures (5 and 6) show the results plotted graphically in the same way as aforementioned. The results show that the plasticity index in the (<63 µm) fraction of bulk samples is higher than the bulk samples before attrition and wet sieving (Table 3 and Figure 6). It means that the plasticity index has positive correlation with the clay grain size. This is due to the fact that (<63 µm) size contains more clay than the bulk sample. As a result of the process of the attrition and wet sieving, the clay content can increase the plasticity index of clay.

The bulk samples after attrition and wet sieving (<63 µm) are plotted graphically in the region of the kaolinite. While some samples plotted in the region of the plastic kaolin (Figure 6). According to the clay workability sheet (Bain and Highly, 1978), the following bulk samples (An, Bn, Cn, and Dn) fall within the region of the optimum molding properties; the bulk samples (En and Fn) fall within the acceptable molding properties expect for the bulk sample (Gn) (Figure 5). Figures (3, 4, 5, and 6) indicate that Jarash clay could be suitable for pottery and the clay bricks industry.

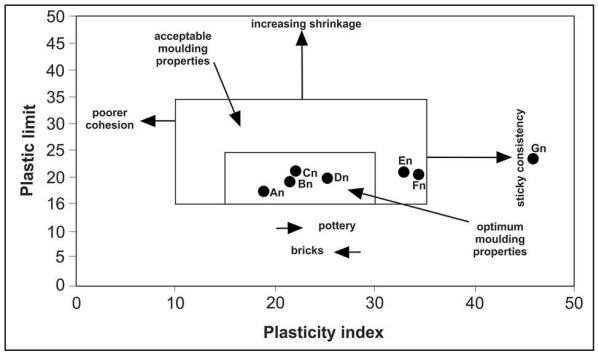

Figure 5. Clay workability chart for samples after wet sieving and attrition (<63 µm) [The standard figure (modified after Bain and Highly, 1978)].

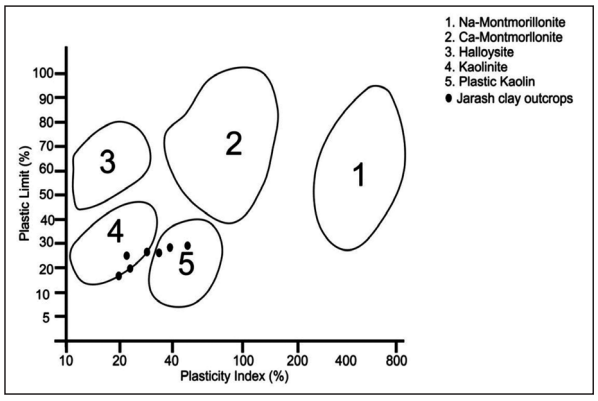

Figure 6. Clay identification for bulk samples after wet sieving and attrition for Jarash clay (<63µm) [The standard figure modified after (Bain, 1971)].

Table 4. Showing the grain size of the tested bulk samples after wet sieving.

*Size (m*m)		Sample No						
		Bulk An	Bulk Bn	Bulk Cn	Bulk Dn	Bulk En	Bulk Fn	Bulk Gn
+2	Wt. (g)	179.5	13.50	100.9	53.8	80.9	194.2	51.0
	(%)	20.37	1.54	11.46	6.08	9.07	21.8	5.675
+1	Wt. (g)	49.1	5.9	43.8	47.8	77.6	60.34	19.2
	(%)	5.57	0.671	5.0	5.4	8.7	6.8	2.14
+0.5	Wt. (g)	66.4	15.3	44.2	20.7	61.6	26.9	27.9
	(%)	7.54	1.74	5.027	2.34	6.9	3.02	3.105
+0.25	Wt. (g)	32.4	40.23	29.2	51.4	82.2	28.9	47.4
	(%)	3.68	4.58	3.32	5.80	9.21	3.24	5.274
+0.125	Wt. (g)	35.1	44.08	38.2	81.0	50.2	59.58	68.74
	(%)	3.98	5.014	4.35	9.15	5.63	6.7	7.65
+0.063	Wt. (g)	97.8	220.0	123.3	70.7	59.7	51.6	155.4
	(%)	11.10	25.03	14.011	7.99	6.7	5.79	17.3
-0.063	Wt. (g)	420.7	540.0	500.0	560.0	480.0	470.0	520.0
	(%)	47.75	61.425	56.832	63.24	53.8	52.72	57.9
Total	Wt. (g)	881	879.01	880.0	885.4	892.2	891.52	898.64

Results of Grain Size Analysis for Samples after Wet Sieving and Attrition

Grain size analysis is used to determine the amount and the percentage of the different grain sizes which consist mainly of gravel, sand, silt, and clay in the sample. Table (4) shows the percentage of different grain sizes for the seven bulk samples. Figure (7) shows results of grain size analysis for the bulk samples from Jarash clay after attrition and wet sieving (<63µm), and figure (8) illustrates the bulk representative samples of Jarash clay ranging from sandy clay to clayey sand.

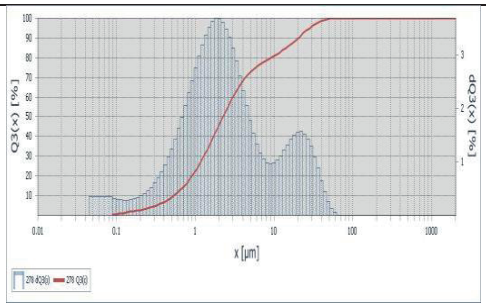

Sample No.: Bulk An

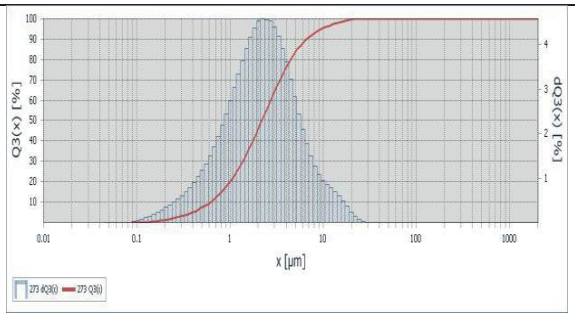

Sample No.: Bulk Bn

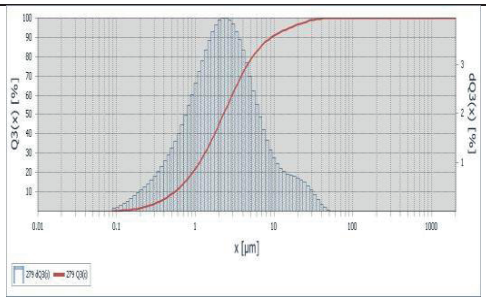

Sample No.: Bulk Cn

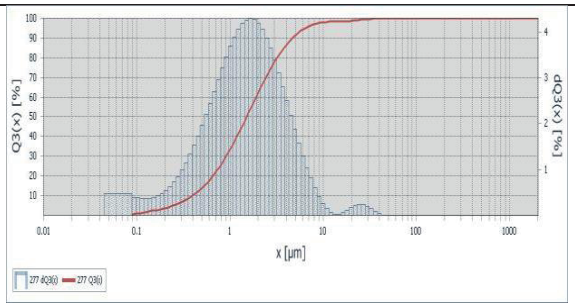

Sample No.: Bulk Dn

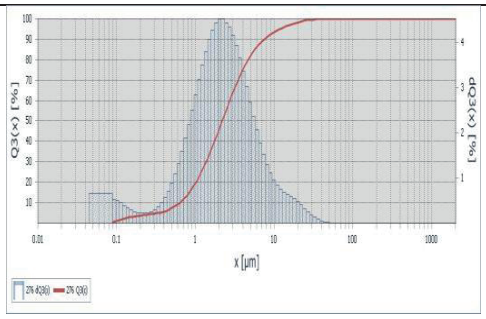

Sample No.: Bulk En

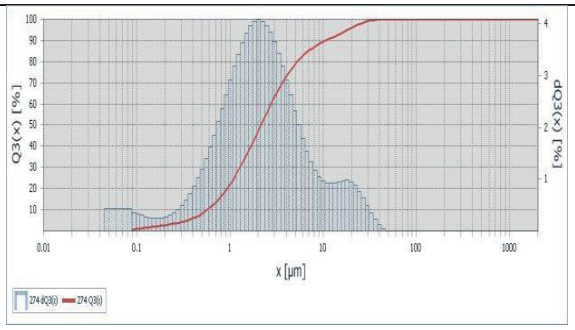

Sample No.: Bulk Fn

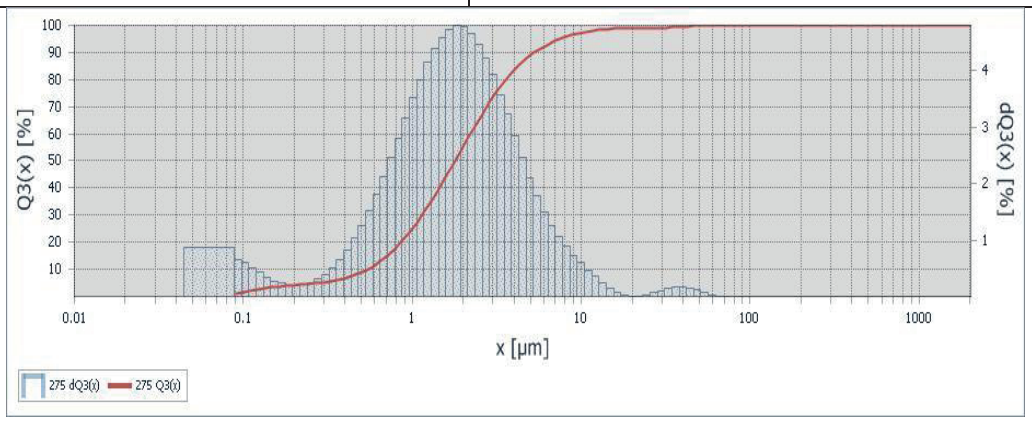

Sample No.: Bulk Gn

Figure 7. Grain size analysis of the bulk samples from Jarash clay after attrition and wet sieving (< 63µm).

Table (5) presents the physical, chemical, mineralogical, and technical properties of Jarash clay deposits after attrition and wet sieving. Values of major chemical components such as SiO_2, Al_2O_3, and Fe_2O_3 are (61.0%) (Range = 47.5 - 78.1%), (19.77%) (Range = 10.8 - 26.33%), and (4.58%) (Range = 1.41 - 10.15%) respectively. While other minor components such as K_2O, TiO_2, CaO, MgO, and MnO are of small values. The low Al_2O_3 content and the high Fe_2O_3 content indicate low-grade clay deposits.

Many localities in Jordan and in the world are correlated to Jarash clay. For instance, the (Kaolin A3) from Hiswa clay deposits in Jordan is considered as low-grade, Another example, kaolin from Oboro deposits in Nigeria is considered low-grade as well. The aforementioned clay deposits are used and applied as raw materials for ceramic tiles, pottery, and brick-making (Mark, 2010; Al-Momani, 2000). Similarly, Jarash clay deposits could be suitable for pottery, ceramic tiles, and brick-making industries.

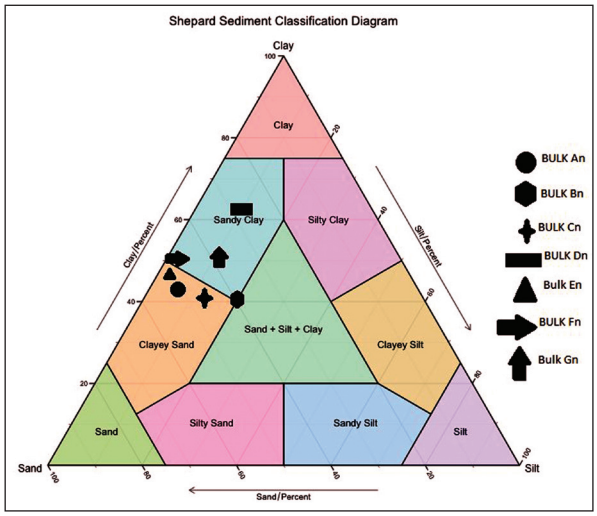

Figure 8. Shepard sediment classification for the bulk samples (Based on Shepard, 1945; Poppe and Eliason, 2008).

Table 5. Comparison between chemical, physical and the technical properties of Jarash clay with properties of other clay deposits from different countries.

The Present Study			I	II
Chemical composition				
SiO_2%		61.00	60.21	58.73
Al_2O_3%		19.77	19.05	19.25
Fe_2O_3%		4.58	3.70	9.15
TiO_2%		1.75	--	0.83
Na_2O%		0.06	0.42	0.09
K_2O%		1.27	2.16	1.39
MnO%		0.006	--	0.04
MgO%		0.59	1.50	0.16
CaO%		1.22	0.30	0.05
P_2O_5%		0.09	-	0.08
LOI		9.35	10.2	7.14
Technological properties				
Plastic limit (wt%)	**Range**	15.9 - 26.3	19.0	18.09
	Average	10.74		
Liquid limit (wt%)	**Range**	34.2 - 71.5	42.4	30.05
	Average	48.18		
Plasticity index (wt%)	**Range**	18.3 - 45.2	23.0	11.96
	Average	19.74		
Physical properties				
Bulk Density (g/cm^3)	**Range**	0.86 - 1.22	1.66	0.69-1.33
	Average	0.99		
Oil Absorption (g/100g)	**Range**	23.35 - 46.5	--	21.81-35.34
	Average	33.1		
Specific gravity	**Range**	2.01- 2.7	--	-
	Average	2.24		
Whiteness (%)	**Range**	25.4- 54.9	--	-
	Average	40.1		
Other properties				
pH	**Range**	6.73 - 8.45	--	5.30- 6.50
	Average	7.74		
Moisture content	**Range**	0.25- 6.81	--	-
	Average	2.40		
EC (mS/cm)	**Range**	108.1- 573	--	-
	Average	281.7		

I. Oboro clay deposits in Nigeria (Mark, 2010) Used as Clay refractory and ceramic
II. Hiswa clay Kaolin A3 (AL-Momani, 2000) Used as ceramic tiles.

Results of X- Ray diffraction (XRD) and Scanning electron microscope (SEM) are matching with the results of mineralogical composition presented before in figures (4 and 6). This means that the kaolinite content is one of the major constituents in Jarash clay. Figures (9 and 10) show typical X-ray diffraction analysis of the bulk samples before and after attrition and wet sieving (<63µm) respectively. Also, Jarash clay contains small or trace amounts of muscovite/ ilite, and smectite.

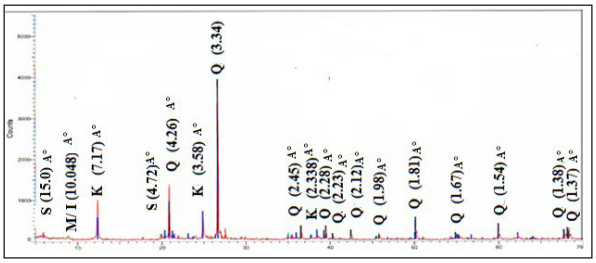

Figure 9. Typical XRD pattern for the representative sample before attrition scrubbing and wet sieving, with the d-spacing for the major peaks between brackets (Q: Quartz, K: Kaolinite, S: Smectite, M/ I: Muscovite/ Ilitte). The unit of d-spacing (in Angstrom A°).

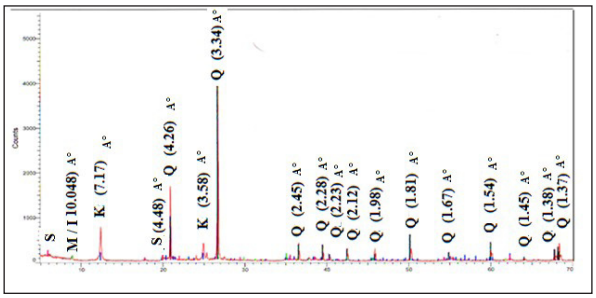

Figure 10. Typical XRD pattern for the representative sample after attrition scrubbing and wet sieving (<63µm), with the d-spacing for the major peaks between brackets (Q: Quartz, K: Kaolinite, S: Smectite, M / I Muscovite / Iilite). The unit of d-spacing (in Angstrom A°).

The crystal shape and texture of Jarash clay images obtained by scanning electron microscope are presented in figure (11). The clay samples, as shown in the SEM images, consist mainly of Kaolinite. Figure (11) shows the euhedral to pseudohexagonal shape of Kaolinite in particles sized less than 2 µm.

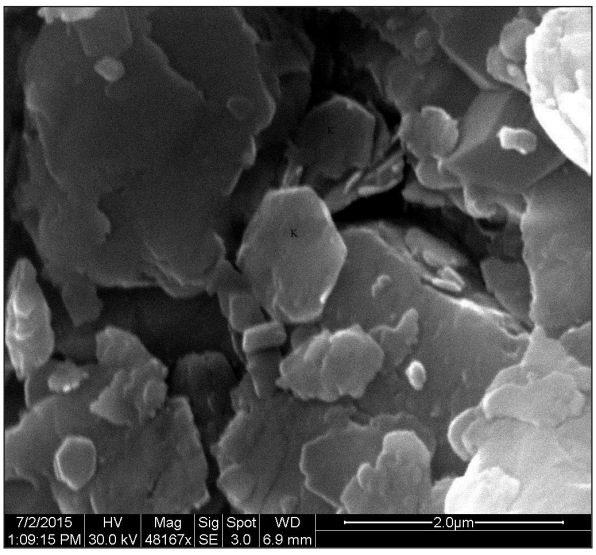

Figure 11. SEM Image of pseudohexagonal of kaolinite (48167x).

Conclusion

The results obtained by analyzing Jarash clay indicated that the plasticity index in the (<63 µm) size of Jarash clay after attrition and wet sieving is higher than that before attrition and wet sieving. It means that the plasticity index has positive correlation with the clay grain size. This is due to the fact that (<63 µm) size contains more clay than the bulk samples. As a result of the process of attrition and wet sieving, the clay content enhances the plasticity index of Jarsh clay.

According to the Shepard sediment classification diagram, the bulk representative samples of Jarash clay range from sandy clay to clayey sand.

The bulk samples of Jarash clay before attrition and wet sieving are plotted graphically in the region of the kaolinite in the identification chart of Bain (1971). While some samples were plotted in the region of the plastic kaolin. The contents of kaolinite and plastic kaolin may be affected by the variations of liquid limit (LL), plastic limit (PL), and plasticity index (PI) for different samples of Jarash clay.

Using the clay workability sheet (Bain and Highly, 1978), most of the bulk samples of Jarash clay fall within the region of the optimum molding properties, and the acceptable molding properties. This indicated that Jarash clay could be suitable for pottery, and the clay bricks industry.

In addition, the physical characteristics (whiteness, bulk density, oil absorption, and specific gravity), grain size analyses, chemical characteristics, and technical characteristics (liquid limit (LL), plastic limit (PL), and plasticity index (PI)) of Jarash clay deposits after attrition and wet sieving confirm that Jarash clay deposits could be suitable for pottery, ceramic tiles, and brick-making industries.

Acknowledgements

The financial support from the Deanship of Scientific Research and Graduate Studies at Yarmouk University is gratefully acknowledged. The authors wish to thank the editor of JJEES and the referees for their insightful comments and suggestions which greatly improved the presentation of this paper. Special thanks are due to Dr. Mohammad Al-Qudah for his assistance to improve this paper.

References

[1] Abu Hamad, A. A., Amireh, B., Jasper, A., and Uhl, D. (2016). New Palaeobotanical data from the Jarash Formation (Aptian–Albian, Kurnub Group) of NW Jordan. The Palaeobotanist 65: 19–29.

[2] Ahmad, F., Abu hamad, A., Obidat, M. (2012). Palynological study of the Early Cretaceous Kurnub Sandstone Formation, Mahis area Central Jordan, Acta Palaeobotanica, 2: 303-315.

[3] Al-Momani, T. (2000). Characterization, Industrial Utilization and Environmental Impact of the Hiswa Clay Deposits, South Jordan. Ph.D. Thesis, University of Jordan, Jordan.

[4] Amireh, B. (1996). Sedimentolgy and Paleography of The Regressive-Transgressive Kurnub Group Early Cretaceous of Jordan. Sedimentary Geology. Elsevier Science publishers.

[5] Amireh, B., and Abed, A. (1999). Depositional Environments of the Kurnub Group (Early Cretaceous) in northern Jordan. Journal of African earth Sciences, 28: 449-468.

[6] Aras, A., Albayrak, M., Arkan, M., and Sobolev, K. (2007). Evaluation of Selected Kaolin clay as Raw Material for Turkish Cementand concrete industry. Clay Minerals, 42 (2): 233-244.

[7] ASTM D 4318: Standard Test Method for Liquid Limit, Plastic Limit, and Plasticity Index of Soils.

[8] ASTM D 854-00: Standard Test for Specific Gravity of Soil Solids by Water Pycnometer.

[9] Baba, A., Mosobalaje,M., Ibrahim, A.,and Girigisu,S. (2015). Bleaching of a Nigerian kaolin by oxalic acid leaching. Journal of Chemical Technology and Metallurgy. 50 (5): 623-630.

[10] Bain, J. A., 1971. A Plasticity chart as an aid to the identification and assessment of industrial mineral. Clay minerals 9:1-17. 9, a.

[11] Bain, J.A., and Highly, D.E.(1978).Regional appraisal of clay resources challenge of the clay mineralogist. In: Mortland M. M and farmer V. C. (eds) Proc. Int. Clay Conference. Elsevier. Amsterdam, 437-446.

[12] Bloodworth, A.J. Highley, D.E. Mitchell, G. J. (1993). Industrial Mineral laboratory manual Kaoline, British Geological Survey, p8.

[13] British Standard, BS 3483, Part B7 (1974). British Standard Methods for Testing Pigments.

[14] Diko, M. L., Ekosse, G.E., Ayonghe, S.N. and Ntasin, E. (2011). Physical characterization of clayey materials from Tertiary volcanic conesin Limbe (Cameroon) for ceramic applications. Applied Clays Science, No. 51: 380-384. DOI:10.1016/J. Clay.2010.11.034.

[15] Diko, M., Ekosse, G. and Ogola, J. (2016). Fourier transform infrared spectroscopy and thermal analyses of kaolinitic clays from South Africa and Cameroon. Acta Geodynamica et Geomaterialia, 13 (2): 149-152.

[16] Ediz, N., Tatar, I., and Aydin, A. (2015). Pre-Concentration and flotation of Alunitic Kaolin and its possible use in ceramic tileindustry. Physicochemical Problems of Mineral Processing. 51(1): 213-231.

[17] Ekosse, G. E. (2010). Kaolin deposits and occurrences in Africa: Geology, mineralogy and utilization. Applied Clay Science, 50(2): 212–236.

[18] Khoury, H.N. (2002). Clays and clay minerals in Jordan. University of Jordan. Special Publication, Amman-Jordan. pp. 15-19.

[19] Khoury, H. N., Hodali, H., Hourani, M., Mubarak, Y., Faqir, N., Hanayneh, B., and Esaifan, M. (2008). Mineral Polymerization of Some Industrial Rock and Minerals in Jordan. University of Jordan. Amman-Jordan. pp. 15-19.

[20] Mark, U. (2010). Characterization of Ibere and Oboro Clay Deposits In Abia State, Nigeria For Refractory Applications. International Journal of Natural and Applied Sciences, 6(3): 296-305.

[21] Murray, H.H. (1988). Kaolin Minerals: Their Genesis and Occurrences. Bailey, S.W., editor. Hydrous Phyllosilicates. Volume 19. Reviews in Mineralogy. Washington, DC: Mineralogical Society of America. Chapter 4, pp. 67 – 90.

[22] Murray, H. (1999). Applied clay mineralogy today and tomorrow. Clay Minerals. 34, 39-49.

[23] Murray, H. (2007). Applied Clay mineralogy occurrences, Processing and application of Kaolin's, Bentonies, Palygorskite-Sepiolite, and common clays. Developments in Clay Science-2, Elsevier Radarwef, Amsterdam. Netherlands.

[24] Poppe, L. J., and Eliason, A. H. (2008). A Visual Basic program to plot sediment grain-size data on ternary diagrams. Computerand Geosciences. 34: 561-565.

[25] Preston, M. and Tatarzyn, J. (2013). Mineral Processing Optimizing Plants efficiency With Attrition Scrubbers. Yan-Tai Jin-Peng Mining Machinery Company. China.

[26] Royal Jordanian Geographic, Jarash maps sheet. (2003). 1:25.000, Center, Amman, Jordan.

[27] Sandgren, Metsoper- Erik. Berglind, B. Modigh, S. (2015). Basics in mineral processing handbook. Metso Corporation, Finland.

[28] Shepard, F.P. (1945). Nomenclature based on Sand-Silt-Clay ratios. Journal of Sedimentary Petrology. 24 (3): 151-158.

[29] Sawariah, A. and Barjous, M. 1993. The geology of Suwaylih map sheet No. 3154-II. Natural Resources Authority, Amman, Jordan.

[30] Yasin, S., and Ghannam, A. (2006). Kaolinite, National Resource Authority, Hashemite Kingdom of Jordan.

JJEES
Jordan Journal of Earth and Environmental Sciences

Volume 9, (Number 2), August, 2018
ISSN 1995-6681
Pages 89 - 101

A Comparative Study of Ringiculidae and Acteonidae (Architectibranchia, Gastropoda) from the Campanian Amman Silicified Limestone Formation and some Similar Species from the Fringing Reefs of the Gulf of Aqaba in Jordan

Ikhlas Alhejoj[1*], Klaus Bandel[2], Abdalla M.B. Abu Hamad[1]

[1]Department of Geology, the University of Jordan, 11942, Amman, Jordan.
[2]Geologisch-Paläontologisches Institut und Museum Hamburg, Universität Hamburg, D-20146 Hamburg, Germany

Received 6 February, 2018; Accepted 27 May, 2018

Abstract

Two gastropod genera of Heterostropha and Architectibranchis were recorded from the Campanian Amman Silicified Limestone Formation. Representatives of these two gastropod genera are still living until now in the reef environment of the Gulf of Aqaba, and can be found near the Marine Biological Station of Jordan. An analytical comparison between the Campanian gastropods and the recent gastropods is attempted in the present study. The fossil shells have been transformed into silica and during this process of transformation from aragonite biocrystals of the crossed-lamellar structural type, they have retained the morphology of their micro-structure of crossed lamellae. The embryonic and larval shell of *Acteon* from the Cretaceous have the same size and morphology as that of the acteonid *Pupa* from Aqaba, and both also resemble each other regarding the adult shell morphology and ornament. The two genera of *Ringicula* recognized from Aqaba differ from each other predominantly regarding their size; one being larger than the other. They closely resemble the fossil *Ringicula* with some distinct characters of the inner lip of their aperture.

Keywords: Ringiculidae, Acteonidae, Cretaceous, Amman Silicified Limestone Formation, Marine Gastropods.

1. Introduction

An amazing continuity exists in regard to some species of gastropods which lived in the sea of the shallow Tethys Ocean that covered northern Jordan during the Campanian and those which now live in the Gulf of Aqaba in Jordan. For example, the species belonging to the families Ringiculidae and Acteonidae live in the sea at Aqaba and have been recovered from the Campanian rocks at Amman and Irbid. The Amman Silicified Limestone Formation of Jordan contains fossil-rich Upper Cretaceous deposits that have been studied for example in the general description of the oyster fauna of Amman Silicifed Limestone Formation as provided by Aqrabawi (1993). These form thick coquina beds covering most of Jordan, and reflecting local highs and sea-level lowstands. Fossilized microorganism assembleges and macrofauna including bivalve, gastropod, ammonite, and fish teeth fragments have been documented and studied (Farouk et al., 2016; Powell,1989)

In this article, the morphology, and environments of the studied species of the genera of Ringiculidae and Acteonidae (gastropods) from Amman Silicified Limestone Formation are described and compared with some similar species from the fringing reefs of the Gulf of Aqaba in Jordan.

2. Sample Collection and Treatment

The material described in this study were collected from Wadi Kafr, southeast of Kafr Yuba village (29°51'0" N, 35°30'0" E) in Irbid, about 63 Km northeast of Amman City (Fig.1a**).** The silicified fossils were found embedded in marls with a composition of calcium carbonate. They were carefully treated with a solution of hydrochloric acid to dissolve the carbonated matrix, and the rocks were then rinsed in water on a screen with a 0.5mm mesh. After a major cleaning, the dried fossils were studied under a binocular microscope, and were documented using the Scanning Electronic Microscope of the University of Jordan. The gastropods in the current study were described based on previous studies, and on new investigations. Regarding the recent gastropods, the samples were collected from the area next to the Marine Science Station along the marine reserve area (E34°58.210; N29°27.293) using a net with a 150 µm mesh width. The samples were collected in a plastic bucket, and were transferred to the laboratory. The gastropod specimens were deposited in the University of Jordan at the Department of Geology under collection numbers AM2033-2050.

* Corresponding author. e-mail: i.alhejoj@ju.edu.jo

3. Geological Setting

During the upper Cretaceous time, the type of sedimentation within the Jordanian shelf sea of the Tethys Ocean switched from predominently benthic to predominantly pelagic source of material (Bandel and Salameh, 2013).Within the deposition of the sediments of the Belqa Group (Quennell and Burdon, 1959), that switch occurred at the base of the formations with the names Umm Ghudran = Ain Ghazal, (Amman, Al Hisa Phosphorit = Ruseifa, and the Muwaqqar throughout Jordan). The predominant type of rocks found in the Belqa Group consists of chalky limestones. Only close to the shore environments of the Tethys Ocean in the SE of Jordan, dolomites and sandstone are intercalted indicating the intermediate closeness of the shore of Gondwana Continent (Schandelmeier et al. 1997; Bandel and Kuss 1987; Bandel et al. 1987). Bandel and Mikbel (1985) confirmed the data of Bender (1968) according to whom, Amman Silicified Limestone Formation occured on a large scale in Jordan with its typical lithology (Fig. 1b). Only in the southeast of the country, it wedges out and is replaced by continental varicolored sandstone with plant fossil (Bender, 1974; Bender and Mädler 1969; Berndt, 2002). During its deposition mainly at Campanian times, the shore was laid in the far south of Jordan and on the other side of the Gulf of Suez (Bandel et al., 1987; Klitzsch, 1986). The sea had covered much of the northern Gondwana continent during the Coniacian, (withdrew during Santonian to flood and withdrew during the Campanian and flood far at Maastrichtian), but at the low stages of the sea level, continental sand reached the area from Gondwana, and a terrestrial flora was able to grow leaving traces in SE Jordan.

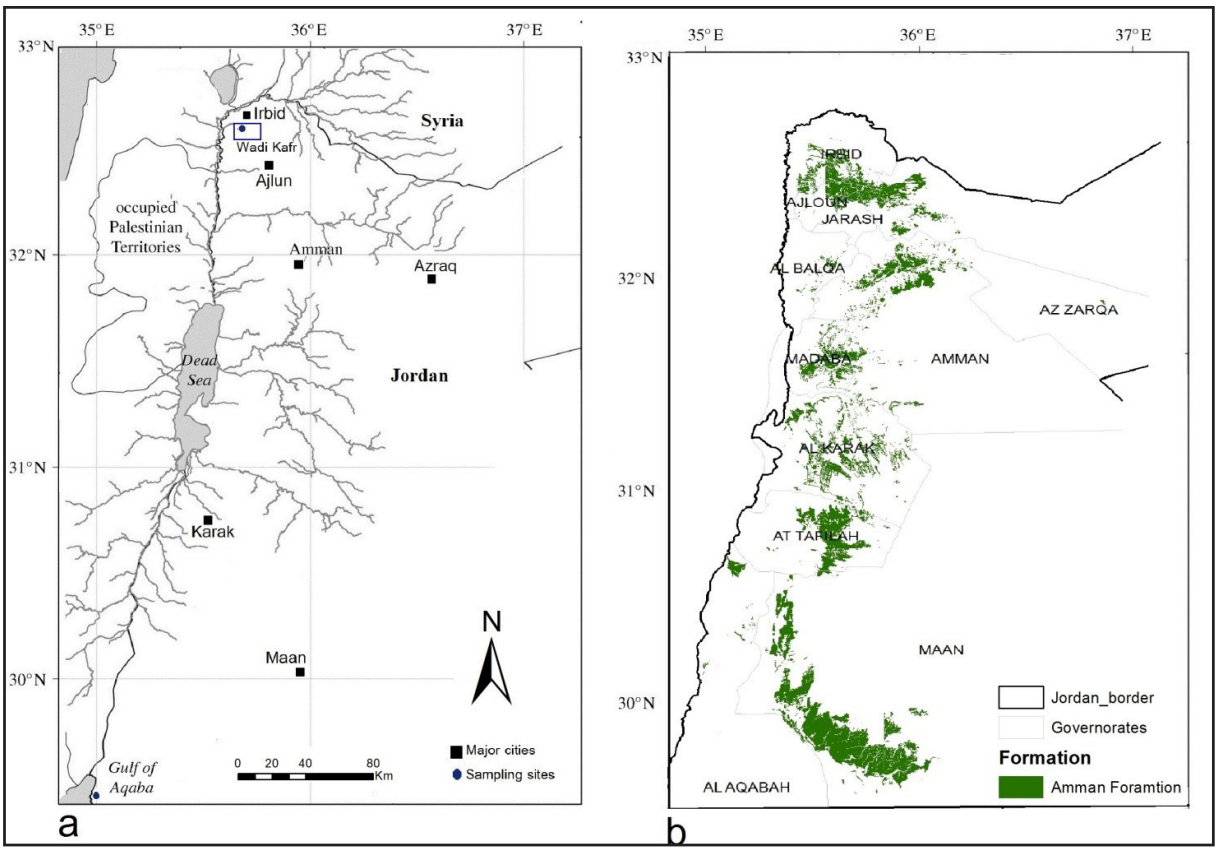

Figure 1. a. Map of sampling locations, **b**. Map showing distribution of Amman Silicified Limestone Formation deposits in Jordan.

During the upper Conician to upper Eocene Belqa Group, the deposition is dominated by the skeletal parts of pelagic organisms (predominantly coccoliths) (Bender, 1968). These deposits are widely distributed, and cover much of the Jordanian plateau extending from the Yarmouk River in the north to Ras En Naqab-Batn El Ghul escarpment in the south (Powell, 1989).

The Amman Silicified Limestone Formation disconformably overlies the Coniacian-Santonain Wadi Umm Ghudran Formation. The type section of Umm Ghudran is found in Wadi Umm Ghudran, which lies twelve km WSW of Irbid. The type for the Ain Ghazal Formation lies just to the southeast of central Amman within the city proper. The base of Umm Ghudran- Ain Ghazal Formations in both cases is well-defined by the last hard massive limestone bed of Wadi Sir Formation formed predominantly by skeletal products of benthic organisms. The top of the formation is recognized with the appearance of a thick chert bed of the base of the Amman Silicified Limestone Formation near Irbid and in the case of the sections within Amman also by a more or less silicified bed with an oyster coquina.

The Umm-Ghudran Formation was considerd to be Santonian in age (Bender, 1968; Parker, 1970; Quennell and Burdon, 1959; Wetzel and Morton, 1959) with the base inpart being Coniacian in age (Bandel and Geys, 1993). The Amman Silicified Limestone Formation has been determined to be Campanian in age based on occurrences of *Baculites cf. ovatu* fossils and micro planktonic assemblages (Haggart, 2000; Farouk et al., 2016; Wetzel and Morton's, 1959).

It is of variable thickness in different locations of Jordan.

Table 1. lithostratigraphic units of upper Cretaceous in Jordan (Masri, 1963; Farouk et al., 2016; Powell, 1989).

Age		Group	Formation Masri 1963	Formation Powell 1989	Formation Farouk et al. 2016	Lithology
Paleogene	Eocene	Belqa	Muwaqqar	Umm Rijam	Muwaqqar	Chert
	Paleocene			Muwaqqar		Chalk
Upper Cretaceous	Maastrichtian					
	Companian		Amman	Al Hisa Phosphorite	Al Hisa Phosphorite	Phosphorite and oysters
				Amman Silicifed Limestone	Amman Silicifed Limestone	Chert
	Santonian			Ghudran	Umm Ghudran: Dhiban Chalk Member / Tafilah Member / Mujib Chalk Member; Alia Sandstone	Chalk
	Coniacian	Ajlun	Ghudran	Wadi Sir Limestone / Sandy Phosphorite		
	Turonian		Wadi Sir		Wadi Sir Limestone	Limestone

It may have been totally eroded or is thicker than 100 m. In the area of Wadi Mujib, The Amman Silicified Limestone Formation is approximately 135 m thick (Bender, 1968; Powell, 1988; Powell and Mo'hd, 2011). The transition to Ruseifa Formation with beds of phosphate sand is here- not well-developed, while such deposits in the NNW of Jordan measure about 10 m, and about 25 m at Amman-Ruseifa, and even 40 m at Al Hisa (Beerbaum, 1977). In Wadi Mujib, the sediment formed continued from the base of Amman Silicified Limestone Formation to beyond the end of Ruseifa formation without any notable interruption. In the north and the south of the Mujib area, structural unrest resulted in the elevation of the sea floor to a level where it became eroded, and the sands winnowed from mud forming the phosphate deposits.

The studied outcrops exposed at Wadi Kaf*r* consist of alternating thick massive chert beds and limestone with silicified fossils (Figs. 2a-b). Well-preserved fossils with a thin limestone layer at the boundary to the chert bed are found and collected for the present study (Figs. 2c). Limestone beds with about 3m thickness consisting of fossil fragments were also noticed in the study area (Fig. 2d). The beds of chert are rich in silicified mollusk shells comprising cephalopods, gastropods and bivalves including species close to Nucula, Nuculana, *Barbatia*; others are present as well (Fig. 2e).

The calcareous composition of some specimens has been transformed into silica. The silicification during early diagenesis preserved the delicate shells of a fauna of which most animals had originally lived in, and on the muddy, aragonite-rich, predominantly calcareous sediment. Also, the remains of organisms which had lived in the water column, such as planktonic forminifera and ammonites formed part of the shell coquina. The silicified shells are connected in their origin to the formation of flint nodules and chert layers (Bandel et al., 2000). Chert formed due to the solution and redeposition of siliceous skeletal elements (sponge spicules, diatom and radiolarian sceletons) in the sediment (Bandel and Mikbel, 1985).

4. Overview of the Ringiculidae and Acteonidae Gastropods

Class Gastropoda holds the subclass Heterostropha with Acteon and Ringicula. Within the class, the Heterostropha (Fischer, 1885) (= Heterobranchia Gray, 1840) includes among others the orders Allogastropoda (Haszprunar, 1985) and Opisthobranchia (Milne Edwards, 1848). The members of the families Acteonidae (d'Orbigny, 1843), and Ringiculidae (Philippi, 1853) nowadays represent an exception among the Opisthobranchia since they have a solid well calcified shell (Wenz and Zilch, 1960). Most representatives of this larger group of Gastropoda have reduced their shells and many have even no shell when fully grown, because their earliest shells were lost during the early stages of life. The aperture of the shell of individuals belonging to Acteonidae and Ringiculidae is elongated and narrow, and in some species can be closed with an operculum; however, others do not have a lid. The thick shell is oviform with a short conical apex, and is usually ornamented with spiral groves or rows of pits. The elongated aperture is usually narrow with a posterior notch and enlarged base. The inner lip often has plaits.

Gastropods Ringiculidae and Acteonidae have quite a characteristic shell shape. Here the embryonic and larval shells are coiled to the left while the adult shell is dextrally coiled. The change in the coiling direction occurs within the larval shell where the orientation from the left is lost within the shell that has grown during the larval stage. The transition to the right of the shell of the adult occurs at the phase of the change from a free swimming larva to the benthic crawling young (protoconch to teleoconch transition). The protoconch is composed of one whorl of the embryonic shell with sinistral coiling mode and the shell grown by the larva. During the final growth of the larval shell, the change from the left coiling mode into the dextral coiling mode occurs (Bandel, 1982).

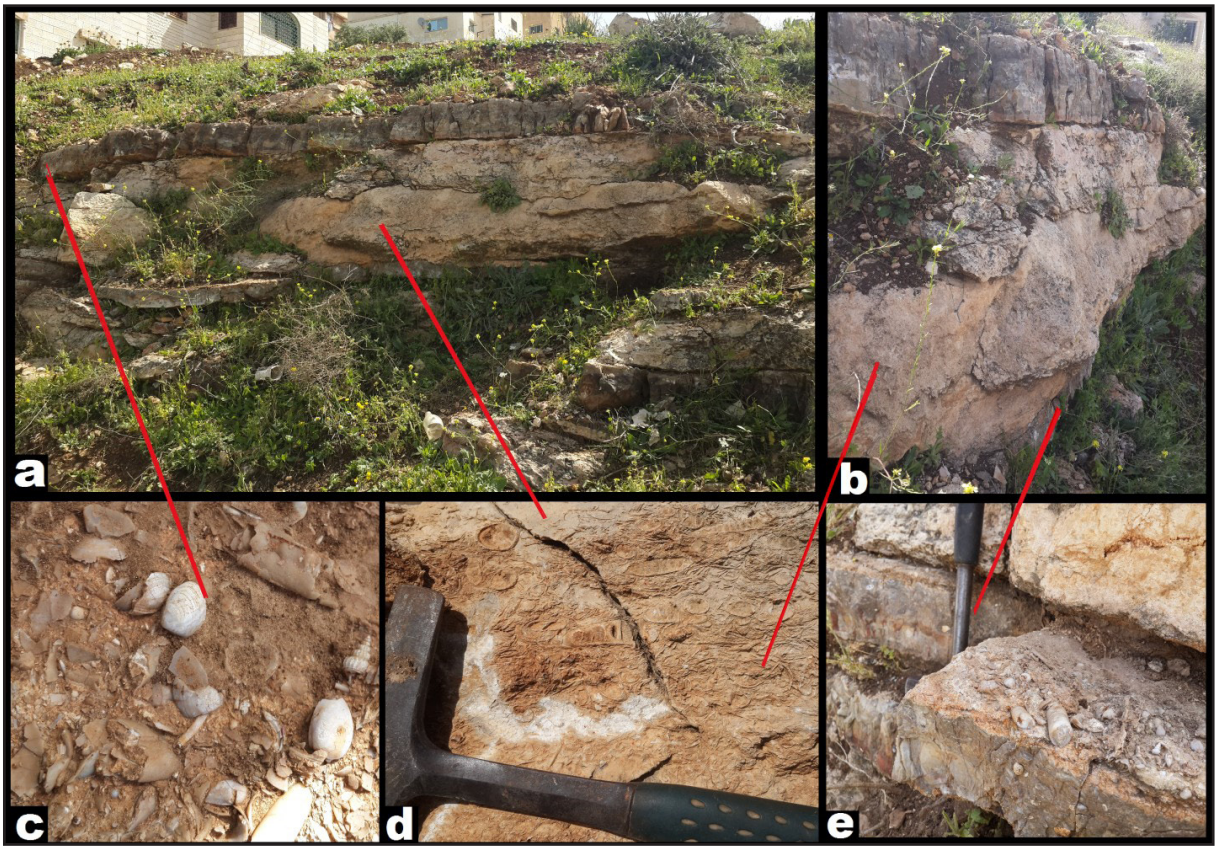

Figure 2. a. Field photograph showing the studied Amman Silicified Limestone Formation exposed at Wadi Kafr, Irbid; **b**. Filed photograph showing an alteration of chert and limestone beds; **c**. Close up of well preserved mollusk fossils such as bivalves, gastropods, and cephalopods from limestone layer at the boundary to the chert bed; **d**. Limestone with reworked mollusca fossils fragments, including turritella and baculites; **e**. Chert beds rich in silicifed fossils from the Amman Silicified Limestone Formation.

The embryonic shell grows during the development of the embryo within the egg, and the larval shell is secreted after hatching from the egg and during life as a free swimming larva. Before hatching, the shell and the soft body detach from each other, and both are connected to each other only by the muscle that is used to pull the soft body into the shell (retractor muscle) (Bandel, 1982; Bandel, 2017).

The change from the embryonic stage to the larval phase of life is also connected to a change in the source of food. The appearance of a first mineral shell here is composed throughout life by aragonite calcium carbonate. The embryo is nursed by the yolk that is contained within the egg, and the larva feeds on algal plankton. To be able to do so, a velum has grown on the embryo still within the egg (Bandel, 1982). The velum consists of two rows of cilia which propels the hatched larva through water and which collects algal cells that come into contact with them and transport them to the mouth. The animal growth now depends on the ingestion and digestion of external food. When the gastropod has concluded its larval life, it changes from a free swimming existence to life on the bottom of the sea (metamorphosis). Growth of the benthic snail is characterized by a shell of the animal after the metamorphosis from the larva (teleoconch) that has a dextral coiling mode (Bandel, 1982; Bandel, 2017).

The protoconch either rests on the teleoconch with angle or is included in its top with an opposite orientation to its columella (axis of coiling). The position of the protoconch depends on the exposure of the apex and the inclination of the shell spindle (columella) (*Acteon*, *Ringicula*) (Bandel 1979). As soon as benthic life is taken up, the mode of locomotion changes and also the mode of feeding. Plankton microorganisms as food are exchanged with feeding on benthic animals. Swimming by the beat of the cilia is changed to crawling with a foot on and in the bottom substrate. Food, thus is no longer collected by cilia, but hunted with the foot and by the mouth parts, and is eaten with the help of teeth present in the anterior part of the digestive tube (oesophagus). Teeth are attached to an elastic ribbon, the radula, which is moved in and out of the mouth and the anterior digestive tube. The teeth take hold of prey, and when the radula is pulled back into the mouth, it transports prey or parts of it into the gut (digestive system) (Bandel, 1990).

The mineral shell of *Ringicula* and *Acteon,* similar to that of most gastropods is composed of calcareous material, and here the modification of aragonite is organized in the bio-crystalline mode of crossed lamellae (Bandel, 1979; Bandel, 1990). Gastropod shells are predominantly composed of a carbonate shell of the calcium carbonate in the crystalline modification of aragonite. The juvenile shells being delicate and thin are rarely well-preserved in the fossil record, but these differ from the gastropods found in Amman Silicified Limestone Formation (Bandel et al., 2000).

5. Fossil Record

Species with *Acteon*-like forms have been existent since the Triassic, and those with *Ringicula*-like shell shape have been known since the Jurassic (Bandel, 2017). Earliest species belonging to the subclass Heterostropha are documented from

Early Devonian (Fryda, 2001). Within the Heterostropha, all those species that change from sinistral to dextral coiling during their ontogeny, or those which have evolved from ancestors that had this development are included. Heterostropha hold the orders Allogastropoda and Euthyneura, the later with the suborders Opisthobranchia and Pulmonata.

Species with shell shape very close to that of modern *Acteon* and to *Ringicula* occur as early as Jurassic (Schröder, 1995; Bandel, 2017) and can be seen related to the Triassic Cylindrobullinidae that may represent the stem group to Acteonidae and Ringiculidae alike (Bandel, 1994). Many of the modern groups of the Opisthobranchia have reduced their shell, and when adult, they become naked. Some of them have only a shell during their embryonic stage, and may leave their shell when changing from larval life to the adult stage.

Hyman (1967) included within the Cephalspidea s.l. (=Tectibranchia) all opisthobranchs with a coiled external shell as is present in the members of the families Acteonidae, Ringiculidae, and several more including **also** the Bullidae, Atyidae, Retusidae, and Cylindrobullidae. The paleontological record allows to trace the general way to the different marine euthyneuran groups by comparing Triassic, Jurassic and Cretaceous species. Within the modern opisthobranch families Acteonidae and Ringiculidae species of the genus *Acteonina* or *Cylindrobullina* from the Triassic and Jurassic are very similar (Bandel, 1994; Bandel, 1996; Bandel, 2017).

One could place *Acteon* (Montfort, 1810) in the suborder Architectibranchia (Haszprunar, 1985), superfamily Acteonoidea (Orbigny, 1842), and could also include in this family *Pupa* (Röding, 1798) with *Pupa solidula* (Linnaeus, 1758).

Ringiculidae can be derived from the gastropods with a shell as found among the fossil Cylindrobullinidae of the Triassic (Bandel, 1984) parallel to the Acteonidae. The stem group to both Acteonoidea and Ringiculioidea alike can be suspected among the Cylindrobullinoidea or relatives of the Zardinellidae (Bandel,1984), both described from the Triassic St. Cassian fauna.

Burn and Thompson (1998) collected the data regarding modern representatives of the Ringiculoidea, and came to the conclusion that even though there are many species in the group, which live in shallow water to the great depth in all seas, very little is known about their anatomy and ecology. Even though young individuals are difficult to distinguish from young Acteonidae, the fully grown ones are quite distinctive from each other. The shape of the radula is quite different in both groups. While in the acteonids, there is a ribbon consisting of many subequal teeth which meet in the middle of the ribbon either having a central tooth between them or meeting without one as such,. In ringiculids, there are only a pair of lateral teeth in the row either with or without a central tooth between them (Bouchet, 1975). Regarding food requirements, it seems that ringiculids usually feed on Foraminifera (Fretter, 1960) or small endobenthic animals.

6. Taxonomic description

Class Gastropoda Cuvier, 1795
Superfamily Acteonoidea d'Orbigny, 1843
Family Acteonidae d'Orbigny, 1843
Genus Acteon Montfort, 1810

The family Acteonidae belongs to the superfamily Acteonoidea, which has recent representatives. Other families such as: Acteonellidae, Tubiferidae, Zardinellidae, are found only as fossils (Gofas, 2015).

Acteonoidea with the given genus name *Acteon* can be traced starting from the Middle Jurassic (Cossmann, 1895; Schröder, 1995; Gründel, 1997; Bandel, 2017) continually to the modern species. The group surrounding *Acteon* and *Bullina* appeared before the Cretaceous; Acteonoidea differ from Cylindobullinoidea in having a spiral ornament. They differ from Actaeonelloidea which also occured commonly in the Cretaceous of Jordan (Mustafa and Bandel 1992) by the same features, but may have folds on their inner lip like these. Ringiculoidea have a thickened margin of their aperture. The Bullinidae differ from the Cylindrobullinidae in the submerged protoconch and the spiral furrows as ornament on the teleoconch. Bullinidae differ from Acteonidae by the absence of folds on their inner lip. The oldest representatives of the Actaeonoidea were included in the family Sulcoactaeonidae (Gründel, 1997) which resemble Bullinidae that are still living in all the essential features especially their shell as described by Rudman (1972).

Most representatives of the Cephalaspidea have a functional shell with nearly cylindrical (subcylindrical) shape, and either an erect or a submerged spire, and are then considered to represent tectibranchiate opisthobranchs. The aperture of the shell is commonly narrow and high, and the inner lip of the aperture (columellar edge of the inner lip). may have folds. Water leaving the pallial cavity usually runs via a slit or sinus of the aperture that is next or near to the suture of the shell. In addition to the growth lines, the shell surface commonly has an ornament of fine spiral furrows and/ or rows of pits.

The shovel-shaped head has posterior extensions (cephalic shield) which cover the anterior shell and mantle opening in many Architectibranchia as was also observed in case of the individuals of *Pupa* from Aqaba. It is also known in *Akera* of the Anaspidea and *Cylindrobulla* of the Sacoglossa. Actaeonidae and Ringiculidae retain the streptoneurous nerve system, while in the other Cephalaspidea, it becomes simplified with the ganglia being concentrated in the head region (Mikkelsen, 1996; Ruthensteiner, 1997).

The Genus Named Acteon (Montfort, 1810)

The shell shape is ovate with a low to moderately elevated spire. The protoconch is heterostrophic, and often partly buried within the teleoconch. About four whorls of the teleoconch are present with the last whorl being very capacious. The sculpture consists of narrow spiral grooves and spiral rows of pits, typically with fine axial costae within the **grooves**. The aperture is large with the anterior end rounded and posterior end constricted. The columella is thick, subvertical, and has a single plait at its posterior end.

Genotype: Voluta tornatilis (Gmelin, 1788) from the North Sea (Thompson, 1988).

The shell of *Acteon* is rather characteristic having a large final whorl, smooth protoconch, an ornament of spiral furrows and one columellar fold. The columellar lip has only one fold compared to that of *Pupa* which has two folds, or that of *Triploca* which has three folds, or *Bullina* where there is no fold at all.

Remarks: Representatives of *Acteon* keep their operculum after metamorphosis. *Acteontornatilis* hatches from its egg mass with an embryonic shell measuring 0,12 mm and grows in the Plankton to a size of 0.32 to 0.35 mm (Thorson, 1946). Eggs are usually enclosed individually in a transparetn capsule. Each egg capsule is attached to the previous one and the next one by a thread (chalaza) of the capsule material. A string of capsules is usually twisted in a spiral coil within a jelly-like mucoid egg mass (Hurst, 1967; Bandel, 1976). Eggs are between 0,05 and 0,4 mm in size. Eggs below 0,17 mm in size usually develop into a planktotrophic veliger, and these of a larger size usually hatch from the egg mass as benthic crawlers.

Acteon hunts worms within the sandy or muddy bottom and sucks them empty. This has been observed in the case of *Pectinaria* by Hurst (1967).

Acteon tornatilis (Linne, 1758) has the oval-cylindrical shell with seven to eight whorls and a short spire measuring less than one third of the total height. Ornament can be seen through the punctate spiral furrows; the columellar portion of the inner lip has one twisted plication. The species lives carnivorously in the Atlantic and Mediterranean Sea (Thompson, 1988).

Species Actaeon cf gracilis Blankenhorn
Plate 1, figs. a-d

Material: Ten specimens from Amman Silicified Limestone Formation, Irbid, Jordan.

Measurements: 7 mm high and 5mm wide, last whorl up to 4 mm high, two folds on the inner lip, up to six whorl-ornament by the spiral lines.

Description: the shell is ovate and convoluted with elongate aperture. Late Cretaceous species from Ripley Formation Mississippi are *Acteon pistilliformis* (Sohl, 1964) with the shell being almost 5 mm high and ovate with a moderately high spire composing about 1/3 of the total shell height. The prococonch is sinistral and attached to the teleoconch with inclined axis. The teleococnh has a channeled suture and rounded whorls. The ornament of the incised spiral grooves with thin raised collabral elements crossing over is wider near the aperture than apically and there are four or five visible on the whorls of the spire. The raised interspaces are wider than the grooves. The aperture is elongate, narrowed posteriorly, and bears a strong oblique fold on the columellar lip. (Occurreence in Ripley Formation of Tennessee and Mississippi.) It resembles *Acteon cicatricosus* (Sohl, 1964) from the same locality that is a little smaller but quite simialar in shape and the ornament of spiral furrows with the interspaces being wider than the grooves. The aperture is elongate, narrowed, posteriorly and bears a strong oblique fold on the columellar lip. The outer lip is crenulated within (Sohl, 1964).

Acteo punctostriatus lives from Cape Cod to Argentina. It is 3-6 cm high, and has a rather high spire (Abbott, 1974). It is more common in shallow water. It resembles the Pacific species from Satonda, Indonesia with almost a 3 mm high ovate shell with a moderately high spire that composes less than one half of the total shell height. The protoconch forms a flattened apex consisting of one whorl in the teleoconch that has a channeled suture and rounded whorls. The ornament consists of incised spiral punctuate. The smooth interspaces of the ornament are wider than the grooves on the lower portion of the body whorl, where there are about eight to twelve spiral rows of pits with a decreasing distance from each other, and are sometimes very indistinctly developed. The aperture is elongate, narrowed in the posterior, and bears an oblique fold on the columellar lip. The outer lip is simple and thin.

Sulcoactaeon sp. from the Jurassic of Sakarahain Madagascar has a smooth protoconch that lies strongly inclined in the apex of the teleoconch forming an angle of about 90° between the axes of the coiling of the larval shell and that of the teleoconch (Plate 1, figs. e-f). Before meeting the teleoconch, the larval shell has turned from the left-handed coiling into dextral coiling. The ornament of the teleoconch consists of strong, about equally wide spiral ribs which are separated from each other by narrower grooves. The groove next to the suture and below it is wider than the following ones and forms a narrow ramp. The shell with two whorls of the teleoconch measures 1.2 mm in height and about 0.8 mm in width. About twenty broad, somewhat angular ribs separated by narrower, rounded grooves ornament the body whorl which occupies two thirds of the shell height. On the whorls of the spire, approximately ten ribs remain visible. The spiral ornament is transected by fine, axially arranged growth lines, best visible within the grooves. Here, they produce a regularly pitted appearance. The inner lip of the aperture is thickened by callus and is raised to cover a slit-like umbilicus. The inner lip is without folds, and is simple and smooth (Kiel, 2006).

The protoconch consists of almost two whorls and is approximately 0.2 mm wide and high. Its smooth whorls have left-handed coiling and a naticoid shape with a wide umbilicus. In the very last portion of the larval shell, the twist from the left into the right coil is apparent. The larval shell is well-distinguished from the teleoconch by an increment of growth as well as the first spiral sculpture of the teleoconch. The axis of coiling of the protoconch is at about a right angle with the spindle axis of the teleoconch.

Sulcoactaeon can be placed within the superfamily Acteonoidea (Orbigny, 1842) and here Acteonidae with *Acteon*-like shell shapes have as characteristic features including an ornament of spiral furrows with pitted appearance.

Remarks: Larva from the plankton at Aqaba are of a heterostrophic species such as Acteon or Pupa with a change in the coiling mode; the initial shell part up to the first growth line is usually with a little less than one whorl representing the embryonic shell and afterwards the sinistral larval shell continues (Plate 1, fig. g).

The Genus Named Pupa (Röding, 1798)

The shell is about 10 mm high consisting of about seven whorls of the teleoconch. It is solid and of oval to egg-shaped outline with short spire and is in general similar to *Acteon*. The aperture is high, with a narrow posterior and widened and rounded anterior. The outer lip is evenly convex, and the columella carries bifid plaits of which the one is continuous to the outer edge and the other is finer inside. *Acteon* has a simple and *Pupa* a bifid columellar plication. The columellar inner lip has two plications. Of the acteonid shells those of

Pupa have double columellar folds.

Genotype is *Pupa solidula* (Linnaeus, 1758) from the Pacific Ocean (Burn and Thompson 1998).

This Acteon occurs within the sea grass environment of the small fringing reef in Aqaba. In 2005 individuals were found at the end of their trail in sand just below the intertidal zone in the lagoon. The animal has an operculum that is elongate and narrow and makes use of it when the animal is withdrawn into its shell. The eggs are in a jelly- mass and are attached to hard substrates noted at the time of October. The animal is white and has a characteristic head with the foot, shovel-like anterior head lappets and lappets of similar shape behind these which cover the anterior portion of the shell when burrowing in the sand.

Living individuals were observed in the shallow sandy bay in front of the small mangrove forest on Lizard Island in the great Barrier Reef of Australia (1991) plowing through the sand and were totally covered by it during motion. The short foot bears a large chitinous operculum. When crawling through the substrate, the posterior lobes of the head-shield direct the substrate onto the shell. Undulatory motions of the margin of the shield push sand to the sides while the animal moves. There are no eyes visible on the head-shield. The exhalent siphon is formed both by an extension of the extreme right corner of the mantel floor and by a prolongation of the left edge of the mantel that covers the inner lip. This exhalent siphon directs fecal material out with the water current. The pallial cavity opens along the right side of the body. The water current entering the pallial cavity is channeled through a ciliated groove in the central line of the head-shield that continues into a cilated groove on the right shell margin.

Species Pupa solidula (Linnaeus, 1758)

Plate 1, figs. (h-j)

Material: Twelve specimens from the fringing reef in Aqaba, Jordan.

Measurements: The shell is 15 mm in length, and 7mm wide. The operculum is small and narrow; in the animals of about 1 cm long, there are seven whorls of the teleoconch.

Description: The shell is ovate and thick. The cephalic shield has two lobes and the posterior shield carries large rounded lobes that protect the neck and front part of the shell. These lobes are held on the anterior portion of the shell when the animal is moving, while the anterior lobes are utilized as burrowing structures on the animal when moving through the sand. Eyes are not seen. The animal is white and the animals collected in October 2005 produced large jelly spawns when held in a glass. The shell is characterized by spiral grooves with pits. The chitinous operculum is elongate and narrow, and serves as functional protection when the animal is withdrawn in its shell.

Differences: The Australian *Pupa nitidula* and *Pupa solidula* are characterized by bright pink or reddish quadrate spots (Burn and Thompson, 1998). Both characters are not present in the species from Aqaba. *Pupa* hunts polychaete worms which are taken hold of by their radula. In the species list from Eilat, a *Pupa* cf. solidula (Linné, 1758) is documented by Edelman-Furstenberg and Faershtein G (2010) with spiral dots.

Remarks: The animals were found in 2005 through the loose sand in the very shallow lagoon.

The Superfamily Ringiculoidea (Philippi, 1853)
Family Ringiculidae (Philippi, 1853)

Ringiculidae is a marine of heterobranch gastropods with a small group of described living species (Bouchet, 2010; Kano, 2016). Shells resemble miniature helmet shells (usually less than 10 mm long) like *Cassis* or *Phalium* and have folds (1-4) on the columellar lip. The whorls of the spire form no apical flattening or ramp, and the spire is small. The apertural margin of the fully-grown shell is strongly thickened and callus is covered in the columellar region. There may also be denticles on the inner side of the outer lip. Ornament consists of spiral incised furrows on a smooth surface or may be absent.

Remarks: The animal can retract fully into its shell, and there is no operculum (Fretter, 1960; Gosliner, 1968). In the active animal, the frontal portion of the shell is covered by the posterior margin of the cephalic shield which develops a siphonal tube at its dorso- medial part, Through it, water can be guided into the frontal mantle cavity that holds one gill. Ringiculids inhabit temperate to tropical seas from littoral zones to great depths. They live by hunting small prey.

Ringiculidae (Philippi, 1853) are represented by small sized species that live in sandy and muddy marine sediments usually on the shelf from just below intertidal areas to deeper water, hunting small animals. Their shell resembles that of a *Cassis* in shape with a strongly thickened outer lip and with folds on the inner lip, but is tiny (1-5 mm). Ornament usually consists of incised spiral grooves commonly crossed by fine axial ridges. The characteristic feature of its protoconch is its missing heterostrophy also in cases where a planktotrophic larva occurs during ontogeny. This character distinguishes them from the similar Acteon, where the heterostrophy in larval shells is always well- developed. This has been so since mid-Jurassic times.

The rounded conical shell is thickened and glossy. It is usually less than 10 mm long. The columellar lip bears one to four strong folds, and the outer lip of the adult is usually greatly thickened**.** Ornament usually consists of incised spiral lines. The spire is small and there is an anterior apertural sinus. There is no operculum in the metamorphosed animal. The protoconch distinguishes this group of the Heterobranchia (=Heterostropha) from the others by being dextral throughout with a plain embryonic whorl and smooth apertural edge.

The Genus Named Ringicula (Deshayes, 1838)

Plate 2, (figs. a-g)

Material: Seven specimens from Amman Silicified Limestone Formation, Irbid, Jordan. Measurements: Height 1.4-6.3 mm, 2.1mm thick folds of inner lip with two strong folds on the columellar part.

Description: The shells resemble miniature helmet shells like *Cassis* or *Phalium* with folds on the columellar lip. The whorls of the spira form no apical flattening or ramp. The apertural margin of the fully-grown shell is strongly-thickened and covered by callus in the columellar region. The columellar lip bears one or several folds, and there may also be denticles on the inner side of the outer lip. The small low spired globose to subglobose shell is either smooth or ornamented with incised spiral lines or furrows. The aperture is narrow with the outer lip being thick and smooth or dented within. The inner lip has a strong callus and three denticles,

two strong folds on the columellar part and further up on the parietal portion a single denticle or fold. The type is *Ringicula ringens* (Lamarck, 1804) from the Eocene of the Paris Basin.

Remarks: *Ringicula* is known since the mid-Jurassic time (Gründel, 1997) and from the Early Cretaceous (Schröder, 1995), and more commonly in the late Cretaceous. It can be differentiated from other gastropods quite easily due to its characteristic shape which since Jurassic time has not changed. Today, the species that are similar in size and shape are found on soft bottom environments mostly in worm seas such as the Caribbean or the Indo-Pacific.

Ringicula buchholzi (Gründel, 1997) is the oldest representative of the genus *Ringicula* from the Callovian in Germany (Gründel, 1997, Pl. 9, figs. 8-12). The protoconch is coaxial consisting of 1,5 smooth whorls with 0,36 mm in diameter. Only the embryonic whorl is sinistrally coiled. The teleoconch consisting of four whorls is almost 4 mm high and 2,5 mm wide. The body whorl has a thickened margin of the outer lip which is thicker in the centre than at the margins, and there are two plicae on the clolumellar portion of the inner lip. Ornament consists of spiral furrows, 5 on the whorls of the spira, sixteen on the body whorl. A similar species, *Ringicula matura* (Schröder, 1995), from the Valendis of Poland differs from *R. buchholzi* by being broader, having a lower spira and on the aperture no inner thickening on the outer lip and only one plica on the columellar lip.

Ringicula from Aqaba appears to be very variable in ornament and shape of the folds on the inner lip of its aperture-so either there are several species, or it is quite a variability within one species.

Ringicula sp1

Plate 3, (figs. a-d)

Materials: twenty-five specimens from Aqaba, Jordan.

Measurements: Fully-grown individuals consisting of 3-3,5 whorls of the teleoconch and the protoconch consisting of 2,5 smooth whorls with only the embryonic one coiled to the left.

Description: The small ones are about 2.5 mm high. The subglobose shell is ornamented with narrow incised spiral furrows in a zigzag pattern and with pits or punctae separated from each other with broad, smooth interspaces. About twenty of these are on the body whorl and the interspaces are a bit narrower anteriorly. A few individuals have on the posterior part of the whorl wider zones without spiral furrows, mostly covering the whole whorl about equally. The aperture is narrow with the outer lip thick, thickened in its margin and crenulated, and often more well- developed in the anterior than in the posterior half, where it may even be smooth. The smoothness is a low central swelling on the central inner side of the outer lip a little anterior to the opposite folds and the swelling of the central inner lip. Thus, this posterior portion of the aperture is narrowed. The inner lip has a strong callus and about three similarly-wide folds. The anterior of these forms the columellar margin of the siphon and is inclined. The next posterior portion of it continues to the margin of the swelling and is oriented vertically to the shell axis. The third fold lies on the inner lip callus and ends on the central thickening formed by it. It is strong, and unites with the plate like the callus ridge forming an L-like shape with it and ending before reaching the posterior end of the outer lip. Thus, there is a furrow between the outer lip and the callus of the inner lip.

Discussion: Two species can be recognized from Aqaba, the second larger *Ringicula sp*2 (Plate 3, figs.e-h) with about 5.3 mm length and 2.9 mm width. It is very similar to *Ringicula sp*1 in shape, environment. Also both have a protoconch that reflects a lecithotrophic development with either a short period in the plankton or crawling young. In the list of species that had been documented by the Wikipedia from the sea near Eilat is the *Ringicula acuta* (Philippi, 1849) illustrated by Edelman & Faerstein, (2010) which most probably is one of the species also encountered in Aqaba (Fig.3a).

The small low globose to nearly globose shell with a low spire is either smooth or ornamented with incised spiral lines or furrows. The aperture is narrow with the outer lip being thick and smooth or dented within, and the inner lip having a strong callus and one to four folds on the columellar part, and further up on the parietal portion a single tooth or fold. This type is named *Ringicula ringens* (LAMARCK, 1804) from the Eocene of the Paris Basin. All its essential featuresresemble those of the species from Aqaba.

Ringicula semistriata (d'Orbigny, 1842) is larger than *Ringicula nitida* (VERRILL, 1873) (A. E. Verrill, 1872) which may be found in the same environment on the US shelf of the Atlantic Ocean. Also its protoconch is larger and it has no central thickening on the inner side of the outer lip. The species *Ringicula nitida (*VERRILL,1873) from the Atlantic Ocean has a small subglobose shell (about 2.5 mm high) that is ornamented with narrow incised spiral furrows with broad smooth interspaces, and consists of 3.5 whorls of the teleoconch. This ornament is quite variable and there may be quite few such furrows present. The aperture of the adult shell is narrow with the outer lip being thick, smooth and with a central inner thickening a little anterior to the opposite fold of the central inner lip. Thus, this posterior portion of the aperture is narrowed. The inner lip has a strong callus and three folds. The anterior of these forming the columellar margin of the siphon is just as strong as the next one posterior to it on the columellar lip; both have the same inclined orientation and a deep groove between each other. The third fold lies on the inner lip callus and ends on the central thickening formed by it. It is strong and unites with the plate like the callus ridge that ends before reaching the posterior end of the outer lip. Thus, there is a low furrow between the outer lip and the callus of the inner lip.

Ringicula nitida is smaller than *Ringicula semistriata* which may be found in the same environment on the Atlantic Shelf of the USA. Its protoconch is smaller but has more whorls. The central thickening on the inner side of the outer lip and the strong folds of the inner lip differ from those of *Ringicula semistriata*. A species of *Ringicula* from Satonda with up to a 2 mm-high shell consists of 4.5 whorls, and is ornamented with narrow incised spiral furrows with broad, smooth interspaces. This ornament is quite variable, and there may be six to ten such furrows present. The aperture is narrow with the outer lip being thick, and a central inner thickening a little anterior to the opposite folds of the central inner lip. These folds make the posterior portion of the aperture narrow. Two small knobs on the inner side of the outer lip are found

between the central swelling and the rounded siphon. The inner lip extends in a callus and three folds. The anterior of these forms the inner margin of the siphon and has the same dimension **as** the posterior portion of it. The third fold lies on the inner lip callus and ends in the callus ridge. There is a broad furrow between the outer lip and the posterior folds on the inner lip. This *Ringicula* from the coast of the Indonesian Island of Satonda resembles *Ringicula nitida* from the Atlantic shelf of the USA, but is a little smaller. Here the central thickening on the inner side of the outer lip is accompanied by anterior denticles which are absent in *R. nitida*.

Difference: *Ringicula sp* is very similar to *Ringicula nitida* in size and shape, but has stronger and zigzaging spiral furrows and a crenulated outer lip margin.

Remarks: The two species from Aqaba live in the muddy sediment of the Gulf of Aqaba from just below the intertidal area in the lagoon of the top of the fringing reef down to depth at the base of the reef and below it.

A very similar shell is also found in the case of the genus *Triploca* that is based on the type *Triploca ligata* (Tate, 1894) from Eocene of Australia (Maxwell, 2009). Its ovate shell has the spire with a little more than half the total height. The protoconch is of about two smooth whorls; the initial whorl depressed. The last whorl is large, evenly convex with small pseudo-umbilicus. The spiral sculpture is of fine grooves with broad flat interspaces. Axial sculpture of fine growth lines is restricted to the grooves. The ovate aperture has the inner lip with three strong folds. The outer lip is thin with shallow spiral grooves within. *Triploca* has three folds on the inner lip instead of one as in *Acteon,* or two as in *Pupa* The genus was thought to represent a member of the Pyramidellidae Gray that is a family with a shell coiled in **a** heterostrophic mode (heterostrophically coiled shell) and that is convergent to, but not part of the Opisthobranchia (nnts). However it represents an independent group of the Heterobranchia. A bit more elongate shell could be placed with *Otopleura,* as is known from the tropical Pacific Ocean near the Philippines (Fig. 3b).

The Genus named Triploca (Tate, 1893)

Plate 3, (figs.i-k)

The species *Triploca sp* from Aqaba

Materials: six specimens from Aqaba, Jordan.

Measurements**: 6.5 mm high, 3.1 mm wide,** nine-whorl shell and a protoconch of about two smooth whorls with three folds on the inner lip.

Description: The shell is ovate. The operculum is thin and brownish and seals the aperture a bit behind the smooth outer and the keeled inner lip. The shell consists of about nie whorls with white protoconch and an axially-ribbed teleoconch, when the shell is fully grown. The ribs are white on a bluish white shell that may have yellowish brown dots. Between the larger axial ribs, there are fine spiral ribs. Only the first whorl of the teleoconch is white as the protoconch.

The species lives together with white “Olivella” and two species of *Nassarius*. The head has the eyes in the triangular tentacles forming sheets with two lobes which lie in the middle and extend over the wide spade-like foot. The color of the animal differs among individuals. *Triploca sp* of Aqaba may represent an *Otopleura* of the Pyramidellidae. *Triploca* is documented by Maxwell, P.A. (2009).

Remarks: The species was found alive in the sand of an intertidal pool as well as within the sea grass of the very shallow lagoon at Aqaba. The head is quite different from that of *Acteon* that is living in a similar environment and also next to *Triploca*. The shell was found in the sand of a tidal pool in the sandy intertidal region.

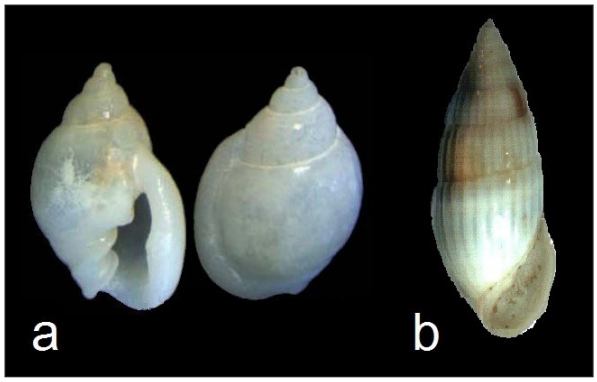

Figure 3. a. Ringicula acuta (Philippi 18490 from the Gulf of Aqaba on the eastern side (copy from Edelman-Furstenberg and Faershtein, G (2010), **b**. Otopleura nitida A. Adams 1854 from the Philippines Pyramidellidae (Gray, 1840) (Source: Wikipedia http://www.biolib.cz/en/image/id101181/?orderby=2&uid=3973)

Conclusion

The two gastropod species described from the Campanian of Jordan closely resemble species which are living near the shore at Aqaba. Even with a distance of approximately 85 Million years between their lifetimes and their existence in two different Oceans - their morphology has changed so little, that the Cretaceous species could be placed within the same genera. Recent comparisons with fossil species are possible, even though the shells of the species from Cretaceous Amman Formation have been transformed into silica. Chert formed due to the solution and redeposition of siliceous skeletal elements when beds were covered by several meters of sediment. The silicified shells are connected in their origin to the formation of flint nodules and chert layers. This change from aragonite to quartz was such that the original type of shell structure as well as the shape of the early ontogenetic shell has been preserved. In the case of *Acteon* and *Ringicula,* the crossed lamellar structure of the shell wall as well the shape of the embryonic and larval shell, and its ontogenetic change from left to right coiling mode were preserved. The amazing continuity of the species that lived in the shallow Tethys Ocean which used to cover northern Jordan during the Campanian and those which live in the Gulf of Aqaba now is quite exceptional. Most groups of gastropods have changed very much from Campanian to now. Relatives of *Acteon* and *Ringicula* have been recognized since the Mid-Jurassic. The larval shell of *Acteon* from Amman Silicified Limestone Formation has the same size and morphology as that of the acteonid *Pupa* from Aqaba, and both also resemble each other regarding the adult shell morphology and ornament. The two genera of *Ringicula* recognized from Aqaba differ from each other predominantly regarding their size; one is larger than the other. They closely resemble the fossil *Ringicula* with distinct characters of the inner lip of their aperture.

Acteon and *Ringicula* gastropods live in sandy and muddy marine sediments from just below the intertidal area to deeper

water where they hunt small animals. The fauna was that of a fully-marine environment in the shallow sea with a soft bottom substrate that was in early deposits usually fully-aerated within the intertidal regime.

References

[1] Abbott, R. T. (1974). American Seashells. -663pp., Van Nostrand Reinhold Company, New York.

[2] Abu-Jaber, N., Jawad Ali, A., Shinaq, R. (1997). Genesis of the Amman Silicified Limestone Formation silicified limestone of Jordan, Africa Geoscience Review, 4: 381-393.

[3] Aqrabawi, M. (1993). Oysters (Bivalvia-Pteriomorphia) of the Upper Cretaceous rocks of Jordan. Paleontology, stratigraphy and comparison with the Upper Cretaceous oysters of northwest Europe. Mitteilungen aus dem.

[4] Bandel, K. (1976). Egg Masses of 27 Caribbean Opisthobranchs from Santa Marta, Columbia.- Studies on Neotropical Fauna and Environment ll (1976), pp.87-118.

[5] Bandel, K. (1982). Morphologie und Bildung der frühontogenetischen Gehäuse bei conchiferen Mollusken.- Fazies, 7: 1-198, Erlangen.

[6] Bandel, K. (1990). Shell structure of the Gastropoda excluding the Archaeogastropoda. – In: Carter, J. G. (ed.), Skeletal Biomineralization: Patterns Processes and Evolutionary Trends, I. – Van Nostrand Reinolds, New York: 117–134.

[7] Bandel, K. (1994). Triassic Euthyneura (Gastropoda) from St. Cassian Formation (Italian Alps) with a discussion on the evolution of the Heterostropha.- Freiberger Forschungshefte, C 452 Paläontologie, Stratigraphie, Facies, Heft 2, Leipzig

[8] Bandel, K. (1996). Some heterostrophic gastropods from Triassic St. Cassian Formation with a discussion of the classification ofthe Allogastropoda. - Paläont. Z., 70, 3/4: S. 325-365, 18 Fig.,Stuttgart.

[9] Bandel, K., and Geys, J. (1984). Regular echinoids in the Upper Cretaceous of the Hashemite Kingdom of Jordan. Ann. Soc.Geol. Nord, 104: 97-115.

[10] Bandel, K., and Kuss, J. (1987). Depositional environment of the pre-rift sediments of the Galala heights (Gulf of Suez, Egypt). Berliner geowiss. Abh. (A), 78: 1-48.

[11] Bandel, K. and Mikbel, S. 1985. Origin and deposition of phosphate ores from the Upper Cretaceous at Ruseifa (Amman, Jordan). Mitteilungen aus dem Geologisch-Paläontologischen Institut der Universität Hamburg, 59: 167- 188.

[12] Bandel, K., Kuss, J., and Malchus, N. (1987). Sediments of Wadi Qena, (Eastern Desert, Egypt).-Journal of African Earth Sciences, Vol. 6, No. 4, pp.427- 455.

[13] Bandel, K., and Salameh, E. (2013). Geologic Development of Jordan Evolution of its Rocks and Life. Jordan University Press (278 pp).

[14] Bandel, K., Shinaq, R., and Nazzal, J. (2000). Palaeoecological and diagenetical significance of a silicified soft bottom fauna of Campanian age (Qatrana Unit, Jordan) Mitteilungen aus dem Geologisch-Paläontologischen Institut der Universität Hamburg, 83: 203-218

[15] Beerbaum, B. (1977). Diagene der marine sedimentaren phosphate lay erstalle von Al-Hasa, Jordan, Germany.

[16] Bender, F. (1968). Geologie von Jordanien. Beiträge zur Regionalen Geologie der Erde, 7. Borntraeger, Berlin, 230 pp.

[17] Bender, F. (1974). Geology of Jordan. Beiträge zur Regionalen Geologie der Erde, 7. Gebrüder Bornträger, Berlin, 196 pp.

[18] Bender, F. and Mädler, K. (1969). Die sandigeSchichtenfolge der Kreide mit einer Angiospermen-Flora in Südjordanien. Beih. geol. Jb., 81: 35-92

[19] Berndt, R. (2002). Palaeoecology and taxonomy of the macrobenthic fauna from the Upper Cretaceous Ajlun Group, southern Jordan. Dissertation, Würzburg

[20] Burdon, D.J., and Quennell, A.M. (1959). Handbook of the Geology of Jordan; to accompany and explain the three sheets of 1:250,000 Geological Map, East of the Rift, by A.M. Quennell Government of the Hashemite Kingdom of Jordan, 82 p. CGMW, Paris, pp. 129–136

[21] Burn, R., and Thompson, T. E. (1998). Order Cephalaspidea. - In: Beesley, P. L., Ross, G.J.B. & Wells, A. (eds.), Mollusca – the Southern Synthesis. – Fauna of Australia, 5: 943–959; CSIRO Publishing, Melbourne.

[22] Edelman-Furstenberg Y, Faershtein G. (2010). Molluscan fauna of the Gulf of Elat: indicators of ecological change. - Geological Survey of Israel, Report GSI 15/10

[23] Farouk, S., Ahmad, F., Powell, J., Marzouk, A. 2016. Integrated microfossil biostratigraphy, facies distribution and depositional sequences of the upper Turonian to Campanian succession in northeast Egypt and Jordan. Facies. 62:8

[24] Fretter, V. (1960). Observations on the tectibranch Ringiculabuccinea (Brocchi). Proceedings of the Zoological Society of London 135:537-549.

[25] Gofas, S. (2015). Acteonoidea d'Orbigny, 1843. World Register of Marine Species. Available at http://www.Marinespecies.org/aphia.phb…..accessed 19march2015

[26] Gosliner, T.M. (1981). Origins and relationships of primitive members of the Opisthobranchia (Mollusca: Gastropoda). - Biol. J. Linn. Soc., 16: 197-225.

[27] Gründel, J. (1997). Heterostropha (Gastropoda) aus dem Dogger Norddeutschlands und Nordpolens. III. Opisthobranchia.-Berliner geowissenschaftliche Abhandlungen E25: 177-223, Berlin.

[28] Klitzsch, E. (1986). Plate tectonics and cratonal geology in Northeast Africa (Egypt, Sudan), Geol. Rdsch. 75, 755-768.

[29] Masri, M.(1963). Report on the geology of the Amman-Zerga area. - Central Water Authority. Amman. Unpubl.

[30] Mikkelsen, P.M. (1996). The evolutionary relationships of the Cephalaspidea s.l. (Gastropoda: Opisthobranchia): A phylogenetic analysis. - Malacologia 37:375-442.

[31] Mustafa, H. and Bandel, K. (1992). Gastropods from lagoonal limestones in the Upper Cretaceous of Jordan. - Neues Jahrbuch Geologie und Paläontologie, Abhandlungen 185:349-376, Stuttgart.

[32] Powell, J.H. (1989). Stratigraphy and Sedimentation of the Phanerozoic Rocks in Centraland South Jordan Part B: Kurnub, Ajlun and Belqa Groups. Geological Bulletin, No. 11. The Hashemite Kingdom of Jordan, Ministry of Energy and Mineral Resources, Natural Resources Authority, Amman (130 pp).

[33] Powell, J.H., and Moh'd, B.K. (2011). Evolution of Cretaceous to Eocene alluvial and carbonate platform sequences in central and south Jordan. GeoArabia 16 (4): 29–82.

[34] Quennell, A.M., and Burdon, D.J. (1959). Geology an Mineral Resources of (former) Trans Jordan.- Colonial Geology and Mineral Resources, 2: 85-115, London.

[35] Rudman, W. B. (1972). The anatomy of the opisthobranch gernus Hydatina and the functioning of the mantle cavity and alimentary canal. - Zoological Journal of the Linnean Society, 51: 121-139.

[36] Schröder, M. (1995). Frühontogenetische Schalen jurassischer und unterkretazischer Gastropoden aus Norddeutschland und Polen.- Palaeontographica, (A) 238:1—95, Stuttgart.

[37] Sohl, N. F. (1964). Neogastropoda, Opisthobranchia and Basommatophora from the Ripley, Owl Creek and Prairie Bluff Formations. - U.S. Geological Survey Professional paper 331 (B): 1-334.

[38] Thompson, T.E. (1988). Molluscs: benthic opisthobranchs (Mollusca: Gastropoda). - Syn. Br. Fauna (n.s.) 8: 1-356.

[39] Thorson, G. (1946). Reproduction and larval development of Danish marine bottom invertebrates with special reference to the planktonic larvae in the Sound (Oresund). Medd. Komm. Danmarks Fisk. Havunders., Ser. Plancton 4:1-523.

[40] Wenz, W., and Zilch, A. (1960). Gastropoda Euthyneura. in Schindewolf, O.H. ed. Handbuch der Paläozoologie. Berlin, Gebrüder Borntraeger V.6. 835 p.

[41] Wetzel, Morton Wetzel, R., and Morton, M. (1959). Contributioná la Géologie de la Transjordanie.- (In:) Notes et Mémoires Moyen-Orient, 7:95-173, Paris.

[42] Wikipedia. (2018). Otopleura nitida. https://en.wikipedia.org/wiki/Otopleura_nitida

[43] Haggart, J.W. (2000). Report on Upper Cretaceous fossils from the Amman Silicified Limest one Formation, Jordan.Paleontological Report JWH-2000- 06, Geological Survey ofCanada, Vancouver.

Plate 1: SEM microphotographs of acteonid gastropods

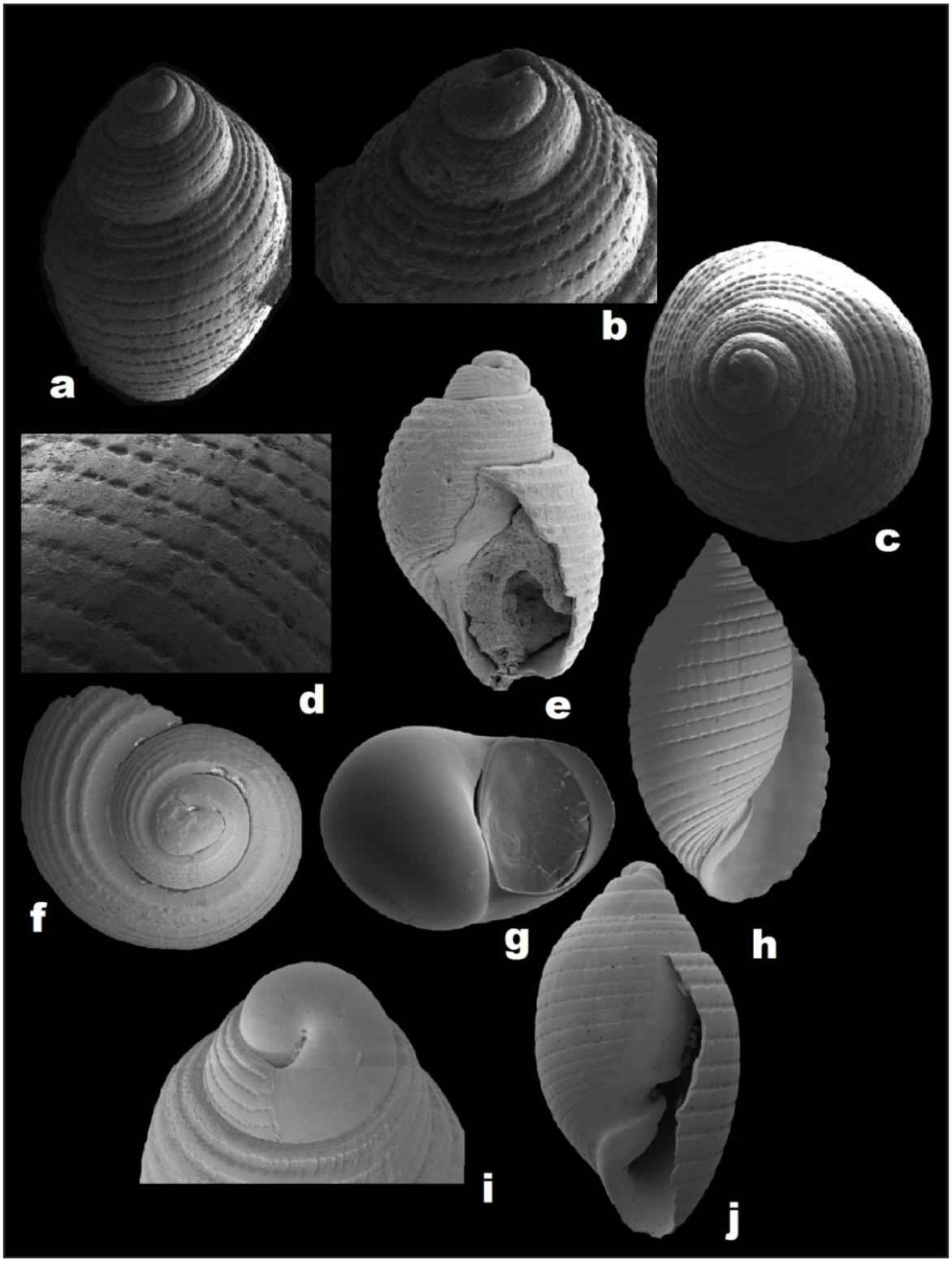

Figure a: Acteon sp from Amman Silicified Limestone Formation, Irbid, Jordan.
Figure b: Acteon with heterostrophic protoconch partly buried within the teleoconch, Amman Silicified Limestone Formation, Irbid, Jordan.
Figure c: Acteon has an ovate shape with four whorls of the teleoconch from Amman Silicified Limestone Formation, Irbid, Jordan.
Figure d: The same as in c showing sculpture of Acteon consisting of punctuated narrow spiral grooves and spiral rows of pits.
Figure e: Sulcoactaeon sp. from the Jurassic deposits, Sakaraha, Madagascar
Figure f: close- up of protoconch of Sulcoactaeon sp. from the Jurassic with a smooth protoconch of almost two whorls and is approximately 0.2 mm wide and high, Sakaraha, Madagascar
Figure g: Larval shell of heterostrophic species from the plankton at Aqaba of with change in coiling mode from right to sinistral larval shell.
Figure h: Acteon sp shell simillar to Pupa sp, Aqaba, Jordan.
Figure i: Protoconch, apical view, Pupa solida, Aqaba, Jordan.
Figure j: Pupa solida, not fully grown, Aqaba, Jordan

Plate 2: SEM microphotographs of Ringiculidae gastropods.

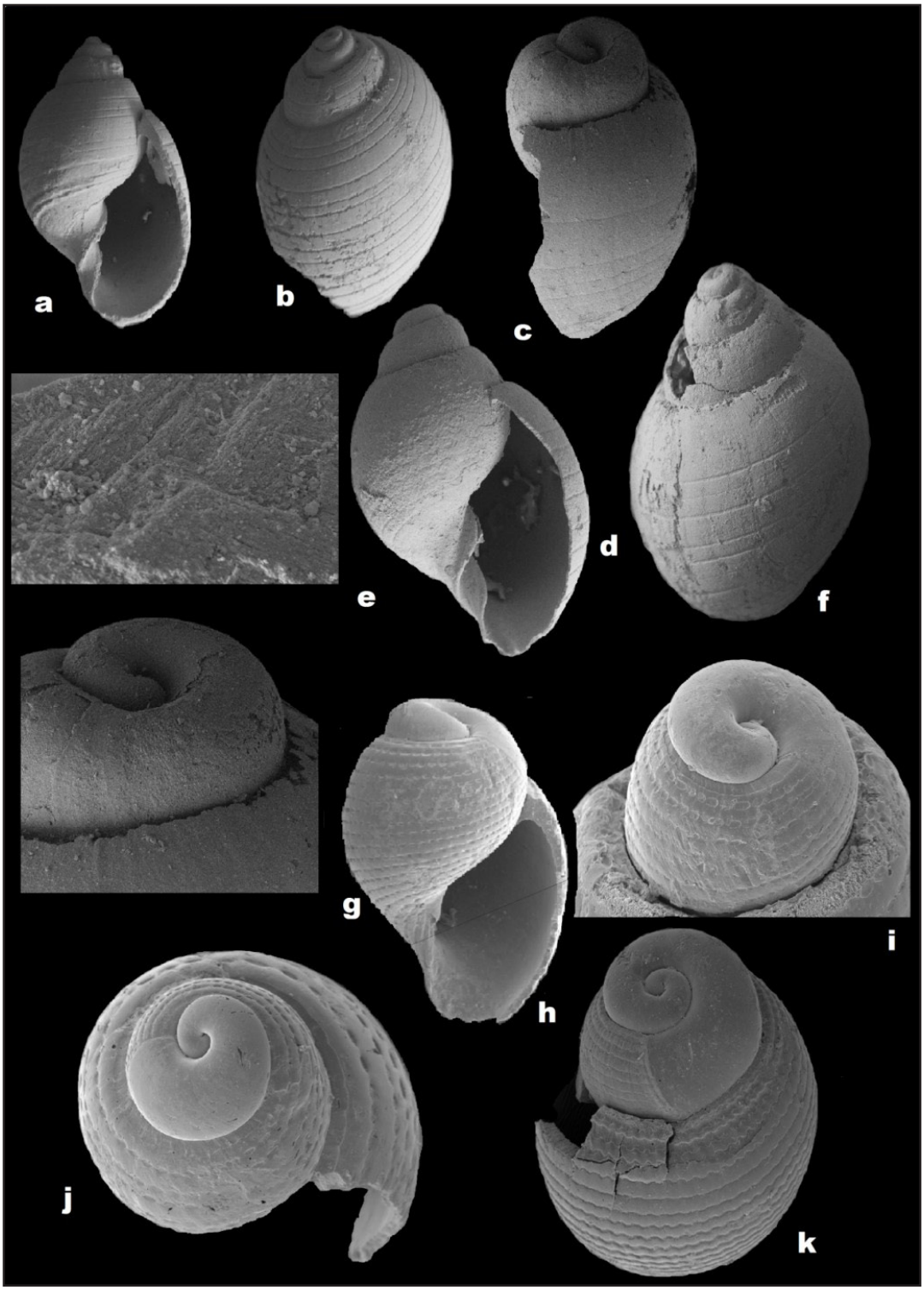

Figure a: Ringicula sp shell from Amman Silicified Limestone Formation at Irbid with narrow thick aperture.
Figure b: Ringicula sp shell from Amman Silicified Limestone Formation, Irbid, Ornament having spiral incised furrows on a smooth surface, Amman, Jordan
Figure c: Larval shell of Ringiculidae showing fold on the inner lip from Amman Silicified Limestone Formation, Irbid, Jordan
Figure d: Apertural view of Ringicula sp shell with two strong folds on the columellar part from Amman Silicified Limestone Formation, Irbid, Jordan
Figure e: Crossed lamellar sculpture structure preserved of Ringicula sp, Amman Silicified Limestone Formation, Irbid, Jordan
Figure f: Ringicula sp sculpture of incised spiral grooves from Amman Silicified Limestone Formation, Irbid ,Jordan.
Figure g: Shell apex, Ringicula sp having narrow protoconch with dome shaped and sculpture of incised spiral grooves from Amman Silicified Limestone Formation, Irbid, Jordan.
Figure h: Apertural view of Ringicula sp showing small low globose shell of the Jurassic from Madagaskar.
Figure i: Protoconch, apical view of Ringicula sp shell from the Cretaceous of Madagaskar
Figure j: Shell apex, punctuated spiral grooves on shell whorls from Mahajanga, Madagaskar
Figure k: shell of Ringicula sp from Eocene, Mississippi.

Plate 3: SEM microphotographs of Ringicula sp and Triploca sp, Aqaba, Jordan

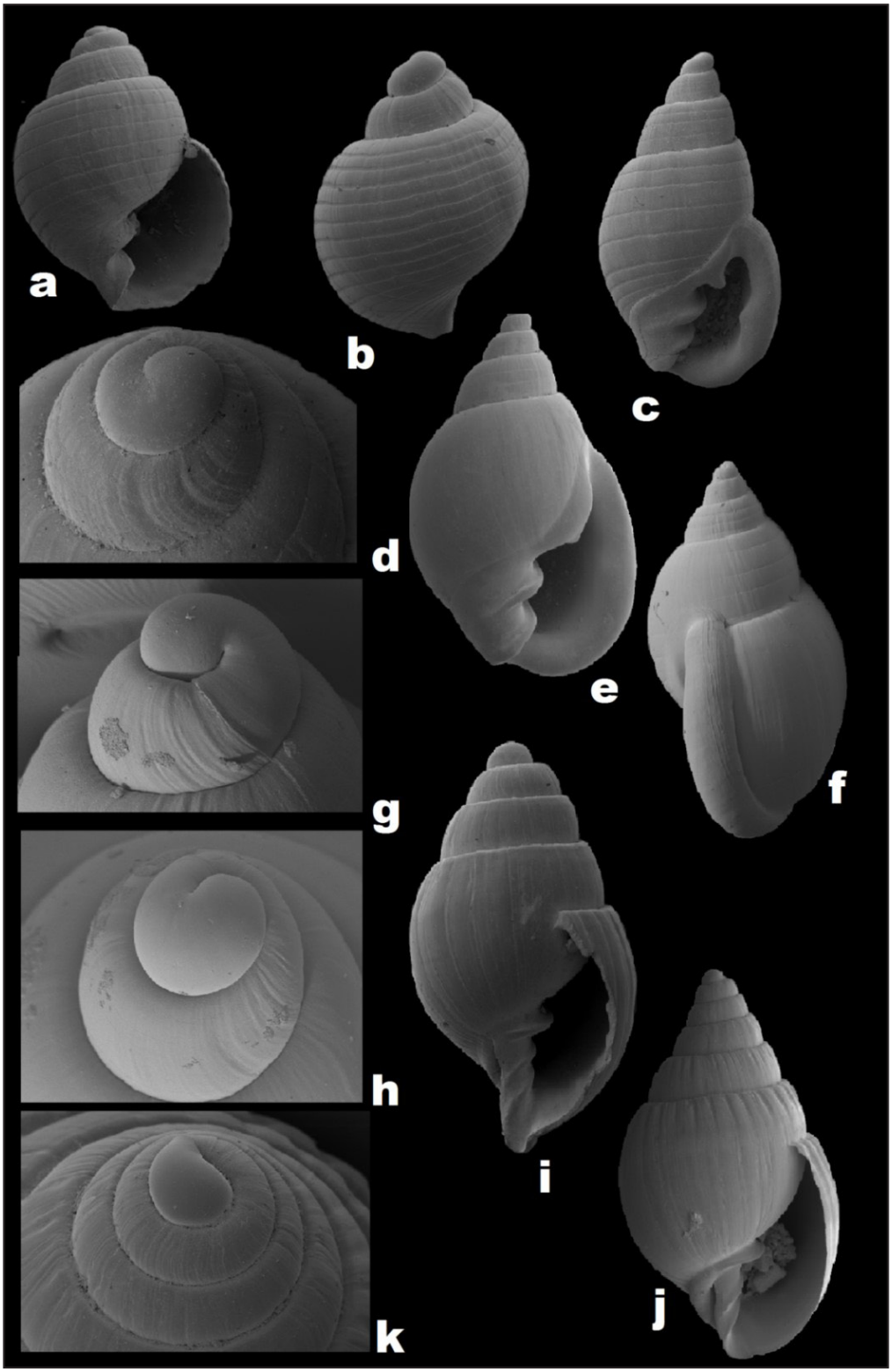

Figure a: Apertural view of Ringicula sp1, Aqaba. Jordan.
Figure b: Ringicula sp1 shell with narrow incised spiral furrows in zigzag pattern and with pits separated from each other with broad, smooth interspaces, Aqaba. Jordan.
Figure c: Ringicula sp1 shell has last whorl large, strongly convex and fold aperture, Aqaba. Jordan.
Figure d: close-up of protoconch, apical view of Ringicula sp1 shell, Aqaba. Jordan.
Figure e: Apertural view of Ringicula sp2, Aqaba. Jordan.
Figure f: Lateral view of Ringicula sp2, Aqaba. Jordan.
Figure g: Shell apex, of Ringicula sp2, Aqaba. Jordan.
Figure h: close- up protoconch, apical view of Ringicula sp2, Aqaba. Jordan.
Figure i: Apertural view of Triploca sp, shell from Aqaba, Jordan.
Figure j: Apertural view, fully grown Triploca sp with axially ribbed teleoconch, Aqaba. Jordan.
Figure k: Shell apex, Triploca sp juvenile, Aqaba. Jordan.

JJEES
Jordan Journal of Earth and Environmental Sciences

Volume 9, (Number 2), August, 2018
ISSN 1995-6681
Pages 102 - 107

A method for Land Degradation Monitoring in Arid and Semi-Arid Regions of Northeastern Jordan Using Landsat images

Hussam Hesham Al-Bilbisi

Geography Department, The University of Jordan, Amman 11942 Jordan

Received 27 February, 2018; Accepted 15 May, 2018

Abstract

This study evaluates land degradation in one of the most important natural grazing regions in the northeastern parts of Jordan. It describes a set of techniques that have been used to develop an operational approach that ensures high accuracy and compatibility for detecting and mapping land degradation in the study area. For this purpose, Landsat-TM and Landsat-8 images acquired in May of 2000 and May of 2014, respectively, were used. The two multi-temporal images were geometrically and radiometrically calibrated to each other, and were used for producing spatially- correct maps of environmental changes over time. Land degradation monitoring, particularly in the vegetation coverage, had been done using NDVI image differencing. The histogram of difference image shows that unchanged pixels were centered around the mean, while the changed pixels were located in the tail regions on either side. The NDVI difference image indicated that negative changes in the middle and southern parts of the study area had occurred between 2000 and 2014.

Keywords: Land degradation, arid and semi-arid, Landsat, NDVI, northeast Jordan

1. Introduction

According to the United Nation Convention to Combat Desertification (UNCCD) (UNEP, 1994), land degradation has been defined as the "Reduction or loss in arid, semi-arid and dry sub-humid areas, of the biological or economic productivity and complexity of rain-fed cropland, or range, pasture, forest and woodlands resulting from land uses or from a process or combination of processes, including processes arising from human activities and habitation patterns, such as soil erosion caused by wind and/or water, deterioration of the physical, chemical,and biological or economic properties of soil, and long-term loss of natural vegetation." It is widely accepted that the lands of arid and semi-arid regions are at the risk of degradation, most of the changes are highly dependent on the biophysical constraints of the land units (Roeder and Hill, 2009). Accordingly, the need to maintain a sustainable use of these lands entails the monitoring of the onset of land degradation so that the problem may be tackled in its early phases. Monitoring will also be required to evaluate the effectiveness of measures to control land degradation (Al-Bilbisi, 2012).

Land degradation overwhelms the whole environment; it has been a major global issue since the twentieth century and will remain high on the international agenda in the twenty-first century (Getzin, 2005; Al-Bilbisi, 2012). Land degradation is actually one of the land surface processes, which physically exhibits an increase in soil bareness and a decrease in the extent of vegetation coverage leading eventually to a reduction in land productivity. Therefore, changes of the vegetation density over time also bear important information on land degradation dynamics which are induced by natural or man-made processes. For this reason, many researchers interested in land degradation processes are concerned about the state and evolution of vegetation cover (Moody and Johnson, 2001).

Remote sensing techniques employing the output of the spectral change data provide a potential means for detecting, quantifying and monitoring changes in the vegetation cover on local, regional and global scales. Information on vegetation is generally obtained by relating vegetation indices (VIs) computed on the basis of satellite remote sensing data to pertinent variables on the terrestrial environment (Leprieur et al., 2000). There are several indices for highlighting vegetation bearing areas on a remote sensing scene; vegetation index, namely Normalized Difference Vegetation Index (NDVI) is a common and widely used index (Mbow et al., 2013; Sommer et al., 2011). It is an important vegetation index, widely-applied in research concerned with global environmental and climatic change (Mbow et al., 2013; Vogt et al., 2011).

Arid and semi-arid areas of northeastern Jordan, where livestock production is the main job for the local population, are considered among the most important natural grazing lands rich in herbaceous rain-fed and pasture plants in Jordan. These areas are increasingly coming under reduction or loss of their biological or economic productivity primarily due to human activities and/or climatic variation, which in turn lead to land degradation (Al-Bilbisi and Tateishi, 2003; Al-Bilbisi et al., 2004). The objective of this study is mapping environmental changes in the northeastern parts of Jordan based on extracted NDVI using Landsat images.

* Corresponding author. e-mail: hbilbisi@ju.edu.jo

  - Volume 9, (Number 2), (ISSN 1995-6681)

2. Study Area

The study area is part of the northeastern desert of Jordan, known as the Northeast Jordanian Limestone Plateau (Figure 1). It is among the most important natural grazing lands in Jordan, rich in herbaceous rain-fed grazing plants, such as *Artimisia Alba* and *Rattamus*. The majority of the population in the study area are involved in livestock production. On the whole, arid to semi-arid climate conditions are dominant in the study area, with low precipitation being less than 100mm and a high potential evaporation ranging between 1500 mm/year and 2000 mm/year, which results in scarce water resources (JMD, 2013). There are noticeable seasonal temperature variations with summers tending to be hot and dry while winters are cool and wet. Mean annual maximum temperatures range between 35-41°C in July, but absolute maximum values can exceed 46°C. Temperatures might reach 0°C in winter, where the minimum annual mean temperatures decline to as low as 0-4°C in January (JMD, 2013). Occasional high intensive/low storms occur resulting in significant runoff and loss of major potential water resources due to the lack of good management and control. In summers, the wind speed ranges between four knots and six Knots, due to depressions that move along the eastern Mediterranean, while in winters, it ranges between five knots and eight knots. There are occasional gales (JMD, 2013).

The study area is a monotonous -flat plateau- and stony desert extending eastwards from the Basalt Shield beyond the eastern borders of Jordan. Small scarps formed by more resistant beds of the Tertiary sedimentary sequence occasionally interrupt it. The land rises in all directions from the eastern margin of the Basalt Shield (Figure 1). The area contains many flats, frequently more than 10 km long but rarely more than 1 km wide (Bender, 1974). Gradients are rarely steep, and there are few breaks of slope. Almost gentle concavo-convex slopes characterize the topography. The ground surface is largely covered by typical desert pavement. The soil consists mainly of limestone rocks or basalt accompanying limestone rock in some areas. According to the Soil Map of the World-Revised Legend (FAO/UNESCO, 1990), the area has mainly two dominant types, namely Gypsisols and Calcisols. Gypsisols formed in the mudflat plains (Qaa). Qaa is the local expression for the fine sediment deposits, which are formed through dissolution from calcium sulphate contained in weathering materials. Much of the drainage appears to be radial, draining to and terminating in a large Qaa. Mudflat plains (Qaa) accumulate from the ephemeral standing water through the many wadis' discharge in the mudflats plains. They comprise fine, soft, various amounts of evaporates and silty clay. The most prominent feature of Calcisols is the translocation of calcium carbonate from the surface layers to an accumulation layer at some depth in the soil. This layer may be soft and powdery, or may consist of hard concretions and can eventually become indurate and cemented. Most Calcisols have a medium to fine texture and a good water holding capacity. They are generally well- drained. These are potentially fertile soils, but their high calcium carbonate content is not favorable for many crops because it may result in iron and zinc deficiency in crops. However, these soils are used mainly for grazing (FAO, 2000).

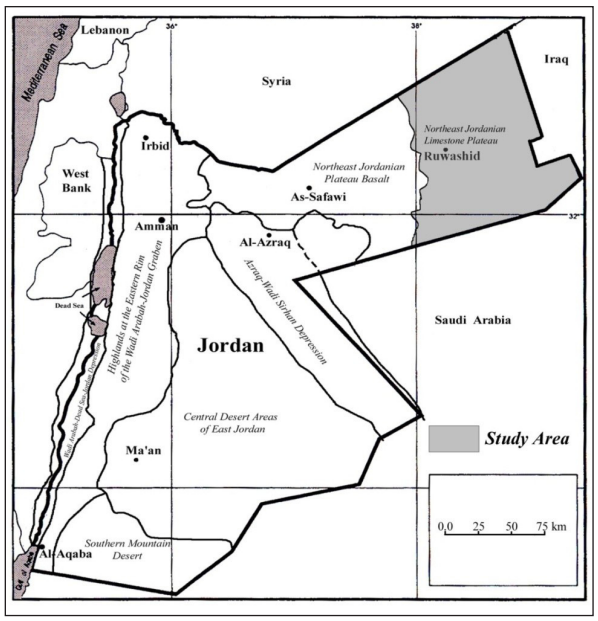

Figure 1. Jordan map showing the main geomorphological units, with the study area in gray color in the northeastern part of the country.

3. Methodology

3.1. Geometric Rectification and Radiometric Calibration

Digital images covering the study area were geometrically and radiometrically calibrated to each other to facilitate their comparison (Lillesand et al., 2014). Geometric correction is a methodology for rectifying satellite images to the same projection system. For producing a spatially-correct map of environmental changes through time, a subset of each of the Landsat TM (Figure 2) and Landsat 8 (Figure 3) digital images acquired in May of 2000, and May of 2014; respectively, were used. The 2014 Landsat 8 image, which was supplied by USGS, had already been rectified and georeferenced to UTM map projection (Zone 36N), and WGS84 datum. Then, this image was employed as the reference scene to which the second scene (TM of 2000) was registered. Using image-to-image registration, the first-degree polynomial equation was used in image transformation. The resultant root mean square error (RMSE) was less than half-pixel (15 m), indicating an excellent registration. The nearest neighbor resampling method was used to avoid altering the original pixel values of the image data.

An important component to the change detection is radiometric calibration and corrections (Chavez and Mackinnon, 1994). Radiometric calibration and corrections can eliminate or reduce the image differences introduced as a result of changing atmospheric conditions. Since both images are acquired within the same season. A histogram matching provided by PCI software was used in this study. After this correction, image statistics and histograms from the two periods were found to be similar and comparable.

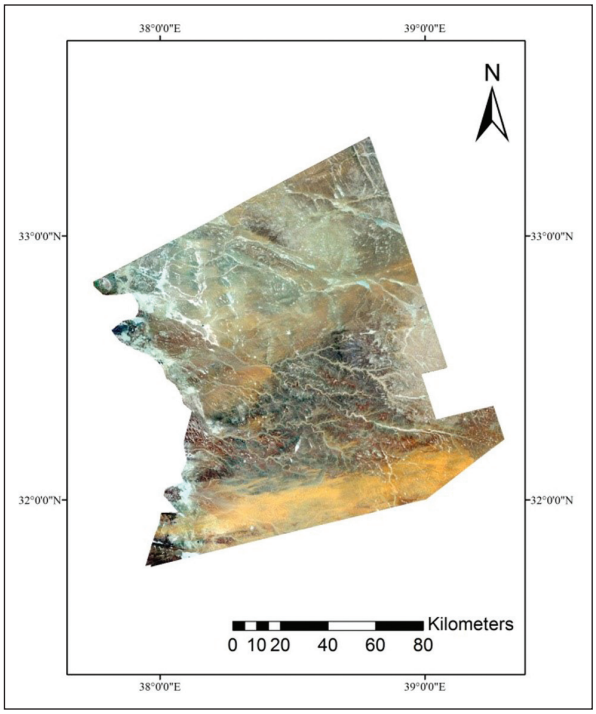

Figure 2. Color composite image of Landsat-TM (2000), bands (MIR, NIR, and Green) exposed through the red, green and blue filters, respectively.

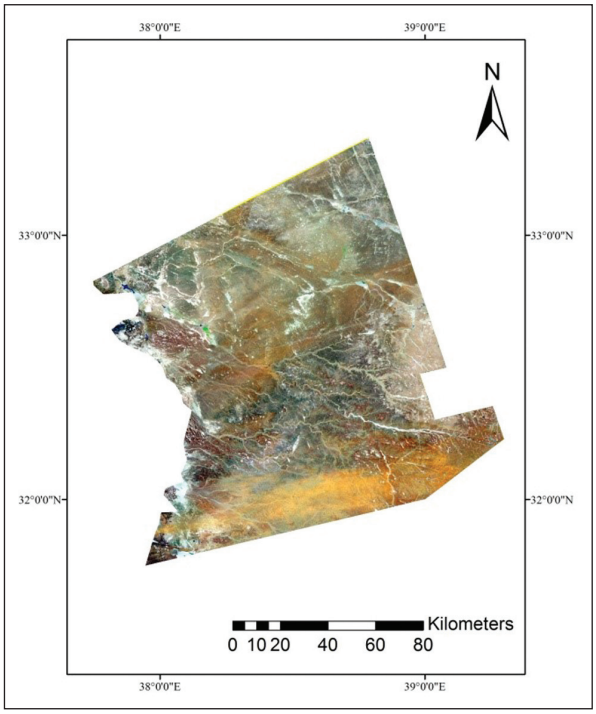

Figure 3. Color composite image of Landsat - 8 (2014), bands (MIR, NIR, and Green) exposed through the red, green and blue filters, respectively.

3.2. NDVI and Image Differencing Generated Image

To facilitate the mapping of land degradation in the arid and semi-arid regions using remote sensing technology, the physical parameters of vegetation must be accurately evaluated. For this purpose, Normalized Difference Vegetation Index (NDVI) (Rous et al., 1974) was used for monitoring land degradation in the study area. NDVI is an algorithm for monitoring vegetation using spectral information of remotely-sensed data, and it can be written as (Rouse et al., 1974):

$$NDVI = \frac{NIR - RED}{NIR + RED} \quad (1)$$

where *NIR* is the spectral response of near infra red band and *RED* is the spectral response of red band. NDVI images were generated for both dates using equation (1) for the purpose of land degradation mapping. NDVI values were expressed in digital values, and were determined as:

$$DN = (NDVI * 100) + 100 \quad (2)$$

Land degradation can be quantified in terms of: (1) soil loss (2) loss of soil quality, e.g., nutrient loss and/or soil compaction (3) a decline in vegetation (forage) production or (4) a change in vegetation species composition contrary to management goals (Pickup, 1989; Behnke and Scoones, 1994; Washington-Allen et al., 1998).

For land degradation mapping, particularly in vegetation coverage, an image differencing method was adopted for pixel-by-pixel comparison and was performed on the NDVI generated images of both dates. Image differencing was calculated as:

$$LATER\ IMAGE - FORMAR\ IMAGE + 25 \quad (3)$$

where 25 is a constant to remove negative values. Subsequently, subtracting NDVI images generated NDVI difference image.

4. Results and Discussion

4.1. Land Degradation Monitoring Using NDVI Image Differencing

This method was performed on the NDVI generated images using Formula (3) where the early image was subtracted from the later image. The resultant NDVI image does not include negative values since a constant (twenty-five) was added during the image differencing. Figure (4) shows the histogram data plot, which was extracted from the resultant image of the generated NDVI difference image.

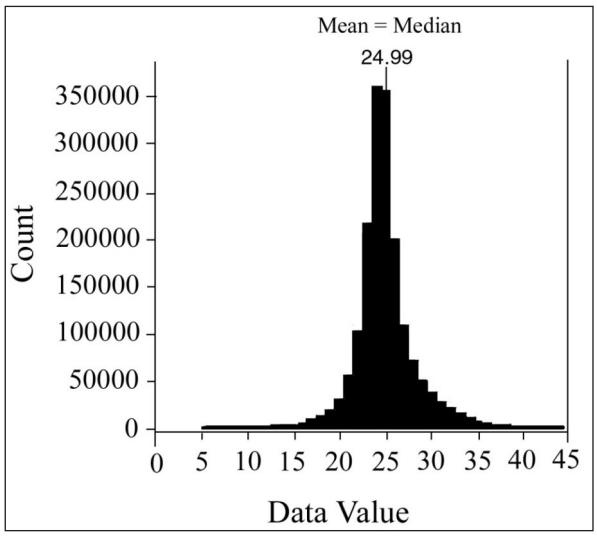

Figure 4. Histogram for the generated NDVI difference image.

When the difference image is Gaussian in nature, unchanged pixels are centered around the mean, while the tail regions on either side of the histogram contain information about the changed area (Qong and Igrashi, 1999). Misregistration is a major problem in image differencing because it may generate artifact changes during the change detection procedure. This problem can be addressed by statistical methods (Prakash and Gupta, 1998). The standard deviation of the difference image establishes a threshold level at which changes were deduced. To contain any misregistration, Singh (1989) recommended a threshold level of ± s (standard deviation) around the mean value (Singh, 1989; Washington-Allen et al., 1998, and Qong and Igrashi, 1999). For image differencing, unchanged pixel values should be equal to zero in theory (in this case it should be equal to 25). For this study, the difference image is Gaussian in nature (Figure 4), where the mean value is equal to the median value (= 24.99), and one-standard-deviation s (threshold) had been used (Washington-Allen et al., 1998, Qong & Igrashi, 1999, and Al_Bilbisi, 2012), s value is 1.15. As mentioned above, since many unchanged pixels are centered around the mean, the mean ± s (standard deviation) threshold level of the difference image was used. All pixel values within the mean ± s (near the Mean) are thus assumed to be unchanged pixels, and tail regions on both sides are assumed to contain information about the positive (gain) and negative (loss) change pixels.

The difference image was density-sliced and color-coded using the above threshold selection method to distinguish unchanged pixels from changed pixels (Figure 5). The threshold boundary between the changed pixels and unchanged pixels is determined according to the following rules, If:

- *NDVI difference image DN <= Mean + s AND >= Mean -s, then unchanged pixels.*
- *NDVI difference image DN > Mean + s, then positively changed pixels (gain).*
- *NDVI difference image DN < Mean - s, then negatively changed pixels (loss).*

The positive changes in the difference image denoted that the NDVI values of the later image were larger than the former one. Similarly, the negative values denoted that the NDVI value of the later image was smaller than the former one. Positive changes represent an increase in the vegetation cover between the two dates. Negative changes represent a decrease in the vegetation cover or a decrease in lower NDVI values. The difference image indicated that significant changes had occurred between 2000 and 2014, particularly in middle and southern parts of the study area; these areas had negative changes (Figure 5).

4.2. Main Possible Reasons of the Land Degradation in the Study Area

Based on the obtained results and the observed ground data, the main possible causes of the land degradation in the study area are:

(I) **Soil Erosion by Wind**: Soil erosion occurs when wind transports soil particles by suspension, surface creep or saltation over distances from a few centimeters to many kilometers. This depends on two factors (1) the ability of the wind to carry particles, and (2) the susceptibility of the soil surface to erosion. Wind erosion is greatest under the following conditions: scarce rainfall, high temperature, high wind velocity, and the lack of vegetation cover for significant parts of the year (CGER, 1997). Several recent studies have supported the view that wind erosion is a principal mechanism for the reduction of soil fertility in arid and semi-arid regions. Soil erosion by wind is the major reason for land degradation in the study area (Figure 6), where wind erosion caused sand drifts that covered and destructed the vegetation cover in this area.

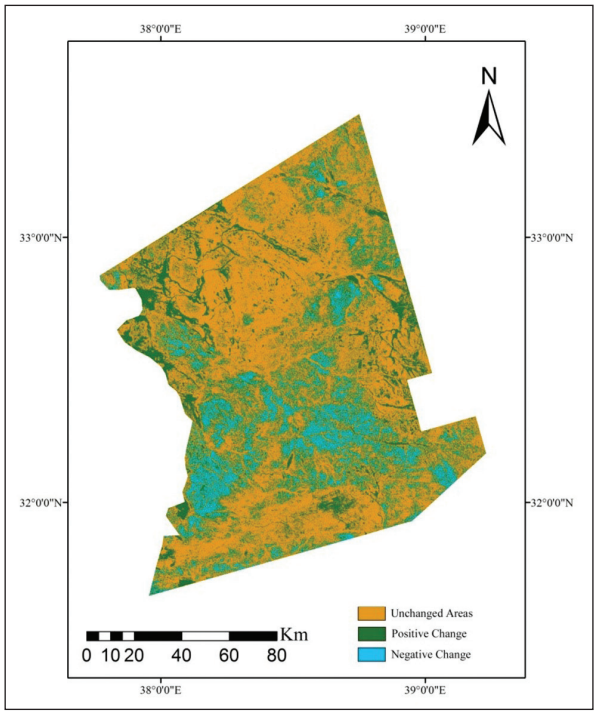

Figure 5. Density sliced NDVI difference image of the study area.

Figure 6. Sand drifts covered the vegetation in the study area.

(II) **Over-Grazing**: land degradation as a consequence of over-grazing occurred as a result of the removal of edible species which encouraged the inedible species to grow up (Figure 7). Then, if pressures continued, the modification of soil and water conditions worsen to the extent that all the vegetation gets removed and soil erosion becomes a major problem. It is clear that plant destruction is not solely achieved by eating, and the trampling of plants, the disturbance of root systems by scuffing and compaction of the surface will also reduce rainfall infiltration and all of that contributes to damage and cause the desertification.

Figure 7. Anabasis (inedible plant species) a consequence of overgrazing in the study area.

(III) **Soil Salinization**: The low rate of rainfall and the high rate of evaporation are the main causes behind soil salinization in the study area. In some areas, the surface of the soil is covered by a thin layer of calcium carbonate (Figure 8) contained in weathering materials to the extent that dry fragments do not slake in water and plant roots cannot penetrate; since salt tolerance of most plants is relatively low, therefore, the productivity rapidly declines, and as a result land degradation occurs

Figure 8. Thin layer of calcium carbonate causing soil salinization in the study area.

Conclusion

The methodology developed in this research to map land degradation using Landsat-TM and Landsat-8 images was based on an adequate understanding of the landscape features, and NDVI generating images. The NDVI image differencing method was used for land degradation monitoring, particularly in vegetation coverage. The difference image indicated that negative changes mostly in the middle and southern parts of the study area had occurred between 2000 and 2014. Based on the observed ground data, the main possible causes of the land degradation in the study area are soil erosion by wind, over-grazing and soil salinization. Therefore this area needs more attention from decision-makers to minimize the effects of land degradation in this region.

Acknowledgement

The author would like to express his great gratitude for The University of Jordan for the funding support during my sabbatical year 2014-2015 spent at Mu'tah University.

References

[1] Al-Bilbisi H. (2012). A two decades land use/cover change detection and land degradation monitoring in central Jordan using satellite images. Jordan Journal of Social Sciences, 5(1): 133-149.

[2] Al-Bilbisi, H., Tateishi R., and Tetuko, S.S.J. (2004). A technique to estimate topsoil thickness in arid and semi-arid areas of north-eastern Jordan using synthetic aperture radar data, International Journal of Remote Sensing, 25(19): 3873-3882.

[3] Al-Bilbisi, H., and Tateishi, R. (2003). Using satellite remote sensing data to detect land use/cover changes and to monitor land degradation in central Jordan. Journal of the Japan Society of Photogrammetry and Remote Sensing, 42(6): 4-18.

[4] Behnke, R.H., and Scoones, I.(1994). Rethinking range ecology: Implications for rangeland management in Africa. In Behnke R. H., Scoones, I., and Kerven, C. (eds.), Range Ecology at Disequilibrium, London: Overseas Development Institute, International Institute for Environment and Development, and Commonwealth Secretariat, London, 1-30.

[5] Bender, F. (1974). Geology of Jordan, Gebrider Borntraeger, Berlin.

[6] CGER, Center for Global Environmental Research, (1997). Databook of desertification/land degradation. National Institute forEnvironmental studies, Japan, pp 64.

[7] Chavez, P. S., JR. and MacKinnon, D. (1994). Automatic detection of vegetation changes in the southwestern United State using remotely sensed images. Photogrammetric Engineering and Remote Sensing, 60: 1025-1036.

[8] FAO (1990). Guidelines for soil description, 3rd ed., Rome, 70pp.

[9] FAO (2000). Land Cover Classification System (LCCS) - Classification concepts and user manual-. Rome, pp 179.

[10] Getzin S. (2005). The suitability of the degradation gradient method in arid Namibia. African Journal of Ecology, Volume 43 (4): 430 -351.

[11] JMD (Jordan Meteorological Department) (2013). The official web site, <http://www.jmd.gov.jo>.

[12] Lillesand, T.M., Kiefer, R.W., and Chipman, J.(2014). Remote sensing and image interpretation. 7th ed. John Wiley & Sons, Inc. New York, USA.

[13] Leprieur, C., Kerr, Y. H., Mastorchio, S., and Meunier, J. C. (2000). Monitoring vegetation cover across semi-arid regions: comparison of remote observations from various scales. International Journal of Remote Sensing, 21(2): 281-300.

[14] Mbow, C., Fensholt, R., Rasmussen, K., and Diop, D. (2013). Canvegetation productivity be derived from greenness in a semi-arid environment? Evidence from ground-based measurements.Journal of Arid Environments, 97: 56–65.

[15] Moody, A., and Johnson, D.M. (2001). Land-surface phenologies from AVHRR using the discrete Fourier transform, RemoteSensing of Environment, 75: 305-323.

[16] Pickup, G. (1989). New land degradation survey techniques for arid Australia: Problems and prospects. Australian Rangeland Journal, 11: 74-82.

[17] Prakash, A., and Gupta, R. P. (1998). Land-use mapping and change detection in a coal mining area- Acase study in the Jharia coalfield, India. International Journal of Remote Sensing, 19: 391-410.

[18] Qong, M., and Igarashi, T. (1999). Environmental changes deduced from satellite data in arid regions- A case study in the lower reaches of the Hotan and YARKANT rivers, China, Journal of Arid Land Studies, 9: 153-167.

[19] Roeder A., and Hill J. (eds.), (2009). Advances in remote sensing and geoinformation processing for land degradation assessment. ISPRS Series. London. ISBN-10: 0415397693.

[20] Rouse, J.W., Haas, R. H., Schell, J.A., and Deering, D.W. (1974). Monitoring vegetation system in the Great Plains with ERTS. 3ed ERTS Symposium, NASA SP-351, NASA, Washington, D. C., 1: 309-317.

[21] Singh, A. (1989). Digital change detection techniques using remotely-sensed data. International Journal of Remote Sensing, 10: 989-1003.

[22] Sommer, S., Zucca, C., Grainger, A., Cherlet, M., Zougmore, R., and Sokona, Y. (2011). Application of indicator systems formonitoring and assessment of desertification from national toglobal scales. Land Degradation and Development, 22: 184–197.

[23] Tucker, C. J., Pinzon, J. E., Brown, M. E., Slayback, D. A., Pak, E.W., and Mahoney, R. (2005). An extended AVHRR 8-km NDVIdata set compatible with MODIS and SPOT Vegetation NDVI data. International Journal of Remote Sensing, 26, 4485–4498.

[24] UNEP (1994). United Nations Convention to Combat Desertification, Interim Secretariat for the Convention to Combat, <http://www.unep.ch/inch.html> .

[25] Vogt, J.V., Safriel, U., Von Maltitz, G., Sokona, Y. (2011). Monitoring and assessment of land degradation and desertification: towards new conceptual and integrated approaches. Land Degradation and Development, 22: 150–165.

[26] Washington-Allen, R. A., Ramsey, R. D., Norton, B. E., and West, N.E. (1998). Change detection of the effect of severe drought on subsistence agropastoral communities on the Bolivian Altiplano. International Journal of Remote Sensing, 19: 1319-1333.

JJEES

Volume 9, (Number 2), August, 2018
ISSN 1995-6681
Pages 108 - 115

Jordan Journal of Earth and Environmental Sciences

Are Clay Minerals in Jordanian Soils Antibacterial?

Jwan H. Ibbini[1], Mohammed I. Al-Qinna[1], Kholoud Y. Mashal[1], Jamila Abuidhail[2], Karem H. Alzoubi[3] and Majed M. Masadeh[4]

[1]Department of Land Management and Environment, Faculty of Natural Resources and Environment, Hashemite University, Zarqa-Jordan
[2]Department of Maternal, Child, Family Health Care Nursing, Faculty of Nursing, Hashemite University, Zarqa-Jordan
[3]Department of Clinical Pharmacy, Faculty of Pharmacy, Jordan University of Science and Technology, Irbid-Jordan
[4]Department of Pharmaceutical Technology, Faculty of Pharmacy, Jordan University of Science and Technology, Irbid-Jordan

Received 16 April, 2018; Accepted 20 May, 2018

Abstract

Clay separates have been recently evaluated for their antibacterial potential. The current research is conducted to investigate the antibacterial effects of clay fractions from Jordanian soils and their relation to the physical and chemical properties of the soils. Thirty three soil samples were collected from different sites in the country with a high clay content (mainly from northern and middle governorates). The physical and chemical properties of bulk soil and clay fractions were characterized. Thereafter, the clay fractions were screened for their antibacterial properties *in vitro* against common bacterial pathogens and clinical isolates known for their multidrug resistance.

Seven clay fractions showed antibacterial properties against one or more of the tested pathogens in liquid culture. The X-ray diffraction (XRD) and X-ray Florescence (XRF) results of the antibacterial clay were correlated with the bacterial growth inhibition to understand the antibacterial mechanisms.

Correlation analyses using Pearson's product moments and backward elimination stepwise regressions indicated that the tested microbial strains are being significantly affected by different physical and chemical properties of the soil (e.g. EC, CEC, Available water), soil solution ionic concentrations (e.g. HCO_3^- and SO_4^{2-}, Na^+, and Ca^{2+}), clay fraction composition (Clay-Fe-oxide, Clay-$CaCO_3$), and clay type (smectites, quartz, and englishite). On the other hand, Fe_2O_3, Al_2O_3, and MgO clay compositions were found to be the most effective factors governing the antimicrobial activity. Thus, each microbial strain has a specific inhibitor control that interacts with its antimicrobial mechanism. As a conclusion, this study indicates the bactericidal effect of some clay mineral fractions from Jordanian soils, which still need to be clinically tested before use in medical applications.

Keywords: Soil texture, clay fractions, chemical properties, microbial activity, antibacterial clay, XRD, XRF.

1. Introduction

Natural clays have been used in ancient and modern medicine (Carretero et. al., 2002, 2006; Wilson 2003). Applications of clay minerals ranged from geophagy (Wilson, 2003; Ferrel, 2008) to apical applications (Carretero et. al. 2006 Gomes et. al., 2007). Geophagy, is the practice of eating earth materials containing clay minerals to physically sooth an infected and inflamed gastrointestinal lining (Dory-Lefaix et al., 2006). Alternatively, clays have been used topically in mud spas (pleotherapy) to adsorb toxins from skin, and to provide heat to stimulate circulation for rheumatism treatment (Carretero et. al., 2006).

Clay minerals are ubiquitous in natural soils. They have a small particle size of less than 2.0 μm in diameter and bulk density of 2.65 g/ cm^3 as defined by stock's low (Moore et. al., 1997). This provides a high specific surface area for a cation exchange capacity, and high absorptive and adsorptive capabilities. For that, they have been used in a variety of cosmetics and pharmaceutical formulations. For example, the extremely fine particles of smectites (expandable clay minerals) and kaolin group minerals are used to remove oils, secretions, toxins and contaminants from skin by absorbing and adsorbing moisture and impurities from the skin. Clay also serves to cleans and refresh the skin surface, and aids in the healing of topical blemishes in many cosmetics (Williams and Haydel, 2010).

Multidrug resistant organisms (MDROs) are microorganisms, predominantly bacteria, that are resistant to one or more classes of the commonly used antimicrobial agents (Barie, 2012). The widespread use of antibiotics, misuse and\ or overuse of antibiotics, and the ability of microorganism to develop drug resistance contribute to the emergence of new multidrug resistant bacteria (Freber, 2002; Barie, 2012; Orsi et al., 2011; Siegel et al., 2006).

Common MDROs include, but not limited to, *Staphylococcus aureus*, *Klebsiella pneumonia*, *Acinetobacter baumannii*, *Pseudomonas aeruginosa*, *Escherichia coli,* and *Clostridium difficile* which are common causes of human infections worldwide (Siegel et al., 2006).

As the rise of bacterial antibiotic resistance continues to risk human health, this elevates the need to properly detect, prevent and effectively treat these infections. The overuse and misuse of common antibiotics in recent decades stimulates the need to identify new antimicrobial compounds. Therefore,

* Corresponding author. e-mail: jhibbini@hu.edu.jo

natural products including clays that display antibacterial properties are of special interest (Bush, 2004).

Recent scientific attention was drawn toward clay minerals in the published literature. Two French green clays were reported to WHO in 2002 by a French humanitarian Line Brunet de Courssou during her work in the Ivory cost of West Africa. The French clay was used to heal Buruli skin ulcer, a necrotizing disease, caused by *Mycobacterium ulcerans* (Williams et al., 2004). Since then, natural clay minerals have been identified to have the ability to kill a variety of pathogenic bacteria (Haydel et al., 2008; Ma'or et al., 2006; Park et al., 2009; Williams et al., 2004).

Locally, the historical use of red soil in Jordan is still practiced by some communities to treat skin infections such as infant diaper rash. The idea of this study was established from the observation of traditional use of red soil to treat diaper rash among infants in Jordan (Abuidhail, 2011). This triggered the initiation of scientific investigation of the antimicrobial properties of clay minerals found in Jordan's soil. In the Jordanian culture, it was known that mothers brought red soil, cleaned it, filtered it, then took the fleecy material and put it on the nappy rash after applying some olive oil. Using red soil was known to be dangerous, because the soil may be contaminated. It may increase the severity of skin problems as nappy rash changing it to a severe skin infection (Abuidhail, 2008). However, the identification of new inhibitory agents other than antibiotics can open a wide door for the potential of producing an inexpensive alternative that is a property of Jordan and to present such finding for utilization in the Jordanian Pharmaceutical industry.

Therefore, this research is aimed at mineralogically characterizing clays in the Jordanian soil, in order to identify their antibacterial effectiveness. It will provide theoretical guidance to promote the production of antibacterial products from natural clay minerals for complementary therapies.

2. Materials and Methods

2.1. Study Area and Soil Sample Collection

A soil map of Jordan (Hunting Technical Services and Soil Survey and Land Research Centre, 1994) was implemented to allocate the potential sites for clays in Jordan. This was achieved based on field surveying in the northern regions of Jordan. Thirty-three surface (0-20cm) sampling sites were selected. At each site, three sub-samples were taken that are 30m apart. Two surface soil samples were obtained from each location; one undisturbed soil sample using core method (6 cm in diameter), and one disturbed sample using auger method. the samples were labeled and brought to the laboratory for physical and chemical analyses. The spatial location of the sampling sites was recorded using handheld GPS with 3m accuracy (Figure 1).

2.2. Clay Physical and Chemical Analyses

Disturbed soil samples were air dried, ground, then sieved through a 2-mm sieve. The percentage of coarse fractions (> 2 mm in diameter) in each soil sample was collected and estimated. All soil samples were analyzed for the major soil physical and chemical properties (Table 1) following ISO and SSSA procedures. Core samples were used to determine the soil physical properties while maintaining the exact field soil structure.

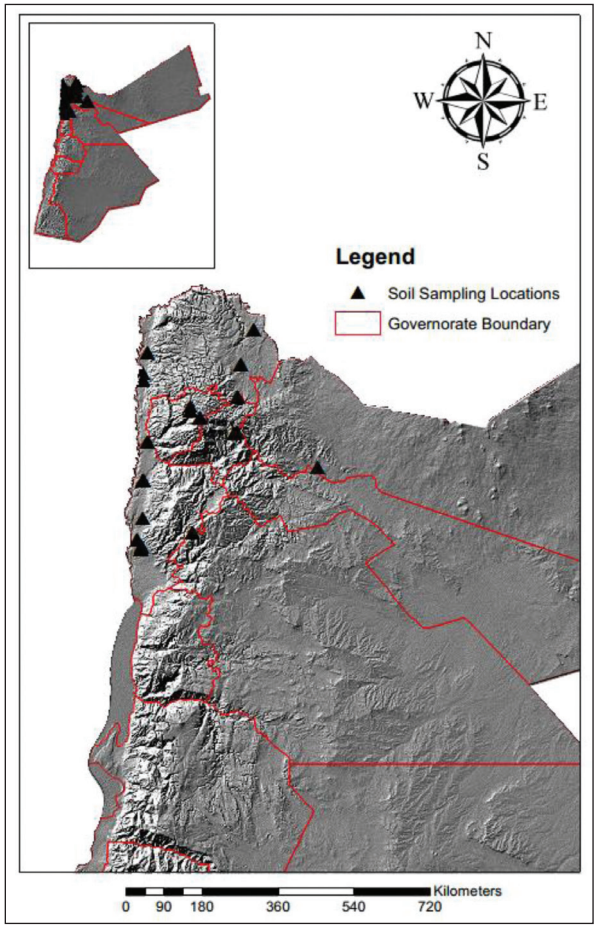

Figure 1. Soil sampling points across the northern parts of the country.

2.3. Clay Fractionation and Diffraction

Based on several trials to search for the best fractionation procedure, clay separation was achieved using the centrifuge technique. Although the gravitational decantation method is much easier, however it is not acceptable since the sedimentation takes a long time (at least 8 hours per sample), and Brownian motion interferes with settling for particles finer than 0.5 micrometers (Poppe et al., 2001). The centrifuge separation technique was achieved based on use of only 10 grams of soil per run and ending by only 0.5 to 1.0 g clay. Thus, this step had taken about a year to finish.

Clay separates were analyzed using the same analytical procedures stated above (Table 1) only the pH and ECe were done in a 1:5 clay:water suspension using a pH meter and EC meter, respectively. Seven samples which showed active microbiological properties were qualitative mineralogicals analyzed as oriented mounts on glass slides from 3u to 60u two-theta. X-ray diffraction and XRF analyses were prepared and analyzed according to the established analytic procedures at the "Water, Environment and Arid Region Research Center" in Al-Bait University using X-ray diffraction (XRD) and XRF systems. The XRD was from PANanalytical B.V. LR 39487C made in Netherlands. And the XRF was from PHILIPS Analatical X-Ray B.V. LR 39487 C made in Holland.

Table 1. Soil Physical and Chemical Analyses procedure following SSSA and ISO.

Soil Physical Property	Method	Reference
Soil Water Content	Gravimetric Method	Petersen and Calvin, 1986
Soil Dry Bulk Densities (ρB)	Coring Technique	Blake and Hartge, 1986
Soil Texture	Pipette Method	Gee and Bauder, 1986
Soil Color	Munsell Chart	Lynn and Pearson, 2000
Water Holding Capacity	Ceramic Plate Apparatus	Klute, 1986
Soil chemical property		
Cation exchange capacity (CEC)	1 M NH4OAc (pH 7.0)	Page et al., 1982
Organic carbon	Wet Oxidation method	Walkley and Black,1934
Active or amorphous iron oxide	Tamm's Reagent	Loppert and Inskeep, 2001
pHe	Paste extract (pH meter)	Sparks etal., 2001
ECe	Paste extract (EC meter)	Sparks etal., 2001
Ionic concentrations of soil solution		
Ca^{2+}, and Mg^{2+}	EDTA titration	Sparks etal., 2001
Na^{+}, and K^{+}	Flame photometer	Sparks etal., 2001
Cl^{-}	Silver nitrate titration	Sparks etal., 2001
HCO_3^{-}	Acid titration	Sparks etal., 2001
SO_4^{2-}	Turbidimetric	Sparks etal., 2001

2.4. Bacterial Strains and Growth Conditions

Staphylococcus aureus ATCC 29213, *Pseudomonas aeruginosa* ATCC 254232*, Escherichia coli* ATCC 35318, and *Klebsiella pneumoniae* ATCC 33495 obtained from the American Type Culture Collection, Methicillin-Resistant *Staphylococcus aureus* (MRSA), *Candida albicans* and *Escherichia coli* (Extended Spectrum Beta Lactamase) ESBL obtained from the Specialty Hospital Laboratories (Amman-Jordan), were used for all studies. *Staphylococcus aureus* ATCC 29213 and methicillin-resistant Staphylococcus aureus (MRSA), were grown on Blood agar , *Pseudomonas aeruginosa* ATCC 254232*, Escherichia coli* ATCC 35318, and *Klebsiella pneumoniae* ATCC 33495 were grown on Macconkey agar, and *Candida albicans was grown on sabouraud dextrose agar*. All the bacterial and Candida strains were grown at 37°C.

2.5. Antimicrobial Activity of Clay

Clay fractions of each soil sample were obtained and used to screen their antimicrobial effect against the previously described bacteria and yeast sp. by the susceptibility testing on solid medium. A fraction of 200 mg of clay minerals was measured in Eppendorf tubes and was sterilized by autoclaving for fifteen minutes at 121°C.

Eppendorf tube containing (1.0 ml of nutrient broth, 200 mg of clay minerals and 48 µl of 0.5 McFarland standard containing 1.5 $X10^8$ CFU/ml of the bacterial strain were mixed thoroughly for one minute. The tubes were then incubated at 37 °C for twenty-four hours and forty-eight hours in a shaker incubator. To count the microbial population in the clay-bacteria mixture, Petri dish plates containing 20 mL of the solidified Muller Hinton and sabouraud dextrose agar (for Candida) were inoculated with 100 µL of the prepared suspension and spread with a sterile L-shape glass rod. The plates were then incubated at 37 °C for twenty-four hours and the colony counts were then recorded. The same process was repeated after forty-eight hours of incubation.

3. Statistical Analysis

Before commencing with the modeling analysis, the types, strengths, and directions of the relationships between soil physical properties, soil chemical properties, clay specific properties, and the antimicrobial behavior were investigated by applying correlation analysis using Pearson's product moment correlation coefficient (r). Correlation analysis was useful for detecting the presence of multi-collinearity, which is a crucial characteristic in the modeling process (Howell, 1997). The strengths of the relationships were classified into three levels: weak correlation when $0 \leq |r| < 0.3$, moderate correlation when $0.3 \leq |r| < 0.7$, and strong correlation when $0.7 \leq |r| \leq 1.0$.

The backward elimination Stepwise regression (SWR) technique; as a selection technique, was used to identify the significant soil physical and chemical properties affecting the soil antimicrobial activity (Montgomery et al., 2012). The SWR represents a significant linear model subsetted at a specific significant level (usually 95 %) from the whole linear model (i.e., linear multiple regression including all of the predictors). The backward elimination technique involves deleting the predictor that contributes the least to the model, and thus the final model includes the most significant predictor. The removal of the insignificant predictors was based on Mallows' Cp criterion (Mallows, 1973) and Akaike's information criterion (AIC) (Akaike, 1974).

4. Results and Discussion

4.1. Soil Physical and Chemical Properties

Based on laboratorial results, the Northern regions of the country of Jordan are characterized by stable, well aggregated soils, with dry bulk densities ranging between 1.13 to 1.59 g/cm^3, and high porosity ranging from 40 % to 57 % with a mean of 52 % (Table 2). The water holding capacity (WHC) ranges from 233.5 to 486.0 mm/m, with a saturation percentage ranging from 37.10 to 73.71 %. These physical properties of the soil point to the effectiveness of the clay

content in enhancing the soil friability. The inspected sites' morphology indicates low soil surface crusts with visible continuous porous system and a low gravel content.

Although the effect of organic compounds on aggregate formation is much more stable than clay cementation, however, the measured soil dry bulk densities indicate that even at a low organic matter situation like in Jordan (i.e. average OM% less than 2 %), clay has a distinctive cementing behavior in providing higher porosity and thus reducing the soil bulk density to an average of 1.27 g/cm^3 which allows for a complete interaction with atmospheric air and the diffusion of air from and to the atmosphere. In such a condition, a microbial growth is favored especially if water exists at an optimum condition.

In regard to the soil color inspection using Munsell Chart, the Northern regions inspected in this study are characterized by having a yellowish red color with various hue magnitudes ranging from 5 to 10, and variable value and chroma. The majority of the soil samples range between 5YR to 7.5YR 4/4 indicating a strong yellowish red color attributed to the solid matrix formation (clay minerals and oxides).

According to the soil samples' texture analyses, the upper north regions of Jordan are classified as having a good potential for a high clay separate content. As indicated by the texture triangle (Figure 2), the soil texture ranged from Clayey to Silty clay to Silty Clay loam classes with a high clay content ranging from 24 % to 68 % by weight with an average content of 46 % and a standard deviation of 12 % (Table 2).

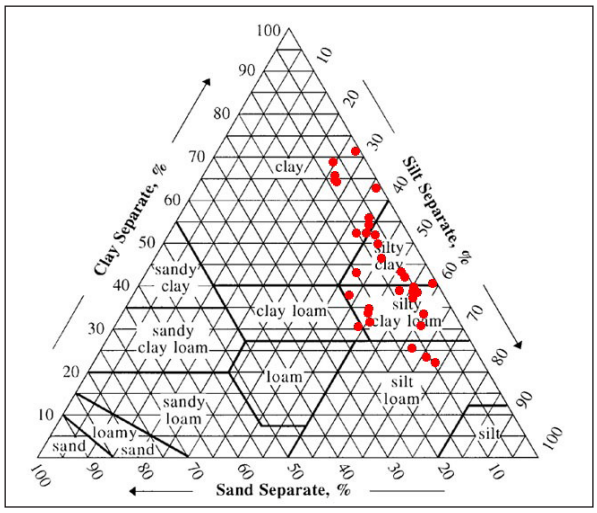

Figure 2. Soil textural class distribution of the soil samples.

Table 2. Soil physical and chemical properties of the inspected sites.

	Maximum	Minimum	Mean	Std Dev
Soil Physical Properties				
Soil bulk density, ρb (g/cm^3)	1.59	1.13	1.27	0.09
Soil Air Dry Water Content, θg (g/g)	0.075	0.043	0.043	0.018
Saturation Percentage, θs (%)	73.71	37.10	57.05	11.25
Available Water, AW (m/m)	0.486	0.233	0.366	0.064
Water Holding Capacity, WHC (mm/m)	486.0	233.5	366.5	64.48
Sand Content (%)	21.8	1.8	9.7	5.0
Silt Content (%)	61.6	23.9	45.2	9.4
Clay Content (%)	67.9	23.9	46.3	12.0
Soil Bulk Chemical Properties				
Potential of Hydrogen, pH	8.41	6.80	7.96	0.34
Electrical Conductivity, EC (µS/ cm)	1834.00	327.39	682.74	331.82
Cation Exchange Capacity, CEC (cmolc/kg)	86.99	2.60	34.08	20.08
Organic Matter Content, O.M (%)	1.60	0.55	0.98	0.37
Nitrogen-N, (ppm)	0.224	0.034	0.108	0.046
Phosphorus, P (ppm)	22.00	1.20	11.58	5.91
Ionic concentrations of the Soil Solution				
Chloride, Cl^- (meq/L)	7.25	0.50	2.60	1.70
Bicarbonate, HCO_3^- (meq/L)	13.50	1.50	5.48	2.60
Sulfate, SO_4^{2-} (meq/L)	4.75	0.69	2.27	1.15
Sodium, Na^+ (meq/L)	42.13	1.52	4.98	6.89
Potassium, K^+ (meq/L)	3.92	0.05	0.63	0.87
Calcium, Ca^{2+} (meq/L)	15.50	3.00	6.33	3.10
Magnesium, Mg^{2+} (meq/L)	17.00	1.00	4.99	3.12
Clay Fractions' Chemical Properties				
Calcium carbonate content, $CaCO_3$ (%)	39.04	21.27	29.21	5.69
Amorphous Iron oxide, (mg/kg)	57.24	39.60	49.39	3.93
Cation Exchange Capacity, CEC ($cmol_c$/kg)	119.56	20.65	60.56	23.54
Organic Matter Content, O.M (%)	2.75	0.55	1.64	0.64

In terms of the soil bulk chemical analyses, the results indicate that these soils are moderately alkaline as indicated by the associated soil pH, ranging from 6.80 to 8.41. Also, the soils are characterized by low salinity with an EC ranging from 1834 to 327.39 µS/cm, where the variation in EC may be attributed to salt removal for being located within sub-humid regions (i.e. located within regions having an average annual rainfall of 300 to 400 mm).

The soil organic matter (OM) is very low ranging from 0.55 % to 1.6 %, which remains within the typical range of the Jordanian environment associated with a low organic addition and a high organic decomposition being located within typical thermic temperature regime. The soils cation exchange capacity (CEC) ranges from 2.60 to 87 cmolc/kg due to the presence of 2:1 clay minerals and due to the low organic matter content. The soil with higher CEC will be capable to adsorb more cations from the soil solution.

In terms of the Ionic concentrations of the soil solution, the chemical results show that sodium is the dominant cation ranging from 1.52 to 42.13 meq/L, whereas the dominant anion is bicarbonate ranging from 1.50-13.50 meq/ L (Table 2). These results are consistent with the fact that most of the soil samples are calcareous being originated from a limestone parent material.

The chemical Properties of the clay fractions show a calcareous behavior as the $CaCO_3$ % ranged from 21.27-39.04 %. The clay fractions CEC ranges from 20.65 cmolc/kg to 119.56 cmolc/kg. The existing differences between CEC results of clay fractions are due to the differences in the mineralogical composition of these samples. On the other hand, the iron content in the clay fractions ranges from 39.6 to 57.24 mg/kg.

4.2. X-ray Diffraction

The X-ray diffraction (XRD) analyses of the soil samples showed a varying composition of clay minerals and non-clay minerals (Figure 3). The most abundant clay minerals are the Kaolinite and smectite group, while the non-clay minerals were mainly calcite and quarz. The smectite clay mineral group has high CEC, which explains the variation among the chemical composition of the soil samples. The soils rich in these minerals have a higher capability to adsorb more cations from the solution and replace them with ones in the exchange sites. On the other hand, the Kaolinite clay mineral group has a different structure and holds lower CEC. Generally, the adsorption mechanisms of clay and non-clay minerals to micro-organisms vary according to the clay structure and its chemical property. Both clay and non-clay mineral surfaces can adsorb bacteria through electrostatic and hydrophobic interactions (Yee and Daughney, 2000).

4.3. X-ray Fluorescence

The results of X-ray fluorescence (XRF) analysis of the major chemical components are shown in Figure 4. The results were in consistence with the XRD analyses, where silica and aluminum, which compose the crystal structure of Smectites and Kaoline minerals, were the predominant elements present. These elements are followed by calcium, iron and sodium. In addition, one of the samples shows higher phosphorus concentration, which is consistent with the presence of Englishite mineral, that is mainly phosphates. The presence of Ca^{2+}, Mg^{2+}, Na^{+}, and K^{+} ions are unlikely to contribute to antibacterial activity, because these ions are essential to bacterial cells (Stotzky, 1989). However, the presence of TiO_2, which is present in all samples, is known to irreversibly adsorb *E. coli* through acid-base attractions occurring between the Waal O antigens lipopolysaccharide and the metal oxide (Jucker et al., 1997).

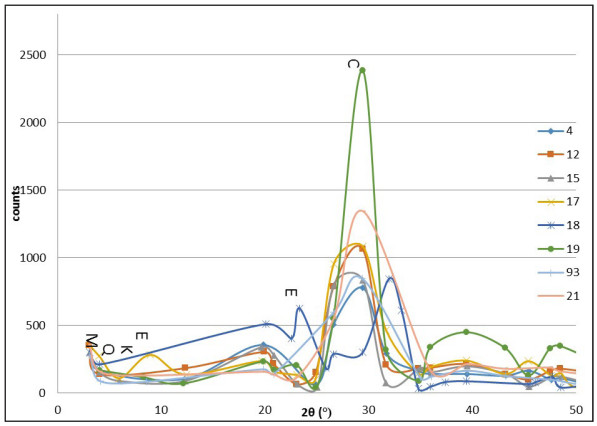

Figure 3. X-ray diffraction spectra of the selected clay separates (E= Englishite, K=Kaolinite, M= Montmorillonite, Q= Quartz, C= Calcite).

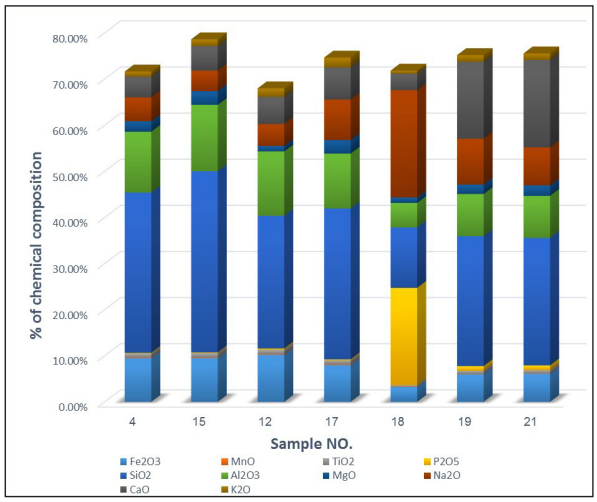

Figure 4. X-ray fluorescence (XRF) analysis of the selected clay separates.

4.4. Microbial Activity

Based on Well Agar Diffusion laboratorial experiment for testing the microbial activity of seven strains using nine fractioned clay samples, the counts after twenty-four hours and forty-eight hours incubations are presented in Table (3). According to the antimicrobial activity results, it seems that each fractioned clay sample has a different effect regarding the microbial strain. Some clay samples may depress the growth substantially as being exclusively effective/elective on specific strains. This indicates that the antimicrobial activity of the clay samples vary significantly according to the strain type and thus suggesting a unique inhibition mechanism of the clay minerals against each microbial strain.

For example, the *E. coli (ESBL)* is being inhibited in all the samples except for sample number twenty-one. On the other hand, the *C. albicans* microbial strain is being inhibited using only two samples number seventeen and twenty-one.

4.5. Correlation between Microbial Activity and Soil Physical and Chemical Properties, Clay Fraction Properties, and XRF Results

In order to investigate the antimicrobial effects of the physical and chemical properties of the soil (including ionic concentrations of the soil solution), the multivariate correlation analysis was achieved using the Pairwise correlation method (Table 4). According to the correlation matrix, there exist moderate and weak relations between the soil physical and chemical properties and antimicrobial activity. In general, the importance of the soil physical and chemical properties varies according to the microbial strain type. Thus, relations are variable and do not direct nor reflect a general conclusion other than that the soil behaviors vary depending on the existing environmental conditions at the field and the management pursued at the micro-scale. The potential medical effect of the clay is still vague, however it appears from these correlations that the chemistry and type of the soil clay are going to be the determinant of the effectiveness of these soils.

Similar to the previous correlation, the antimicrobial effects of the clay fraction properties were investigated using the multivariate correlations analysis (Table 5). The correlation matrix indicates that only Clay-Fe-oxide, Clay-OM, and Clay-pH have a moderate positive correlation with the antimicrobial activity. The reduction effect of Clay-Fe-oxide, Clay-OM, and Clay-pH on the microbial growth is significantly clear concerning *K. pneumoniae, C. albicans, and E. coli (ESBL)*. However, other microbial strains such as *S. aureus, P. aeruginosa,* and *E. coli* were non-significantly affected by the clay fraction properties

The bactericidal mechanism was not due to the physical attraction between clay and bacteria, thus suggesting a chemical transfer or reaction. It was found that the pH and the oxidation state, buffered by the clay minerals through the cationic exchange at the clay surfaces are key to controlling the solution chemistry and redox reactions occurring at the bacterial cell wall (Williams and Haydel, 2010). A group of researchers suggest that the healing power may be attributed to the antibiotic-producing bacteria they have found living in the soil (Falkinham et al., 2009). In contrast, other studies suggested that the acidic environment of hydrated minerals contributes to the antibacterial activity by increasing the availability and toxicity of metal ions in the solution chemistry and redox-related reactions occurring at the bacterial cell wall (Williams and Haydel, 2010; Cunningham T., *et.al*., 2010). A Study investigating different clays from Swaziland, Botswana, and South Africa also revealed antibacterial activity, and attributed that to the low pH and the availability of certain ionic species such as Cu, Al, S and Cl (Sisai *et.al*., 2010).

The correlation matrix generated between the antimicrobial activity and XRF results indicates that the clay composition is more effective in microbial inhibition (Table 6). The matrix indicates the presence of strong relations between the antimicrobial activity and different clay fraction composition, especially MnO, TiO_2, MgO, CaO, and K_2O. The strong relations are microbial strain specific and not effective for all strains. On the other hand, SiO_2 seems to have a moderate inhibition control over all microbial strains.

Results obtained in this study showed that each of the short listed clay minerals was active against one or more of the tested pathogens, and none showed an activity against all the bacteria, this was investigated in another study (Lynda Williams, 2017) and justified by the fact that bacteria are metabolically diverse, and they evolve different adaptation mechanisms to thrive in a variety of environments; some can even live in extreme environmental conditions. Therefore, antibacterial clay can be effective against a specific type or group of bacteria.

Table 3. Antimicrobial activity of seven strains using nine fractioned clay samples

Sample |ID No.	S. aureus		P. aeruginosa		E. coli		K. pneumoniae		C. albicans		E. coli (ESBL)		MRSA	
McFarland standards	1.5 X10^8 CFU/ mL		1.5 X10^8 CFU/ mL		1.5 X10^8 CFU/ mL		1.5 X10^8 CFU/ mL		6.0X10^8 CFU/ mL		1.5 X10^8 CFU/ mL		1.5 X10^8 CFU/ mL	
	24 hrs	48 hrs	24 hrs	48 hrs	24 hrs	48 hrs	24 hrs	48 hrs	24 hrs	48 hrs	24 hrs	48 hrs	24 hrs	48 hrs
4	616	TMTC	N.G	N.G	TMTC	TMTC	TMTC	TMTC	TMTC	TMTC	N.G	N.G	201	TMTC
12	TMTC	TMTC	N.G	N.G	TMTC	TMTC	TMTC	TMTC	TMTC	TMTC	352	TMTC	TMTC	TMTC
15	TMTC	TMTC	N.G	N.G	N.G	N.G	76	N.G	TMTC	TMTC	N.G	N.G	TMTC	TMTC
17	TMTC	TMTC	TMTC	TMTC	TMTC	TMTC	N.G	N.G	1008	N.G	N.G	N.G	TMTC	TMTC
18	83	TMTC	TMTC	TMTC	TMTC	TMTC	TMTC	TMTC	TMTC	TMTC	N.G	N.G	227	TMTC
19	488	TMTC	TMTC	TMTC	TMTC	TMTC	7	N.G	TMTC	TMTC	N.G	N.G	40	325
93	TMTC	TMTC	TMTC	TMTC	TMTC	TMTC	N.G	N.G	TMTC	TMTC	N.G	TMTC	TMTC	TMTC

TMTC: Too many to count. NG: No growth.

Table 4. Correlation between antimicrobial activity and soil physical and chemical properties including soil solution ionic concentrations

Microbial Strain Type	pH	EC	Clay	CEC	O.M	Cl^-	HCO_3^-	SO_4^{2-}	Na^+	K^+	Ca^{2+}	Mg^{2+}	θg	bulk density	Available water	θs	P	K	N
S.aureus	-0.0463	0.0466	-0.0777	-0.1162	0.1696	0.0123	0.2908	-0.0013	-0.0864	0.0279	-0.0685	0.1248	-0.1089	-0.1028	-0.3136	0.0159	-0.0204	0.1194	0.0661
P. aeruginosa	-0.0131	0.1259	0.1037	-0.0287	0.2409	-0.0365	0.2208	0.0204	-0.0804	0.1014	-0.1282	0.0376	-0.0423	-0.0850	0.0201	0.2506	0.1676	-0.1627	0.1810
E.coli	-0.0522	0.3843	-0.0244	-0.1393	0.1476	0.0796	0.2005	0.2676	0.0176	0.2722	-0.0439	0.1541	-0.0447	-0.1408	0.0616	0.2322	0.3374	-0.0297	0.1070
K.pneumoniae	0.0308	0.4810	-0.2082	-0.3906	0.3253	0.2905	0.5149	0.3809	-0.0059	0.2666	-0.0176	0.2054	-0.3093	-0.0881	-0.0378	-0.0376	0.5017	0.1272	0.3786
C. albicans	0.0308	0.4810	-0.2082	-0.3906	0.3253	0.2905	0.5149	0.3809	-0.0059	0.2666	-0.0176	0.2054	-0.3093	-0.0881	-0.0378	-0.0376	0.5017	0.1272	0.3786
E.coli (ESBL)	0.1941	0.0119	-0.1381	-0.2061	0.2915	0.0350	0.4386	0.0252	-0.0812	-0.0412	-0.1797	-0.0175	-0.3000	-0.0225	-0.2607	-0.1387	0.2494	0.1676	0.3278
MRSA	-0.2028	0.3682	-0.0781	-0.2501	0.2717	0.1581	0.3475	0.2025	-0.0902	0.2778	-0.0064	0.2828	-0.1758	-0.1367	-0.1754	0.0960	0.1069	0.0576	0.1687

The strengths of the relationships were classified into three levels: weak correlation when $0 \leq |r| < 0.3$, moderate correlation when $0.3 \leq |r| < 0.7$, and strong correlation when $0.7 \leq |r| \leq 1.0$.

Table 5. Correlation between antimicrobial activity and clay fraction properties

Microbial Strain Type	Clay-$CaCO_3$	Clay-CEC	Clay-Fe-oxide	Clay-OM	Clay-pH	Clay-EC
S.aureus	-0.0810	-0.2503	0.2929	0.1649	0.0273	0.3389
P. aeruginosa	-0.0783	-0.0408	0.1284	0.2173	-0.0242	0.0357
E.coli	0.1337	0.0599	0.2732	0.1688	0.1765	-0.0752
K.pneumoniae	0.0581	-0.1014	0.5022	0.3561	0.4011	-0.1340
C. albicans	0.0581	-0.1014	0.5022	0.3561	0.4011	-0.1340
E.coli (ESBL)	-0.1988	-0.2295	0.4753	0.3554	0.2663	0.1407
MRSA	0.0874	-0.2889	0.2696	0.3088	0.1462	0.1800

The strengths of the relationships were classified into three levels: weak correlation when $0 \leq |r| < 0.3$, moderate correlation when $0.3 \leq |r| < 0.7$, and strong correlation when $0.7 \leq |r| \leq 1.0$.

Table 6. Correlation between antimicrobial activity and XRF results

Microbial Strain Type	Fe_2O_3	MnO	TiO_2	P_2O_5	SiO_2	Al_2O_3	MgO	Na_2O	CaO	K_2O
S.aureus	-0.4712	-0.5333	-0.5733	0.4800	-0.4383	-0.5068	-0.3679	0.5083	-0.0892	-0.7214
P. aeruginosa	0.6563	0.1833	0.5988	-0.4827	0.5159	0.6288	0.0894	-0.6799	-0.0349	0.0604
E.coli	0.0819	-0.0913	0.1740	-0.2478	0.3528	0.1563	0.4667	-0.3008	0.3604	0.0041
K.pneumoniae	-0.0518	0.1833	0.1388	-0.4496	0.4153	0.0518	0.7449	-0.2621	0.6267	0.4570
C. albicans	-0.0518	0.1833	0.1388	-0.4496	0.4153	0.0518	0.7449	-0.2621	0.6267	0.4570
E.coli (ESBL)	0.2432	0.3064	0.1859	0.1340	0.0838	0.2523	-0.0892	0.0665	-0.7128	0.0160
MRSA	-0.6432	-0.7500	-0.7047	0.3852	-0.4976	-0.6852	-0.3048	0.4613	0.4148	-0.7328

The strengths of the relationships were classified into three levels: weak correlation when $0 \leq |r| < 0.3$, moderate correlation when $0.3 \leq |r| < 0.7$, and strong correlation when $0.7 \leq |r| \leq 1.0$.

4.6. Stepwise Regression Analyses

The backward elimination stepwise regression analysis was useful to indicate the significant factors governing the antimicrobial activity based on soil physical and chemical properties, clay fraction properties, soil solution ionic concentration, and XRF results. Table (7) shows that each microbial strain is being affected by different soil factors. The positive or negative sign of each soil factor is indicative of the effect of the parameter on the antimicrobial activity as being either inhibitor or catalyst of microbial growth.

Table 7. Stepwise Multiple Regression Results for soil physical and chemical factor selection governing microbial reduction.

Microbial Strain	R^2	RMSE	P-value	Equation
S.aureus	0.1148	27.9	0.0537	(-10.864) + 0.004 * Clay-EC (µs/cm)
P. aeruginosa	0.0108	33.49	0.5656	(0.912) + 0.255 * clay content (%)
E.coli	0.9900	0.05	<.0008*	(-354.147) -57.153 * CaO (%) + 20.042 * Na^+ (meq/L) -1.442 * Ca^{2+} (meq/L) + 797.648 * AW (m/m)+ 0.143 * K (ppm)
K.pneumoniae	0.9900	0.11	0.0014*	(-55.258) -263.952 * Fe_2O_3 (%)+ 5619.897 * MgO (%) -0.845 * CEC (cmolc/kg) + -0.382 * Clay-$CaCO_3$ (%) + 3.138 * P (ppm)
C. albicans	0.9900	0.03	0.0014*	(61.185) + -65.988 * Fe_2O_3 (%) + 1404.974 * MgO (%) -0.211 CEC (cmolc/kg) -0.095 * Clay-$CaCO_3$(%) + 0.784 * P (ppm)
E.coli (ESBL)	0.0574	41.63	0.4121	42.910) -0.522 * CEC (cmolc/kg) -6.218 * K+(ppm)
MRSA2	0.5625	38.73	0.0522	(235.000) -149999.732 * MnO (%)

** Highly significant at 95% confidence level.*

Therefore, different antibacterial clays may exhibit different modes of action, some of which may react with bacteria by adsorption, or interact with soil solution ionic species. The same conclusion was made by (Williams, 2017) saying that different mechanism could apply to the bactericidal effects of the soil clay fraction type, or clay physical and chemical properties, or through specific ionic species of the soil aqueous solution.

Conclusion

Jordanian soils exhibit a high clay content that reaches up to 57 %. These soils were found to have a good potential for their inhibitory effect against some pathogenic bacteria. The correlation between the tested microbial strains and soil bulk physical and chemical properties, and soil solution ionic concentrations, indicated that some of these properties have moderate relations especially soil EC, CEC, available water, HCO_3^-, and SO_4^{2-}, P, and K. However, the effect of each soil property is variable according to the microbial strain.

Correlations with the clay-separate properties and clay composition indicated that Clay-Fe-oxide, Clay-OM, and Clay-pH are the most effective factors governing the microbial activity positively of the *K. pneumoniae, C. albicans, E.coli (ESBL)*, and *MRSA* bacterial species. On the other hand, the Clay-EC is found to be positively effective in inhibiting the *S. aureus* growth.

The X-ray diffraction indicated that these soils are in majority composed of Kaolinite, Smectite, Englishite, Calcite and Quarz. The correlations with clay-fraction composition revealed that MgO is a strong inhibitor of the *K. pneumoniae and C. albicans* growth and a moderate inhibitor of the *E.coli* growth. On other hand, Fe_2O_3 *and* TiO_2 were found to be moderate to strong inhibitors of the *P. aeruginosa* growth, while Na_2O and P_2O_5 were found to be moderately effective in inhibiting *S. aureus and MRSA.*

The backward elimination stepwise regressions were able to identify the most common significant factors governing each microbial growth. These factors vary by the microbial strain suggesting the presence of different antibacterial mechanism (e.g. absorption, adsorption, toxicity, etc). Therefore, further

specific investigations are encouraged to understand the mechanisms of the microbial inhibition**.**

Acknowledgement

The authors would like to thank the Scientific Research Support Fund (SRSF) for financing this research. Further gratitude is expressed to the following research assistants who helped with the experimental lab work, namely Kamal Hijjawi, Enas Al-Suhaim, Hana Al-Nounah, and Sabal Al-Hmoud. The research team would like to acknowledge the Center of Water and Environmental Studies at Al-Bait University for conducting the XRD and XRF analysis.

References

[1] Abuidhail, J.(2011) "Rural Jordanian Mothers as a Vulnerable Population Group," was accepted for podium presentation at Guaranteed Symposium, "New Perspectives in Promoting Comprehensive Women's Health across the Lifespan, through the 2011 MNRS Annual Research Conference in Columbus, Ohio, March 25-27, 2011.

[2] Abuidhail, J. (2008). Rural Jordanian mothers' cultural health beliefs, knowledge and practices of postnatal care. Thesis of Doctor of Philosophy. Glasgow Caledonian University/ Scotland/UK.

[3] Barie, P.S. (2012). Multidrug-resistant organisms and antibiotic management. Surg Clin North Am., 92(2):345-91.

[4] Bush, K. (2004). Why it is important to continue antibacterial drug discovery. American Society for Microbiology News. 70: 282-287.

[5] Carretero, M.I. (2002). Clay minerals and their beneficial effects upon human health. A review. A pplied Clay Science. 21: 155 – 163.

[6] Carretero, M.I., Gomes, C. S. F., and Tateo, F. (2006). Clays and human Health. In: Bergaya F., Theng, B.K.G; Lagaly G.,editors. Handbook of Clay Science. Elsevier Ltd.

[7] Cho S.S., Choi Y.H., Simkhada J.R., Mander P., Park da J., and Yoo, J.C. (2012). A newly isolated Streptomyces sp. CS392 producing three antimicrobial compounds. Bioprocess Biosyst Eng. 35(1-2): 247-54. Epub 2011 Sep 10.

[8] CLSI (2009). "Methods for dilution antimicrobial susceptibility test for bacteria that grow aerobically. Approved standard. Eighth edition. Villanova, PA: 2009. Available from http://www.clsi.org/source/orders/free/m07-a8.pdf. Accessed 14 September 2011.".

[9] Cunningham, T.M., Koehl, J.L., Summers, J.S., Haydel, S.E. (2010). pH-Dependent Metal Ion Toxicity Influences the Antibacterial Activity of Two Natural Mineral Mixtures. PloS ONE 5(3): e 9456. doi:10.1371/journal.pone.009456

[10] Dane, J.H. and Topp, G.C. (2002) Methods of Soil Analysis, Physical Part, 3rd ed. SSSA, Madison, WI.

[11] Dory-Lefaix, M.T., and Tateo, F. (2006). Clay and clay minerals as drugs. In: Bergaya F., Theng, B.K.G; Lagaly G., editors. Handbook of Clay Science. Elsevier Ltd.

[12] Falkinham, J.O. 3rd, Wall T.E., Tanner J.R., Tawaha K., Alali F.Q., Li C., Oberlies N.H. (2009). Proliferation of Antibiotic-Producing Bacteria and Concomitant Antibiotic Production as the Basis for the Antibiotic Activity of Jordan's Red Soils. Applied and Environmental Microbiology, 2009; 75 (9): 2735 DOI: 10.1128/AEM.00104-09

[13] Ferrel, R. E. (2008). Medicinal clay and spiritual healing. Clays and Clay Minerals. 56: 751 – 760.

[14] Freber, D. (2002). Livestock feed ban preserves drugs power. Science, 295(5552): 27- 28.

[15] Gomes, C. S. F., and Silva, J. B. P. (2007). Minerals and clay minerals in medical geology. Applied Clay Science. 36: 4 – 21.

[16] Gutierrez-Fernandez, A., Inada, M., Balbín, M., Fueyo, A., Pitiot, A.S., Astudillo, A., Hirose, K., Hirata, M., Shapiro, S.D., Noël, A., Werb, Z., Krane, S.M., López-Otín, C., and Puente, X.S. (2007). Increased inflammation delays wound healingin mice deficient incollagenase-2 (MMP-8). FASEB J., 21(10):2580-2591.

[17] Haydel, S.E., Remenih, C. M., Williams, L. B. (2008). Broad Spectrum in vitro Antibacterial Activities of Clay Minerals Against Antibiotic Susceptible and Antibiotic Resistant Bacterial Pathogens. Journal of Antimicrob and Chemotherapy. 61: 353-361.

[18] Kim, J., Dong, H., Seabaugh J., Newell, S. W., and Ebrel, D.D. (2004). Role of microbes in the smectite to illite reaction. Science. 303:380 – 382.

[19] Kostka, J.E., Dalton D.D., Skelton H., Dollhopf S., Stucki J. W. (2002). Growth of iron (III-reducing bacteria on clay minerals as the sole electron acceptor and comparison of growth yields on a variety of oxide iron forms. Applied and Environmental Microbiology. 68: 6256 – 6262.

[20] Ma'or, Z., Henis, Y., Along, Y., Orlov, E., Sorensen, K. B., and Oren, A. (2006). Antimicrobial properties of Dead Sea black mineral mud. International Journal of Dermatology. 45: 504 –511.

[21] Moore, D.M., and Renolds, R.C. (1997). X-ray diffraction and the identification and analysis of clay minerals. New York: Oxford University Press.

[22] Orsi, G.B., Falcone, M., and Venditti, M. (2011). Surveillance and management of multidrug-resistant microorganisms. Expert Rev Anti Infect Ther. 9(8): 653 – 79.

[23] Otto, C.C., Cunningham, T.M., Hansen, M.R., and Haydel, S.E. (2010). Effect of Antibacterial Mineral Leachates on the Cellular Ultrastructure, Morphology, and Membrane Integrity of Escherichia coli and Methicillin-Resistant Staphylococcus aureus. Annals of Clinical Microbiology and Antimicrobials. 9:26.

[24] Park, S.K., Lee, C.W., and Lee, M.Y. (2009). Antibacterial effectof minerals from ores indigenous to Korea. Journal of Environmental Biology. 30(1): 151 – 154.

[25] Sadaf, F. R. Saleem, et. al. (2006). Healing potential of cream containing extract of Sphaeranthus indicus on dermal wounds in Guinea pigs. J. Ethnopharmacol, 107(2): 161-163.

[26] Siegel, J.D., Rhinehart, E., Jackson, M., Chiarello, L. (2006). Healthcare infection control practices advisory committee: Management of multidrug-resistant organisms in health care settings, Am. J. Infect Control; 35(10 Suppl 2):S165-93.

[27] Sisai, F. M., Georges-ivo, E. E., Berhanu, A. G., Isaac, M., Stephan, H.C. (2010). Microbiological characterization of southern African medicinal and cosmetic clays. International Journal ofEnvironmental Health Research. 20(1): 27 – 41.

[28] Sparks, D. L., Page, A. L., Helmke, P. A., Loeppert, R. H., Soltanpour, P. N., Tabatabai, M. A., Johnston, C. T., Sumner, M.E. (2001). Methods of Soil Analysis, Chemical Part, 3rd ed. SSSA, Madison, WI.

[29] Tramontina, V. A., Machado, M. A., Nogueira, Filho Gda, R., Kim, S. H., Vizzioli, M .R., Toledo, Sd. (2002). Effect of bismuth subgallate (local hemostatic agent) on wound healing in rats. Histological and histometric findings. Braz. Dent. J. 13(1): 11-16.

[30] Williams, L. B., Haydel, S. E. (2010). Evaluation of the Medicinal Use of Clay Minerals as Antibacterial Agents. International Geology Reviews. 52(7/8): 745-770. doi:10.1080/00206811003679737

[31] Williams, L.B., Haydel, S.E., Giese, Jr. R.F., Eberl, D.D. (2008). Chemical and mineralogical characteristics of French greenclays used for healing. Clays and Clay Minerals. 56(4): 437 –452.

[32] Williams, L.B., Holland, M., Ebrel, D.D., Brunet, T., Brunet, C.L. (2004). Killer clays! Natural antibacterial clay minerals. Mineralogical Society Bulletin. 139: 3- 8.

[33] Williams, L.B., Metge, D.W., Eberl, D.D., Harvey, R.W., Turner, A. G., Prapaipong, P., Peterson, A. T. (2011). What makes a naturalclay antibacterial?. Environmental Science and Technology. 45(8): 3768 – 3773.

[34] Williams, L. B. (2017). Geomimicry: harnessing the antibacterial action of clays. Clay Minerals. 52: 1-24.

[35] Wilson, M. J. (2003). Clay mineralogical and related characteristics of geophagic materials. Journal of Chemical Ecology. 29: 1525 – 1547.

[36] Wu, T., Xie, A., Tan, S., Cai, X. (2011). Antimicrobial effects of quaternary phosphonium salt intercalated clay minerals on Escherichia coli and Staphylococcus aureus. Colloids and Surfaces B: Biointerfaces. 86: 232-236.

[37] Yee, N., Fein, J.B., Daughney, C.J. (2000). Experimental study of the pH, ionic strength, and reversibility behavior of bacteria - mineral adsorption. Geochim Cosmochim Acta, 64: 609–617.

JJEES
Jordan Journal of Earth and Environmental Sciences

Volume 9, (Number 2), August, 2018
ISSN 1995-6681
Pages 116 - 126

Post-Cretaceous Mesostructures and Their Formation Mechanisms, Jordan

Ikhlas Alhejoj[1*], Mohammad Alqudah[2], Khitam Alzughoul[1], Arwa Tarawneh[1]

[1]Department of Geology, the University of Jordan, 11942, Amman, Jordan
[2]Department of Geology, Yarmouk University, Irbid, Jordan

Received 2 June, 2018; Accepted 3 July, 2018

Abstract

In the current work, a variety of deformational mesostructures (tectonic and nontectonic) in the Upper Cretaceous rocks of Jordan are described and attempts have been made to explain their textures, formation and the mechanisms of development. The structures include: undulations, brecciated chert, slickensides, nodules of limestone, deformed fossils, boudinage, geodes, stylolites, flow channels and flowage structures.

These structures have been described in previous studies with no correlation to the factors responsible for their formation. In this article, three types of deformation forces or a combination of them are ascribed for these structures: stress fields acting in ENE-WSW, NW-SE and NNW-SSE directions, shock waves produced by earthquakes or meteoritic impacts, and compaction resulting in density inversion and over-pressurized groundwater.

Keywords: Deformation structures, geodes, undulations, flowage structures, slickensides, stylolites and boudinage structures.

1. Introduction

The Late Cretaceous deposits in Jordan hold different lithological, paleontological and mineralogical layers from detrital to carbonate rocks changing into chalky rocks at the end of this period. The area where these rocks are found has been strongly affected by sea level fluctuations and tectonic movements reflected in the sedimentary deposition and structural geology. The deformation rate of the rocks depends on many factors, including lateral stress fields, confining pressure, temperature, stress rates, and most importantly competence-incompetence behavior of rock materials (Means, 1976; Earle, 2015). The Upper Cretaceous deposits are found distorted in many areas in Jordan and the deformed structures are considered to represent a record of the history of the area related to the paleostress fields that caused the deformation. Rock deformation can develop during deposition or shortly after burial but before the sediment was lithified or cemented. On the other hand, deformation can be the result of post-deposition processes, usually associated with tectonic activity, earthquakes, shock waves, and differential load pressure. The present work is organized to introduce a variety of deformation structures in the Upper Cretaceous rocks in Jordan and study their relationship to tectonic and non-tectonic deformation. Each of the deformation structures is discussed individually below.

1.1. General Geological and Tectonic Overview of Jordan

The history of Mesozoic deposition in Jordan reflects the Tethys Sea level fluctuations and its relation to the geological development of the Arabian Plate. In Jordan, the Cretaceous deposits comprise three lithostratigraphic groups: the Kurnub, the Ajlun and the Balqa Groups which are bound and divided by regional unconformities (Powell 1989; Powell et al., 1996; Flexer et al., 2005).

Generally, most of the deformation structures investigated in this study are found in the Upper Cretaceous rocks from Ajlun and the Balqa Groups. Late Cretaceous sediments are exposed almost all over Jordan from the north of Irbid to the south of Ras en Naqab escarpment (Fig. 1a). During the Cenomanian and Turonian, the Ajlun Group was deposited when Jordan was located at the northwestern margin of the Arabian-Nubian shield, comprising Formations: Na'ur Limestone, Fuheis, Hummar, Shueib, and Wadi (As)-Sir Limestone (Burdon, 1959; Bender, 1974; Powell, 1989) (Fig. 1b). The thickness of this group increases towards the north with maximum reaching about 600 m in Irbid and decreases in the southern part of Jordan (Powell, 1989). The depositional environment of this group is shallow marine mainly depositing limestone with intercalated clay, marl and gypsum beds from Shueib Formation (Powell, 1989; Bandel and Salameh, 2013).

The Ajlun Group is covered by Balqa Group, which is composed of chalk, chert, marls, and phosphorites reflecting changes in the chemistry and temperature of the sea in Coniacian time (Bandel and Salameh, 2013). The Formations included in this Group, from older to younger, are: Umm Ghudran Formation, Amman Silicified Limestone Formation with much chert (Santonian and Campanian), Ruseifa Formation with much phosphatic sand (Campanian), and the Muwaqqar Chalk Marl Formation (Maastrichtian) at the top (Bandel and Salameh, 2013).

Umm Ghudran Formation is characterized by chalk-rich sediments covering most of Jordan's territory. In the south-

* Corresponding author. e-mail: i.alhejoj@ju.edu.jo

east carbonates grade into fluvial sands and clays. Phosphates were deposited during the Campanian where the Tethys Sea had been rich in organic matter with oyster bioherms (Powell, 1989). The paleo-climate during the Cretaceous according to Francis and Frakes (1993) was characterized by a cold and warm climate as follows: Albian, warm; Cenomanian, cold; Turonian, cold; Coniacian, warm; Santonian, cold; Campanian, cold and Maastrichtian, cold.

Jordan was part of Gondwanaland when that land fragmented into smaller plates one of which is the Arabian- Africa Plate. The Syrian Arc represents a fold-thrust belt which extends from NW Sinai through the Jordan Rift Valley northward to Central Syria, which was active during the Coniacian - Miocene, and is still today (Chaimov et al., 1992; Diabat, 2009). As result of the Syrian Arc compressive stresses with E-W to ESE-WNW, the Shueib Structure and the Amman-Hallabat Structure were formed (Mikbel and Zacher, 1981; Diabat, 2009) (Fig. 2).

Furthermore, a very strong tectonism affected the area creating the Dead Sea transform fault with the N-S/NNE-SSW trending Wadi-Araba-Dead Sea-Rift system. This was initiated with the beginning of the spreading process at the Gulf of Aden during the Late Miocene causing the northward movement of the Arabian Plate, which has been existent since then (Bender 1968, 1974). Along the Dead Sea Transform Fault system, a sequence of pull-apart basins (Gulf of Aqaba, Dead Sea, Lake Tiberias), interrupted partly by transpressional segments, were formed in the consequence of the sinistral transform movement which has caused until today a lateral displacement of Jordan of around 110 km to the north compared to the Sinai-Levant Sub-plate (Quennell, 1959; Freund et al., 1968; Garfunkel, 1981; Bandel, 1981). The rift system is filled by sediments of mid-Miocene to recent ages (Andrews, 1992; Alhejoj, 2013). Regional tectonic and structural elements are studied by Burdon (1959), Salameh and Zacher (1982), Atallah (1992), Diabat et al. (2004), Diabat (2009, 2013, 2015), and others. Eyal and Reches (1983) and Eyal (1996) studied tectonic analysis of the Dead Sea Rift region since the late Cretaceous based on mesostructures in Palestine and Sinai, and identified two tectonic stress fields, each relatively uniformed in both time and space. One stress field, is the Syrian Arc stress with a dominating maximum horizontal compression trending W to WNW, in the Late Cretaceous to Eocene rocks in the folds and plateaus west of the Dead Sea rift. The second field, is the Dead Sea stress with a dominating horizontal extension trending E to ENE.

Few studies on paleostress were carried in the eastern side of the Dead Sea Transform (DST). The first study was carried out by Zaineldeen et al. (2002). Eight paleostress tensor groups (stages) have been identified from their study, ranging from the Late Neoproterozoic to the Holocene period, and have been correlated with the tectonic evolution of the Dead Sea Rift. Diabat et al. (2004) studied the paleostresses at the eastern rim of the DST. Their results summarize the stress field east of the DST in two compression stress systems, namely the NNW-SSE Dead Sea System (DSS), and the Syrian Arc System (SAS) with a stress field in NW-SE direction (Fig. 2). Al Khatib et al. (2010) measured fault slip data in the Upper Cretaceous (Turonian) rocks of Northern Jordan. The orientation of the studied paleostress showed E-W to WNW-ESE compression, and N-S to NNE –SSW extension associated with the formation of the Syrian Arc fold belt which started in the Turonian. Another paleostress has NW-SE to NNW-SSE compression and NE-SW to ENE-WSW extension related to the Dead Sea transform system. Recently, Al Hseinat (2009) has studied the relationship between the formation of the Wadi Shueib fold-belt and the Dead Sea Transform based on anticlines, synclines, monoclines, flower structure, and thrust fault structures. He stated that the formation of the Wadi Shueib Structure is a contraction horsetail formed due to the termination of the Wadi Araba sinistral strike-slip fault.

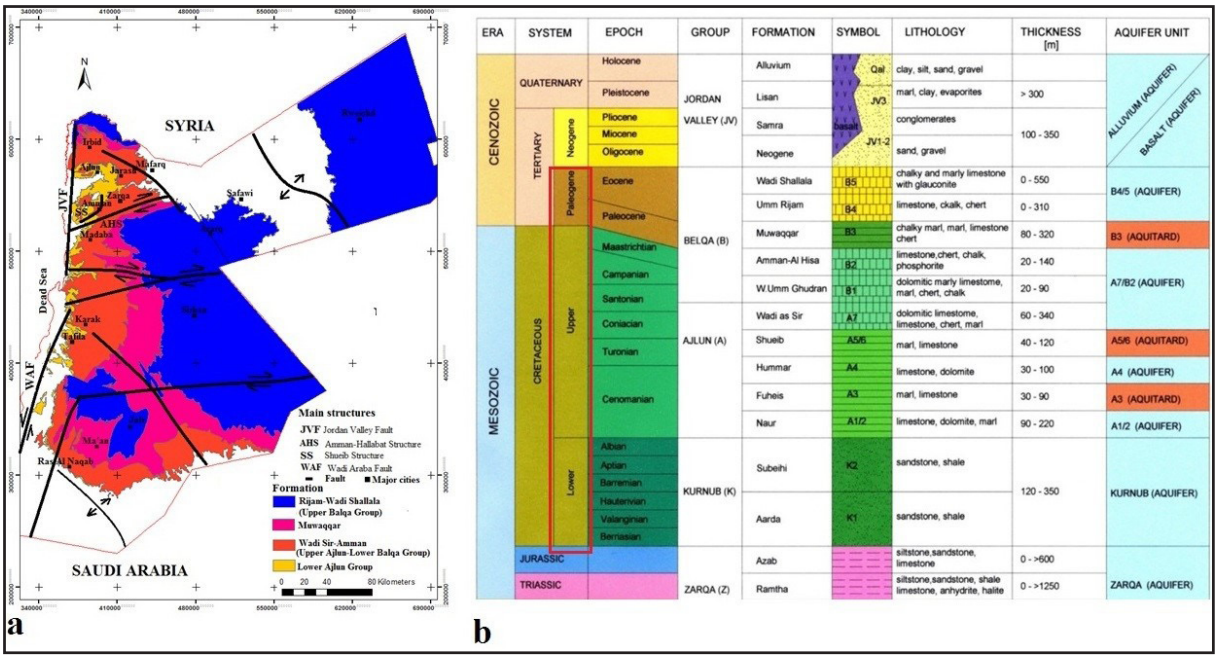

Figure 1. a, Simplified geological map showing the outcrops of Upper Cretaceous Formations and the main structural features in Jordan based on NRA maps (NRA open files) (Jordan Transverse Mercator Projection, JTM). **b**, Sequences of Triassic to Recent lithostratigraphic units in Jordan (Mc Donald and Partners, 1965; Bender, 1968; NRA open files).

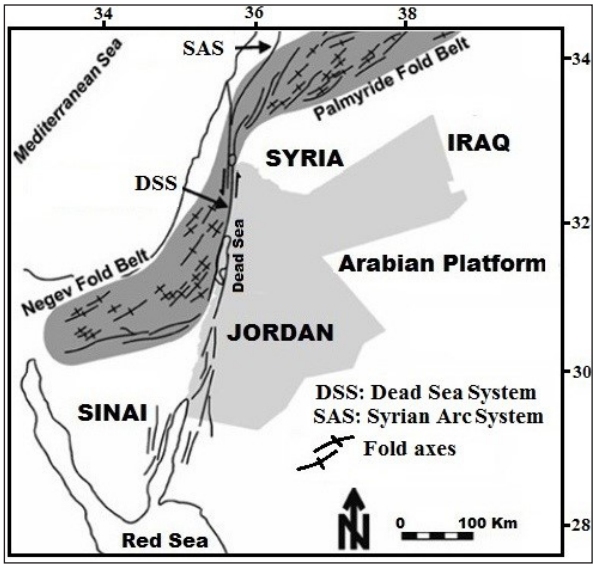

Figure 2. Major tectonic setting of the Dead Sea Transform and the Syrian Arc, in the north-western part of the Arabian plate (modified after Chaimov et al., 1992).

2. Methodology

This work is based on field observation, measurements, and literature review of mesostructures and their formation mechanisms in general and data in the literature about their presence in Jordan. The stress fields which have been active in Jordan since the Upper Cretaceous times are well-known and documented in the geologic literature on Jordan, especially in Burdon (1959), Quennell (1959), Bender (1968), Zaineldeen et al. (2002), and Diabat (2004).

The interpretation of the mechanisms and forces leading to the formation of the different structures is based on field mapping (Fig. 3), measurements of structure and advances in tectonic explanations of deformation.

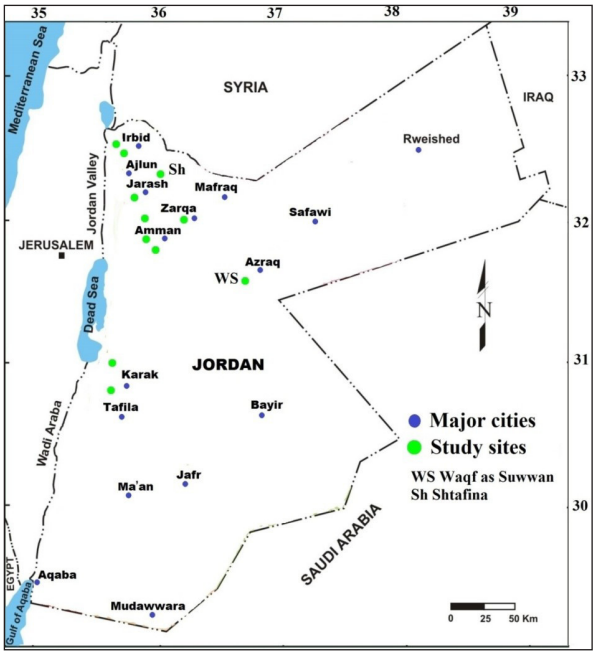

Figure 3. Location map of sampling and measurement sites.

3. Description of the Deformation Structures

3.1. Silica Geode Structures

Geods have a spherical to oval shape with varying diameters between 2cm- 50 cm and are often found in limestone or dolomite beds. In a dolomite bed of the Na'ur Formation at a distance of about 3 km to the north of the University of Jordan, silica geodes were found. Geods are restricted in distribution to an area of about 5000 m² , and are present in one dolomite bed of 1m thick in the middle part of the Formation which is 230 m thick. In a lateral extension, chert lenses and layers are distributed vertically in a range of a few meters in the underlying and overlying limestone beds of the dolomite bed. This structure observed in the south of Ma'an area is chalky limestone and sandstone layers from Wadi Umm Ghudran Formation. They are usually filled with fine- grained quartz crystals (Fig. 4a).

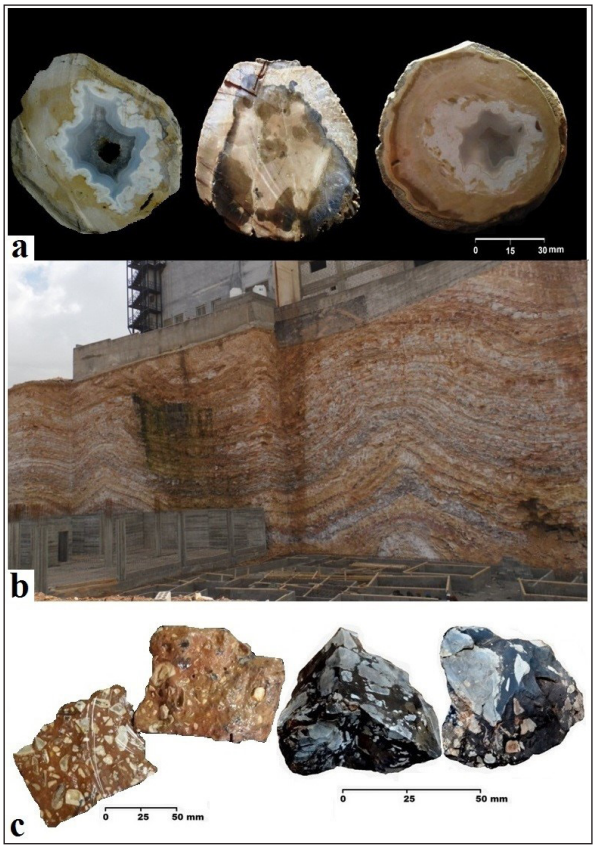

Figure 4. Different deformation structures from the study area, **a**. Spherical and semi-spherical silica geods filled with quartz crystals from Na'ur Formation, North of Amman area, 3km north of the University of Jordan, **b**. Undulations in the Amman Silicified Limestone Formation exposed along Amman – Zarqa, **c**. Chert breccias rocks from Amman Silicified Limestone Formation, Ajlun, Shtafina area.

3.2. Undulation Structure

In the highlands of Jordan extending from Irbid in the north to Karak in the south, the Amman Silicified Limestone Formation shows undulations (folding, disharmonic folding) (Fig. 4b). This Unit, of the Campanian– Maastrichtian age, is composed of chert beds, each a few mm to one meter of thickness. They alternate with silicified limestone, marl, and

silicified phosphate beds, the latter increase upward. The thickness of the Unit can reach 140 m, but in average it is 60 – 70 m (Ruef, 1967). The different chert beds show generally no change in their thicknesses on a scale of kms. But the chalk and marl beds thicken in the fold troughs, and are thin along the flanks. According to Ruef (1967), the cherts are composed of 93 % SiO_2 and about 2 % H_2O. All the chert layers show internal brecciation with very sharp grain edges embedded in a very fine groundmass composed of SiO_2.

The number of undulation reaches thousands, while the overlying and underlying marl and marly limestone rocks of the Amman Silicified Limestone Formation show no undulations at all. The amplitudes of undulations range from decimeter to about 10 m. Undulations are generally convex structures. Concave undulations are very rare. The areal distribution of the undulation is irregular. The strike direction of the undulation axes range from 150˚ to 210˚ (330˚ - 30˚) fluctuating around the N–S direction. Generally, the undulation axes plunge to the north with small varying degrees of up to 15˚ (Table.1).

The verging of undulations (inclination axial surfaces) is generally towards the west. Thickening and thinning of folded beds are present in the less competent, gliding-mobile beds of chalk marl and are almost absent in the chert beds. Thickening is, as expected, found in fold troughs and crests, and thinning along the fold flanks.

Table 1. Field measurements of strikes of horizontal stylolite's peaks, slickensides surfaces with horizontal movements, undulations folding axis and shortening directions in fossils in the different sites in Jordan. In addition hundreds of measurements are found in the literature e.g. Ruef (1967), Salameh and Zacher (1981). For locations refer to Fig. 3. (NF, not found)

Site	Stylolite	Slickensides	Undulations	Deformed fossils
Maan	NF	340˚-20˚ (16) 60˚-75˚ (11)	340˚-10˚ (8) 80˚-90˚ (3)	NF
Karak	352˚-10˚ (25) 115˚-140˚ (12)	330˚-10˚ (27) 70˚-80˚ (12)	350˚-40˚ (25) 70˚-80˚ (10)	N-S
Mujib	350˚-360˚ (3) 110˚-118˚ (12)	350˚-20˚ (24) 65˚-80˚ (12)	0-26˚ (21) 70˚-82˚ (12)	N-S and E-W
Jiza	NF	350˚-10˚ (22) 80˚-85˚ (9)	350˚-112˚ (18) 70˚-72˚ (6)	10˚-20˚ and 70˚
Madaba	350˚-10˚ (17) 115˚-120˚ (8)	350˚-18˚ (33) 70˚-88˚ (8)	15˚-26˚ (17) 90˚-0(6)	N-S and 115˚
Amman	360˚-15˚ (6) 115˚-125˚ (13)	355˚-22˚ (28) 74˚-86˚ (17)	10˚-25˚ (61) 75˚-84(12)	N-S and 120˚
Ajlun	355˚-10˚ (21) 110˚-140˚ (8)	330˚-10˚ (26) 70˚-80˚ (6)	10˚-18˚ (12) 80˚-83˚ (6)	N-S and 115˚
Irbid	350˚-6˚ (16) 120˚-125˚ (3)	350˚-30˚ (18) 70˚-83˚ (6)	5˚-20˚ (32) 80˚-85˚ (8)	N-S and 125˚
Azraq, Hallabat & Waqaf as Suwwan	10˚-12˚ (3) 120˚-130˚ (4)	10˚-20˚ (8) 90˚-100˚ (4)	NF	N-S and 120˚-125˚

3.3. Brecciated Chert

The Amman Silicified Limestone formation does not only show undulations (disharmonic folding), but in addition, its chert beds are strongly brecciated (Fig. 4c). Angular fragments of chert which range in size from a few mm up to 10 cm are sharp – edged without any sign of roundness or even weathering and with no special spatial orientation.

The brecciation is strictly confined to chert beds, and it is evenly distributed between troughs and flanks of folds and along not folded chert layers. The brecciated chert lies in a groundmass of silica SiO_2 of a supposedly younger formation age.

3.4. Deformed Fossils

For a long time, the deformation of fossils has been considered as a significant structural geologic tool, caused by tectonic activity. Such deformation can give important clues on paleo-stress fields and their directions (Sharp, 1847; Breddin, 1956). The comparison of deformed and non-deformed fossils gives evidence about the type of stresses responsible for the deformation, the directions in which these stresses were acting, and the magnitude of the stresses causing them.

In Jordan, different groups of fossils are found deformed in the Upper Cretaceous rocks (Figs. 5a, b). These are widely distributed in Ajlun (Shtafina) (Fig. 5c), Umm Dananier, Wadi Mujib and Jabal Waqf as Suwwan areas as discussed by Alhejoj et al. (2013). Two types of deformation are noticed in the fossils of these areas: ductile and brittle. In the ductile deformations, fossils are found compressed in one direction and expanded in the other direction perpendicular to the first with different shortening or expansion ratios based on the composition of the fossils, the stress field type, its strength, and the relative rheological behavior of the embedding rock and fossil materials. The brittle types of deformation are also present with some fossils showing shear with very prominent shear surfaces as can be seen on the deformed fossils of Jabal Waqf as Suwwan which are also rewelded along the shear planes.

3.5. Slickenside Structures

Slickensides refer to striated, polished rock surfaces of deformation structures along the shear zone movement. They are developed on vertical and inclined to horizontal rock discontinuity surface, and are very common in the Late Cretaceous rocks in Jordan (Fig.6). On a vertical and inclined rock surface, horizontal slickenside movements are both sinistral and dextral. Sinistral slickensides are generally found on rock discontinuity surfaces striking NNW –NNE (330˚ – 30˚) mostly (350˚ – 20˚), whereas dextral slickensides

developed on surface strikings ENE – ESE (60˚ -120˚) but mostly (70˚ -100˚)(Table 1).

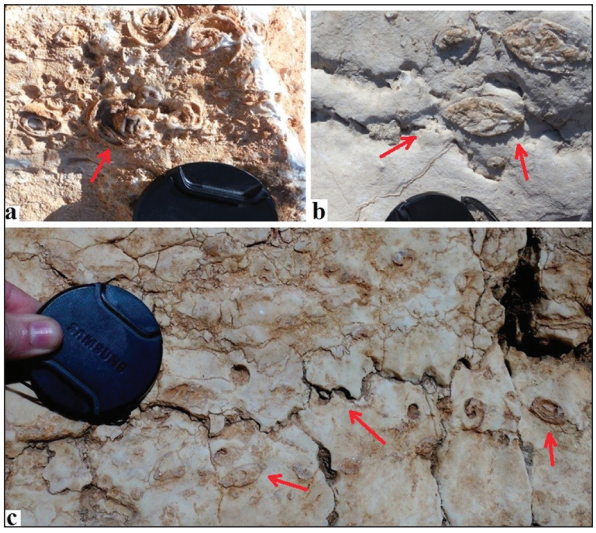

Figure 5. a. Broken fossils from Ajlun area, **b**. Deformed fossils of gastropods (original shape rounded) associated with vertical peak stylolites in Ajlun area, **c**. Deformation of gastropod fossils found together with stylolites from Wadi-Sir Formation in Shtafina area, Ajlun. (Arrows refer to the deformed fossils and stylolites structures).

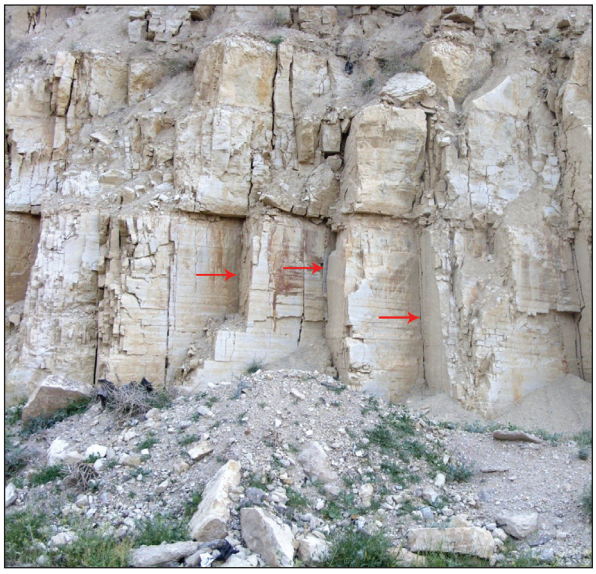

Figure 5. Slickensides in the Upper Cretaceous rocks in Zarqa-Hallabt area (arrows indicate the movement direction).

3.6. Stylolite Structures

Stylolites are secondary structures with a tooth-like shape. They form due to a pressure–solution process affecting mainly sedimentary rocks (Park and Schot, 1968). Stylolites can be classified into sedimentary stylolites and tectonic stylolites. Sedimentary stylolites (Vertical– peak stylolites) are overload structure thought of to be formed during the rock diagenesis (lithostatic pressure), while tectonic stylolites are produced by tectonic processes, and can be used as indicator of paleostress directions (Fabricius and Borre, 2007; Ebner et al., 2010).

Two main types of stylolites are found in the Upper Cretaceous carbonate rocks in Jordan in the form of: horizontal peak stylolites (H–peak stylolites), and vertical peak stylolites (V–peak stylolites) (Fig. 7 and 8a). Oblique stylolites are also observed in the Ajlun area (Fig. 8b).

Stylolites are mainly observed in Wadi-Sir and Hummar Formations which are, to a great extent, composed of almost pure limestone (Fig. 8c). These stylolites are well- developed in the above-mentioned rock Formations, and their peaks may reach a few centimeters in height (Figs. 8d,e).

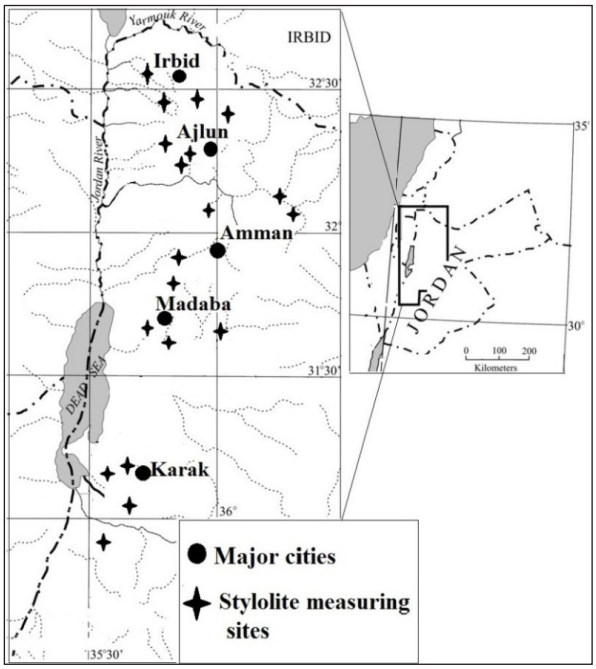

Figure 7. Stylolite measuring locations.

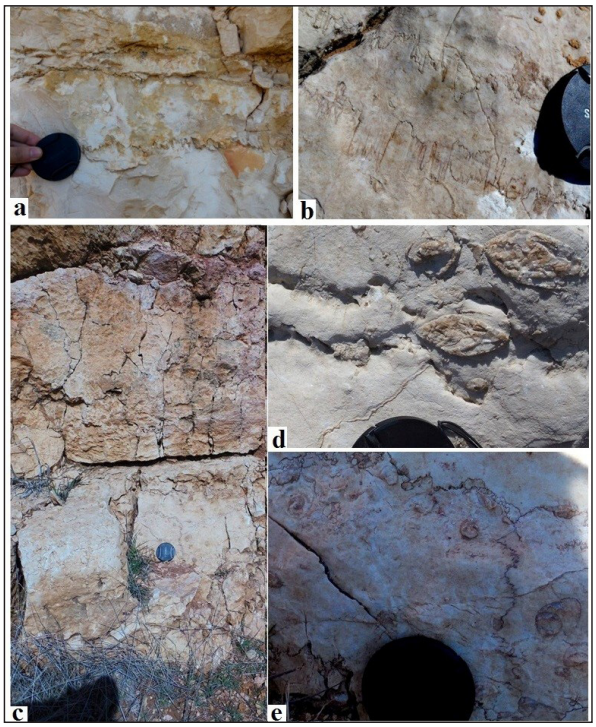

Figure 8. Studied stylolites from Ajlun area, **a**. Vertical-peak stylolite in Wadi-Sir Limestone Formation, Ajlun, **b**. Oblique stylolite in Wadi-Sir Limestone Formation, Ajlun, **c**. Horizontal- peak stylolites in Wadi-Sir Limestone Formation, **d**. Deformed fossils and the stylolites have the same stress field, Wadi-Sir Limestone Formation in Ajlun area, **e**. Close-up of figure (8c) showing tectonic stylolites associated with deformed fossils, Ajlun.

3.7. Flowage Structures

Early Cretaceous sandstones underlie the calcareous Late Cretaceous rock sequences in Jordan (Fig. 9a, b). The transition beds between them are about 10 m thick and consist of marls, clays and silty marls with a density of about 2.30 g/cm^3 and a permeability of about 10^{-7} to 10^{-8} m/s compared to that of the underlying almost pure sandstone (about 1.92 g/cm^3 and 5x 10^{-5} m/s) (Salameh and Udluft, 1985). The transition zone shows a variety of density inversion structures such as the boulders of sandstone which have moved a few meters upward into the marly clayey higher density rocks and vertical flow channels that are up to 20 cm wide and filled with sand, along which the friable to semi-consolidated sand of the Early Cretaceous had moved upwards through the transition zone into the Late Cretaceous rocks or through them to the ground surface (Al-Saqarat, 2009). This structure is clearly exposed in Ajlun area and along Irbid road (Fig. 9c,d).

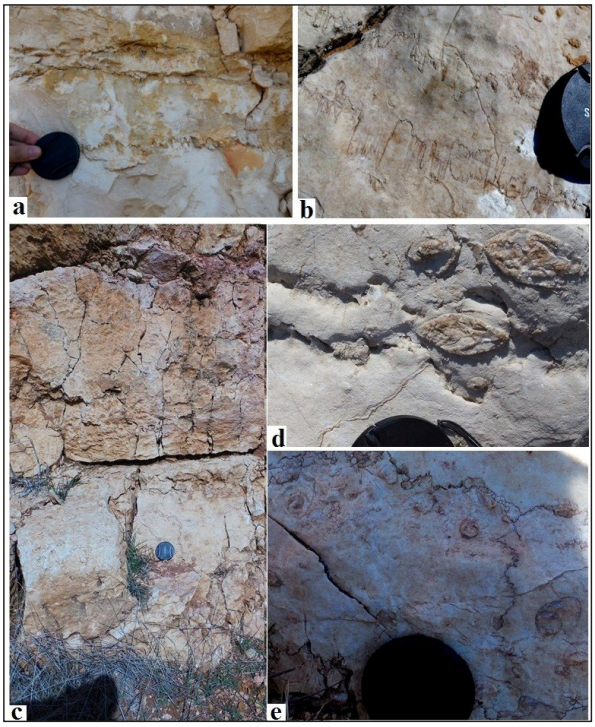

Figure 9. a, Horizontal clay flowage structure in between two hard rock beds of limestone; Ajlun, **b**. Close- up of clay flowage structure between hard blocks of Wadi- Sir Limeston Formation, **c**. General view of clay flowage from Wadi-Sir Limestone Formation in Ajlun area, **d**. Horizontal clay Flowage appears at Irbid city main road.

3.8. Nodular Limestone

The term nodular limestone has been used to include several types of textures that are of genetically different origins. In general, nodular limestone forms by the precipitation of amorphous silica, in the case at hand from spicules of sponges or debris of radiolaria and the post depositional replacement of either the enclosing limestone or chalk by this silica (Boggs, 2009).

Small, irregular rounded and sub-rounded pieces of chert nodules are found within some limestone beds of the Upper Cretaceous rocks of Jordan (Fig. 10).

Figure 10. Nodular limestone in Wadi-Sir Formation as exposed along the Dead Sea road, near Na'ur town.

3.9. Boudinage Structures

Boudinage structures are found in the Upper Cretaceous chert rocks of Jordan. The structure consists of cylinder-shaped pieces of rocks building together thin to thick layers mostly found in the chalky limestone of the Umm Rijam and Shallala Formations, but also in other formations, such as Al-Hisa Phosphorite Formation.

The chert pieces, over- and underlain by the soft rocks of chalky limestone, must originally have built continuous beds of chert, which were then disintegrated into pillow-like pieces. It seems that the incompetent chalky limestone beds reacted to the overburden vertical pressure by flowage, and the rigid competent chert beds reacted by disintegration into pieces. Dissolution of the edges of the chert pieces and borders took place afterwards by the descending water, and their real location changed by pressure and flowage of the chalky limestone components.

Field observation shows that boudinage affects a single layer of chert as a result of its extension in a direction parallel to itself. The boudinage breaks up the layer into a series of discrete segments, each showing a barrel-shaped cross-section, separated from one another by a narrow neck of rock (Fig. 11).

This structure is also found in phosphorite deposits of Al-Hisa Phosphorite Formation, especially in the southern part of Jordan (Fig. 12). The Formation is given Campanian to Maastrichtian age (Bender, 1974). Muwaqqar Formation is of Maastrichtian to Paleocene age (Bender, 1974; Bandel and Salameh, 2013).

Figure 11. Boudinage chert layer bounded by soft chalk layers from Muwaqqar Formation in northwestern Irbid near Al Maqarin area.

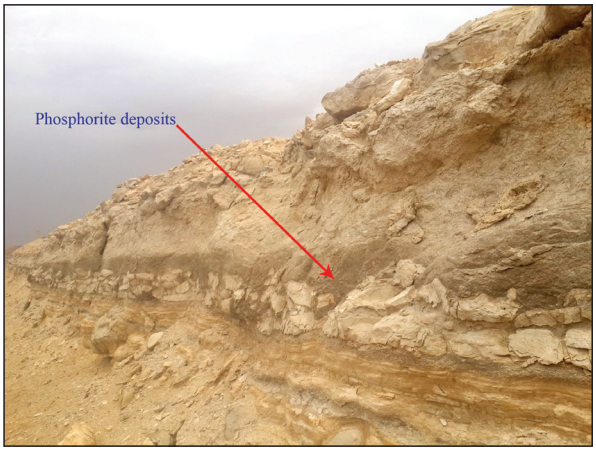

Figure 12. Deformation of phosphorite layer of Al-Hisa Phosphorite Formation is exposed along the Kings Highway, south of the Karak area.

2. Discussion of the Deformation Mechanisms

In the calcareous Late Cretaceous rock sequence in Jordan, a variety of meso structures are present, such as vertical, horizontal and network stylolites, horizontally deformed fossils, slickensides, flow channels, density inversion, undulations among others.

Such structures of tectonic and non-tectonic origins may be used to define the stress fields affecting the rock sequences as well as the type and nature of the stress fields.

Silica geode structures were studied by Salameh and Schneider (1980). The external diameter of the concentrically structured geodes ranges from 8 – 18 cm. Generally, the outer layer is 1 – 3 cm thick, and is composed of silicified dolomite like the host rock. Inwards follow several layers composed of chalcedony, in some geodes alternating with quartz layers. Well crystallized quartz is frequently found inside the geodes.

The structure of the geodes indicates an organic origin, most probably sponges. Hence, the organic matter had influenced the chemical condition of silica precipitation in the geodes. These formations are considered a result of the embedding of the organic matter of sponges in the carbonate sediments of a shallow marine environment to be followed by early diagenetic dolomitization of the carbonate by magnesium – rich pore water in the intertidal environment. After that, opal precipitated from the pore water around the skeleton of organisms. In some cases, the soft silica shrank, and was brecciated (Bandel and Salameh, 2013).

The formation of these geodes and their partially fragmented (brecciated) inner rings are referred to early diagenetic processes accompanied by shrinkage of the still soft silica gel as a result of crystallization and aging.

Because the brecciation of the geods only affects the intermediate and outer chert layers, it can be concluded that a shockwave, during that stage of silica deposition, affected the rocks. After that shockwave, the precipitation of quartz continued filling the geods. Geods totally filled at the time of the shockwaves are, as a whole, brecciated.

In southern Jordan, Makhlouf et al. (2015) studied the quartz geods from the Upper Cretaceous Wadi Umm-Ghudran Formation and stated that their silica composition comes from the weathering of the Amman Silicified Limestone Formation and the infiltration of chemical products by the action of groundwater.

The undulation structure of Amman Silicified Formation was discussed by Ruef (1967). After a rigorous study of the undulations in the Amman Silicified Limestone Formation, he concluded that tectonic forces have to be excluded as initiators of the folding. He favors E-W directed gravity movements (syn-sedimentary gliding) of the mobile sediments, where silica and limy layers served as a means of gliding. According to Ruef , the gravitational movements were intensified by seismic impetus and other non – tectonic factors. Schneider and Salameh (2014) have attributed the triggering of the formation of the undulation to the meteoritic impact event of Jabal Waqf as Suwwan (Salameh et al., 2006 and 2008) which took place in an area lying E and SE of the area of undulation. Here, within the rock sequence, the chert beds played the role of competent beds, and the marl beds the role of incompetent beds which reacted by gliding as well as by the flow of the ductile material collected in folding troughs and crests.

The Suffield Tests explosive TNT experiments (Price, 2001) showed that the maximum principal stress during explosions acted radically generating a series of peripheral folds of small-wave lengths and amplitudes. The stress acted perpendicular to the folding axis. This test supports the hypothesis that a meteoritic impact has caused the undulation in the Amman Silicified Limestone Formation, and that the impact site should lie to the east or west of the Dead Sea area at a few tens to one hundred kms: Waqf as Suwwan lies 80-100 km east of the undulating beds. The general verging of the folding axial planes to the west supports an impact site at around 100 km east of the Dead Sea.

Assuming that an impact was the source of shock waves causing the disharmonic folding, then the internal brecciation of chert beds must be restricted to the consolidated brittle pre-existing chert beds, which is the case in the Jordanian Silicified Limestone Unit. Therefore, the assumption of the impact of shockwaves contradicts and challenges the gravitational gliding which assumes that the rocks were still unconsolidated, and could gravitatively flow. Field evidence does not support gravitational gliding, because of the very low variability in the forms and geometry of the undulation and in the strike and plunge of their axes.

Regarding the brecciated Chert formation mechanism, until now no satisfactory explanation has been provided to clarify the brecciation of the chert beds. Disharmonic folding as a cause of the brecciation is discarded by the fact that not folded chert layers are brecciated.

Agitation during digenesis can also be discarded because chert nodules do not show brecciation. It seems that after hardening, the chert beds were exposed to sudden stresses, which due to their brittle nature had led to their brecciation. Such sudden stress can be referred to the shockwaves of an impact event. Shockwaves of impacts produce love waves, which create horizontal differential rock movements with a reflection of waves within the rock itself and energy remaining in the rock (Hiller and Schneider, 1967). Such mechanism may well lead to brecciation and agitation of the brittle chert beds.

Studied slickensides structures occur on preexisting joint surfaces representing Riedel joints of a tectonic stress

field in a general N–S direction (Burdon, 1959), which is the most recent stress field that has been affecting the Arabian Shield area east of the Mediterranean (Zaineldeen et al., 2002). Some folding structures show also slickensides as a result of differential interlayer movements in the direction of the a-fold axis. These are classified as tectonic slickensides. Tectonic as well as non-tectonic slickensides are found developed on vertical and inclined rock discontinuity surfaces with movements resulting from the overload of the overlying rocks and gravitational sliding. Such Slickensides accompany fault and flexure structures. Tectonic slickensides on inclined surfaces are also present along the major flexures of Suweima – Hallabat and Shueib – Suweileh.

One other studied deformation structure is deformed fossils which were observed, firstly by Alhejoj et al, (2013). They stated that the deformation directions of fossils in the Late Cretaceous rocks of Jordan correlate to the structures produced as a result of unambiguous stress fields. These authors, and formerly Quennell (Burdon, 1959), concluded that Jordan was exposed during its geologic history, in Tertiary and Quaternary times, to different stress fields in an ENE-WSW direction, followed by a NW-SE strong stress field which produced the Syrian Arc, Sweima-Hallabat and Shueib-Suweilih structures. It was finally followed by another strong stress field in a NNW-SSE direction which resulted in the formation of the Dead Sea Transform Fault and the accompanying structures. The studied deformed fossils in the Ajlun area were found horizontally deformed in the same directions of the formerly well-known stress fields producing other structures in the area such as folds, stylolites, reverse faults and flexures. This unambiguously shows that even if other structures indicating stress fields are not found, deformed fossils can well be used as paleostress indicators.

Although, the deformation of Late Cretaceous fossils indicates the three above- mentioned stress fields well-known before namely, ENE-WSW, NW-SE and NNW-SSE, it has not been attempted to obtain information on the history of the stress field evolution from the deformed fossils themselves. Furthermore, deformed fossils in Waqf as Suwwan impact area shows deformation stress directions originating from the center of the impact.

It is worth mentioning that not all deformation of fossils result from tectonic activates, but compaction process can cause deformation of fossils such as the deformed gastropod fossils in the Wadi Mujib area, Jordan (Alhejoj et al., 2013).

An important deformation structures discussed in this work are stylolites especially, horizontal – peak stylolites striking in three directions with trending peaks mainly in 140˚–160˚, rarely in 70˚–80˚ and common in 170˚–190˚. These stylolites are of tectonic origin and reflect the well-known three consecutive stress fields Jordan was exposed to during the Late Tertiary to Recent times. According to Quennell (1959), the first stage of stress was in an ENE – SWS direction, while the second was in NW-SE, and the third was NNW – WSW direction reflected in the formation of the above-mentioned stylolite directions (Fig. 13). The rarely occurring stylolites (Network stylolites) resulted from a combination of tectonic H–peak stylolites and diagenetic V–peak stylolites, and are found accompanying the other two types of stylolites.

Schneider and Salameh (2014) attributed the 140˚-160˚ striking horizontal stylolites and the network stylolites to Waqf as-Suwwan meteoritic impact event which hit the area lying SE of Ajlun and Amman, where most of the 140˚-160˚ striking stylolites are found (Table.1). The stress fields obtained from the interpretation of horizontal–peak stylolites of ENE-WSW, NW-SE, and NNW-SSE are the same which have been obtained from the interpretation of stresses producing the deformed fossils (this study).

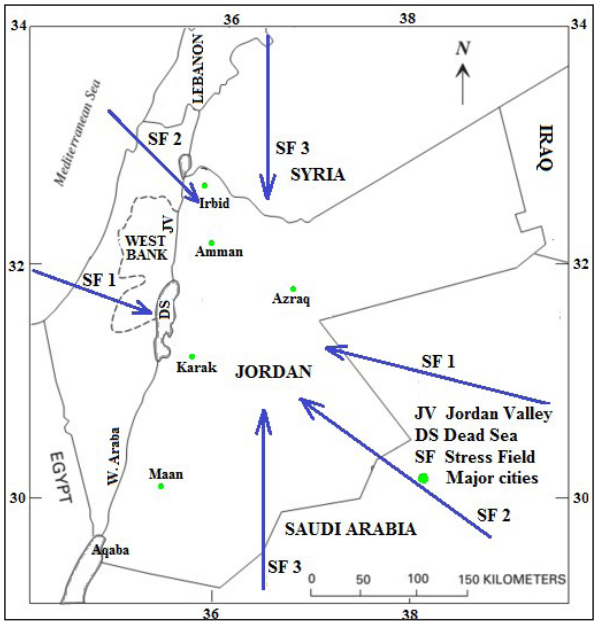

Figure 13. Stress fields affecting Jordan during Neogene to recent times (based on Quennell 1959).

Flowage Structures are also a good example of soft deformation structures. The flow channels seem to have served as escape paths for the over-pressurized Lower Cretaceous semi-consolidated sands caused by the withdrawal (regression) of the Tethys and the very slow process of water pressure releases controlled by very low permeability of 10^{-8}-10^{-9} m/s . The factors which resulted in the upward flow of the sand are: a) the friable nature of the sand b) the increasing pressure in the sand caused by the retreat of the Tethys and the epirogenic upward land movement resulting in lower water pressures in the overlying rock units of Upper Cretaceous age compared to those of Lower Cretaceous age c) a triggering factor causing liquefaction of the over-pressurized friable sands. The triggering factor can be a very strong earthquake, may be > 8 on the Richter Scale, or it could be the result of shock waves like those produced by Waqf as-Suwwan meteoritic impact (Schneider and Salameh, 2014).

The formation mechanisms of Nodular Limestone are interpreted by Abed and Schneider (1980) saying that this structure may have originated by the activities of burrowing organisms such as *ThaIassinoides, Cauianassa or Ophiomorpha*. On the other hand, the origin of this structure also appears to be caused by digenetic processes of highly fractured, disintegrated limestone of about one decimeter in side length. Because crustacean burrows are common in all Cenomanian and Turonian_limestones in Jordan and not restricted to those of the lagoons.The nodules are generally composed in their core part of limestone or dolomitic

limestone surrounded by a veneer of silicified limestone. This shows that after fracturing, solutions infiltrated and caused the deposition of the veneers. Such solutions can be the result of silicate dissolution by acidic water and deposition when the pH of the infiltrating water rises. Fracturing in small pieces can be brought about by shock waves, and dissolution of silicates can be the result of acid rain (e.g. of meteoritic impacts). But it is also likely that these nodules resulted from the general bioturbation in the original sea floor mud of that time. Crab burrows helped in keeping the water of the sediment oxygen-loaded, but that must have ended when digenesis began to transform the mud and sand into nodules. Also the depth of sediment needed for the change from aragonite to calcite and limestone is vital.

The last structure to be discussed is the boudinage structure. Geologic field observation allows this structure to be interpreted as post-deposition process resulting from tectonics causing the formation of the Syrian Arc (Coniacian–Miocene). This produced load pressure and lateral expansion of the soft and gliding-mobile over- and underlying sediments and breaking of the rigid chert into pieces and deforming the phosphorite deposition in Jordan.

Field observation, measurements, previous work and the results of the current work show that the brittle deformed and smashed fossils in soft materials and finely smashed and brecciated chert beds underlain and overlain by less competent limestone rocks indicate the rapidly-acting stress fields (shock waves), which did not allow for the slow accommodation of stresses by ductile deformation.

Stylolites, slickensides and ductile deformed fossils in horizontal direction seem to have developed as a result of gradually developing, long lasting stress fields.

The deep burial of rocks lead to stronger compaction of clays and marls than sandstone. According to Wunderlich (1966) a burial depth of about 500m results in a density inversion between the sandstones with their higher density when deposited at the ground surface, compared to clays and marls under the same conditions. This seems to be the case at the interface of the Lower Cretaceous sandstone and the Upper Cretaceous calcareous rocks where the interface is composed of about 10 m of clays and marls (Bandel and Salameh, 2013). The burial thickness before eroding the top layers covering the Upper Cretaceous rocks which crop out at the ground surface at the present was estimated by Wiesemann (1969) to be at least 1000m. Under this load pressure, the density of the sandstone becomes 2.10 g/cm^3 and that of the clays and marls 2.35 g/cm^3. When adding to this situation the condition that the sandstones are only very weakly cemented in many parts, or even friable, and the groundwater in most parts of them is still confined or over-pressurized, it becomes clear that the layering conditions are label and the system is prune to density inversion and even to releases of over-pressure in them. Actually, density inversion and upward flow channels are very clearly found in the transition zone from the Lower to the Upper Cretaceous. Density inversion and flow along channels may require a triggering factor (activation energy) to liquefy the sandstone. But this is easily provided by earthquakes or meteoritic impact shock waves, such as Waqf as-Suwwan impact (Salameh et al, 2008 and Schneider and Salameh, 2014).

Undulations in the silicified limestone and chert beds without any corresponding undulations in the overlying and underlying limestone sequences and even without any macro or micro structures in them, which might indicate gradually developing regional stress fields, open the door for other interpretations. In addition, the very strongly brecciated chert beds, in fragments up to a few cm, cannot be explained by gradual application of stress fields. Most probably, the undulations and the brecciation of the chert beds are the result of shock waves and the reaction of the competent chert beds relative to the over- and under- lying incompetent limestone beds to these shock waves. Shock waves of a magnitude to produce the wide spread phenomena of brecciation and undulation in an area of 50 by 200 km can only be produced by meteoritic impacts (Schnneider and Salameh, 2014).

Furthermore, the formation of the nodular limestone remains a riddle in spite of the advanced ideas about its origin as a result of crap borrows or biogenic origin. However, looking in details at its outcrops with the very narrow joint spacing of less than 10 cm, it seems that strong sudden forces must have affected this thin bedded limestone that is approximately of a 10 cm layer thicknesses. Thus, these rock pieces moved against each other under shear and torque forces, which had led to the breaking of the edges of rock, composed of almost cubic pieces. These forces acted among others horizontally and affected specific rock types functioning as competent beds represented by the nodular limestone which is generally composed of dolomitic limestone. The shock waves producing the shear and torque stresses resulting in the rounded edges of the nodules and most probably in shattering the beds into pieces might be a very strong earthquake, or more probably a meteoritic impact event.

Finally, boudinage of chert and the phosphorite structure of Upper Cretaceous rocks is mainly a result of the stress field causing the formation of the Syrian- Arc.

Conclusion

Mesostructures in the Upper Cretaceous rocks of Jordan are interpreted to have been produced by a variety of mechanisms:

1. Tectonic stress fields acting in ESE - WSW, NW - SE and NNW-SSE in a sequence producing, in addition to faults and folds, also ductile deformed fossils in horizontal directions, stylolites, boudinage and slickensides. These deformation structures took place contemporaneously with the Syrian Arc and Dead Sea Transform Fault and the stress fields causing them.
2. Shock waves of very strong earthquakes or meteoritic impacts produced brittle deformed fossils embedded in soft materials, very strongly smashed chert beds, undulations in the competent chert beds with no undulations whatsoever in the incompetent over and underlying limestone beds and slickensides.
3. Compaction resulted in density inversions, and hence upward migration of less dense sandstone blocks into the overlying denser but very wet clay and mud layers.

4. Over-pressurized groundwater in the Lower Cretaceous sandstone aquifer caused by the retreat of the Tethys, where the over- pressurized groundwater was triggered by shock waves to cause liquefaction in the friable or very weakly cemented sandstone, ended in the upward migration of its groundwater transporting sand grains into and through the overlying clay and marl layers.
5. Chemical precipitation and replacement of organic matter by silicates produced silica geodes.

References

[1] Abed, A., Schneider (1980). A General Aspect in the Genesis of Nodular Limestones Documented by the Upper Cretaceous Limestones of Jordan. Sedimentary Geology, 26: 329-335. Amsterdam.

[2] Al Hseinat, M. (2009). Structural Analysis of the Wadi Shueib Fold Belt, Jordan. Master Thesis. Yarmouk Universtiy, Jordan.

[3] Alhejoj, I. (2013). Macroaquatic fossils in the Pliocene-Pleistocene deposits of Jordan and their living environments as compared with surviving relatives. Ph.D. Thesis, University of Karlsruhe, Germany.

[4] Alhejoj, I., Salameh, S., and Abu Hamad, A. (2013). Deformed Fossils and Related Structures in Jordan. Jordan Journal of Earth and Environmental Sciences, 5: Pages 31- 44. Jordan.

[5] Al-khatib N, Atallah M, Diabat A (2010). Paleostress analysis of the Cretaceous rocks in northern Jordan. Jordan J Earth Environ Sci., 3: 25–36

[6] Al-Saqarat, B. (2009). Mesostructures in the Upper Cretaceous rocks of Jordan and their deformation mechanisms using geotechnical and mineralogical techniques. Ph. D. thesis, University of Jordan, Jordan.

[7] Andrews, I. (1992). Cretaceous and Paleogene Lithostratigraphy in the Subsurface of Jordan. Subsurface Geology Bulletin No. 5. The Hashemite Kingdom of Jordan, Ministry of Energy and Mineral Resources, Natural Resources Authority, Amman, 60 pp.

[8] Atallah M (1992). On the structural pattern of the Dead Sea Transform and its related structures in Jordan. Abhath AlYarmouk (Pure Sciences and Engineering) 1, 127-143.

[9] Bandel, K. (1981). New stratigraphic and structural evidence for lateral dislocation in the Jordan Rift Valley connected with description of the Jurassic rock column in Jordan. N. Jb. Geol. Palaont. Abb., 161, 271-308, Stuttgart.

[10] Bandel K., Salameh E. (2013). Geologic Development of Jordan - Evolution of its Rocks and Life. - Deposit No.690/3/2013 National library, Amman, 278pp.

[11] Bender, F. (1974). Geology of Jordan. Beiträge zur Regionalen Geologie der Erde, 7. GebrüderBornträger, Berlin, 196 pp.

[12] Boggs, S.Jr. (2009). Petrology of Sedimentary Rocks. Cambridge University Press, Cambridge, United Kingdom.

[13] 600pp.).Breddin H (1956). Die tektonische Deformation der Fossilienim Rheinischen Schiefergebirge. Z.dt.geol. Ges.106:

[14] 227-305.Burdon D.J. (1959). Handbook of the Geology of Jordan:to accompany and explain the three sheets of 1: 250,000Geological Map, East of the Rift, A. M.

[15] Chaimov, T.A., Barazangi, M., Al-Saad, D., Sawaf, T., and Gebran, A. (1992). Mesozoic and Cenozoic deformation inferred fromseismic stratigraphy in the southwestern intracontinental Palmyride fold-thrust belt, Syria. Geological Society ofAmerica Bulletin, 104: 704-715.

[16] Diabat, A. (2009). Structural and stress analysis based on fault-slip data in the Amman area, Jordan. J. Afr. Earth Sci, 54: 155–162.

[17] Diabat, A. (2013). Fracture systemsof granites and Quaternary deposits of the area east of Aqaba: indicators of reactivation and neotectonic activity. Arabian Journal of Geosciences, 6(3): 679- 695.

[18] Diabat, A., Atallah, M., and Saleh, M. (2004). Paleostress analysis of the Cretaceous rocks in the eastern margin of the Dead Sea transform, Jordan. Journal of African Earth Sciences 38: 449-460.

[19] Diabat, A. (2015). Structural and Stress Analysis of the Area between Al-Akeider and Mughayer As-Sirhan, Northwestern Badia- Jordan. Jordan Journal of Earth and Environmental Sciences, 7: 37 – 48.

[20] Ebner, M., Toussaint, R., Schmittbuhl, J., Koehn, D., and Bons, P. (2010). Anisotropic scaling of tectonic stylolites: A fossilized signatureof the stress field?.J. Geophys. Res.115: B06403

[21] Eyal, Y. (1996). Stress field fluctuations along the Dead-Sea Rift since the middle Miocene. Tectonics 15: 157–170

[22] Eyal Y, Reches Z (1983). Tectonic analysis of the Dead Sea Rift region since the late Cretaceous based on mesostructures. Tectonics, 2: 167-185

[23] Fabricius IL and Borre MK (2007). Stylolites, porosity, depositional texture and silicates in chalk facies sediments. Ontong Java Plateau-Gorm and Tyra fields,North Sea. Sedimentology, 54: 183-205

[24] Flexer, A., Hirsch, F., and Hall, J.K. (2005). Tectonic evolution of Israel. In: Hall J.K., Krasheninnikov V.A., Hirsch, F., Benjamini, C., Flexer, A. (eds.) Geological Framework of the Levant, v. II: The Levantine Basin and Israel: Historical Productions-Hall, Jerusalem, pp 523–537.

[25] Francis, J.E., and Frakes, L.A. (1993). Cretaceous climates. Sedimentology Review 1:17-30; London (Blackwell Scientific Publications).

[26] Freund R, Zak I, Garfunkel Z (1968). Age and rate of the sinistral movement along the Dead Sea rift, Nature, 220, 253–255.

[27] Freund, R. (1965). A model of the structural development of Israel and adjacent areas since upper Cretaceous times: Geological Magazine, v. 102, no. 3, p. 189-205.

[28] Garfunkel, Z. (1981). Internal structure of the Dead Sea leaky transform (rift) in relation to plate kinematics. Tectonophysics 80: 81-108.

[29] Hiller, W., Schneider, G. (1967). Geophysik. In: Brinkmann, R., Ed., Lehrbuch der AllgemeinenGeologie, Band 3, Enke, Stuttgart, 396-547.

[30] Macdonald Sir M and Partners (1965). East Bank water resources. Central Water Authority, Amman.

[31] Makhlouf, I., Tarawneh K, Moumani K, IbrahimKM (2015). Recognition of quartz geodes in the Upper Cretaceous Wadi Umm Ghudran Formation, Ras En Naqab, South Jordan. Arabian Journal of Geosciences. 1-13.

[32] Means W.D (1976). Stress and Strain. Springer, New York.

[33] Mikbel, S., and Zacher, W. (1981). The WadiShueib structure in Jordan. N Jaharbuch Geol. Paleontol, Monatshefte, 9:215–

[34] 225, NRA: Natural Resources Authority of Jordan (open files), www.nra.gov.jo

[35] Park,W., and Schot, E.H. (1968). Stylolites: their nature and origin. J. Sediment. Petrol., 38: 175-91.

[36] Powell, J.H. (1989). Stratigraphy and Sedimentation of the Phanerozoic Rocks in Central and South Jordan - Part B: Kurnub, Ajlun and Belqa Groups. Geological Bulletin, No. 11. The Hashemite Kingdom of Jordan, Ministry of Energy and Mineral Resources, Natural Resources Authority, Amman, 130 pp.

[37] Powell, J.H., El-Hiyari, M., Khalil, B.M. (1996). Evolution of Cretaceous to Eocene alluvial and carbonate platform sequences in central and south Jordan. Internal Report, Amman, 57 pp.

[38] Price N J (2001). Major Impacts and Plate Tectonics. Routledge, London, 354 p.

[39] Quennell, A.M. (1951). The Geology and Mineral Resources of (former) Trans-Jordan. – Colonial Geology and Mineral Resources 2: 85-115; London.

[40] Quennell, A.M. (1959). Tectonics of the Dead Sea rift. Int. Geol. Congr. 20:385–403, Mexico.

[41] Reuf, M. (1967). Contributions to the stratigraphy and tectonics of the Cretaceous in Jordan and to the genesis of the folded chertlayers.Ph.D. Thesis. Ruprecht-Karl University.

[42] Salameh, E., and Schneider, W. (1980). The Geods of Upper Cretaceous dolomites/Jordan -Influence of calcareous skeletal debris in early diagenetic precipitation of silica- N. Jb. Geol. Palaeont.Mh. H3, 185-192, Stuttgart, Germany

[43] Salameh, E., Khoury, H., Reimold, W.U., and Schneider, W. (2008). First large meteorite impact structure discovered in the Middle East: Jebel Waqf as Suwwan, Jordan. Meteoric and Planetary Sciences.

[44] Salameh, E., Khoury, H., Schneider, W. (2006). Jebel Waqf as Suwwan, Jordan, A Possible ImpactCrater—A First Approach. Zeitschrift Deutscher Gesellschaftfür Geowissenschaften, 157, 319-325.

[45] Salameh, E.,and Udluft, P. (1985). The hydrodynamic pattern of thecentral part of Jordan. Geol. Jb.

[46] Salameh, E., and Zacher, W. (1982). Horizontal stylolites and paleostress in Jordan. N. Jb. Geol. Palaont. Mh., 8: 509-512, Stuttgart.

[47] Schneider, W., Salameh, E. (2014). Uncommon and Impact-Suspicious Geologic phenomena Across Jordan and Adjacent Areas, Arabian Plate. Open Journal of Geology, 4: 680-717.

[48] Sharp, D. (1847). On slaty cleavage, Geol. Soc. Quart. Jour., 3: 74-105.

[49] Wiesemann, G. (1969). Zur Tektonik des Gebietes östlich des Grabenabschnitts Totes Meer-Jordantal. Beihefte Geologisches Jahrbuch, 81: 215-247.

[50] Wunderlich, H.G. (1966). Wesen und Ursachen der Gebirgsbildung. Bibliographisches Institut (B.I.) AG, Mannheim,Germany.

[51] Zaineldeen, U., Delvaux, D., and Jacobs, P. (2002). Tectonic evolution in the Wadi Araba Segment of the Dead Sea Rift, Southwest Jordan. EGU Stephan Mueller Special Publication Series 2:63- 81.

JJEES
Jordan Journal of Earth and Environmental Sciences

Volume 9, (Number 2), August, 2018
ISSN 1995-6681
Pages 127 - 133

Characterization of Jordanian Volcanic Tuff and its Potential Use as Lightweight Aggregate

Reyad A. Al Dwairi[1], Bety Al Saqarat[2], Fathi Shaqour[2], and Mohmd Sarireh[3]

[1]Department of Natural Resources and Chemical Engineering, Engineering Faculty, Tafila Technical University, Tafila, 6611, Jordan.
[2]Department of Applied Geology and Environment, Faculty of Science, University of Jordan, Amman 11942, Jordan
[3]Department of Civil Engineering (Chair), Faculty of Engineering, Tafila Technical University, Tafila 66110, Jordan.

Received 6 June, 2018; Accepted 5 August, 2018

Abstract

In the current study, Jordanian volcanic tuff (JVT) as a lightweight aggregate is experimentally evaluated. Two types of JVT are investigated, namely zeolitic volcanic tuff (ZT) and the black volcanic tuff (BT), from two volcanic eruptions at Al Hala area in southern Jordan. They are investigated in terms of specific gravity, bulk density, porosity, water absorption, and slake durability using the Los Angeles method. Ten mixtures were prepared using the typical crushed limestone aggregate at first, then volcanic tuff aggregate was used as a replacement for the limestone aggregate at the various ratios of 25, 50, 75 %, followed by a total replacement of 100 % volcanic tuff aggregate. Compressive strength, abrasion, indirect tensile strength, flexural strength, ultrasonic velocity, thermal conductivity, permeability, specific gravity, shear strength and modulus of rupture tests are conducted on the prepared concrete samples.

The results of aggregate characterization indicate that specific gravity ranges from 1.8 to 1.92 for BT and from 1.98 to 1.98 for ZT. Bulk density (kg/m3) ranges from 1189 to 2012 for BT and from 2010 to 2110 for ZT. The two samples possess good porosity with a value of 0.605 (60.5 %), while water absorption for the two samples ZT and BT is 8.7 and 10.2 %, respectively. The above results showed good specifications for JVT to be used as lightweight aggregate. An experimental program based on testing several standard cubes containing different percentages of volcanic tuff as coarse aggregate was prepared.

The results indicated that the best compressive strength obtained is for the mixture of BTC4 as 41 Mpa and with a corresponding density of 1.85g/cm3.

Black volcanic tuff and zeolitic tuff concrete are considered to be light weight concrete compared to the normal weight concrete. The main distinguished characteristic of lightweight concrete is its low density and its higher compressive strength as well.

Keywords: Jordanian Volcanic Tuff, Zeolitic Tuff, Compressive Strength, Flexure Strength.

1. Introduction

Concrete has been one of the most important construction materials over the last century worldwide. Its consumption is increasing in spite of its environmental consequences. The main components of concrete are cement, aggregate and water. The commonly used aggregates are crushed stones or natural gravels that are characterized by high density and low insulation characteristics that make them not environmentally friendly. This has always urged researchers to investigate other options of aggregates such as light weight aggregates in order to produce lightweight concrete (LWC). This issue has become an important interest and research material due to the several resulting advantages, such as savings on reinforcement and foundation costs, in addition to a better fire resistance, heat insulation, sound absorption, frost resistance, superior anti-condensation properties and increased damping (CEB/FIP, 1977).

The main component of LWC is the light weight aggregate (LWA). Volcanic tuff is an excellent light weight aggregate that has been used for many years (Polat et al., 2010), however, they vary in physical and geotechnical characteristics.

Aggregates are commonly defined as natural or artificial incoherent materials possessing different grain sizes that are used in the production of concrete. Lightweight aggregates are formed from materials lighter than water and distinctly more porous than sand, gravel and crushedrock, that are commonly referred to as "dense" aggregates (Klinefelter, 1960; Loughbrough, 1991).

Many materials were used as LWA to produce LWC. Natural materials that are mostly used for the production of lightweight aggregates are sedimentary or very low-grade metamorphic rocks -clay shales (Purbrick, 1991). In addition to the natural or artificial lightweight aggregates, such as Bamboo reinforced, oil palm shells, bottom ash, starch based aggregate, etc. (Ghavami, 1995; Jamal et al., 1997), volcanoclastite and zeolitized rocks can also be used to obtain lightweight aggregates (Colella et al., 2001).

Volcano tuff (clastic) (VT) varies from one location to another based on the weathering rate and zeolitization processes which reflect the mineral content and the quantity of secondary minerals associated with volcanic tuff with zeolites being the most important (Al Dwairi, 2014).

Volcanic tuff in Jordan (VT and ZT) is available in the Northeastern, Central and Southern parts of Jordan (Al

* Corresponding author. e-mail: reyadn@hotmail.com

Dwairi, 2007; Khoury et al., 2015). Volcanic tuffs in Jordan are studied with regard to their mineralogy, petrology and their environmental, industrial and agricultural applications (Dwairi 1987; Ibrahim 1993, Al Dwairi et al. 2009; Al Dwairi 2010, Yasin et al. 2012; Awwad et al.,2012; Al Dwairi et al., 2014; and Al Dwairi et al 2015). Also, Sarireh (2015) had studied the volcanic tuff (black minerals) of Jabal Al-Hala and its physical, chemical, and mechanical properties. The research had presented the properties of Volcanic Concrete (VC) by employing the Volcanic Aggregate (VA) in a concrete mixture in the proportions of 10, 20, 30, 40, and 50 %. The physical tests, such as sieve analysis and specific gravity, density and absorption for both VA and normal weight aggregates (all specific gravities of VA less than those of the normal weight aggregate) were conducted. Also, the density and compressive strength of concrete on the seventh day and twenty-eighth day, flexural strength, and permeability.

The use of volcanic tuff in the concrete industry has been known worldwide. One of the most challenging issues facing the construction sector in Jordan is the increasing cost of the building materials which lead to the increasing cost of construction especially when using traditional building materials.

The present study is aimed at investigating the suitability of the south Jordanian volcanic tuff to be used as light weight aggregate, and attempts to produce a new lightweight concrete mixture by shedding light on volcanic tuff as a promising material used as aggregate.

2. Materials and Methods

2.1. Material

Two locations in Tafila Governorate in southern Jordan were selected to sample volcanic tuff, namely Jabal Al Hala1 (Ataita) and Al Hala 2 volcanic tuff as the map in Figure (1) shows. The two volcanoes are located about 200 km south of Amman City. Al Hala1 is about one km to the southeast of the Rashadiya Cement Plant at an elevation ranging from 1573 – 1643 m above the mean sea level (AMSL), while, Al Hala 2 is about 3km from Al Ees Area at an elevation ranging between 1500- 1524m AMSL.

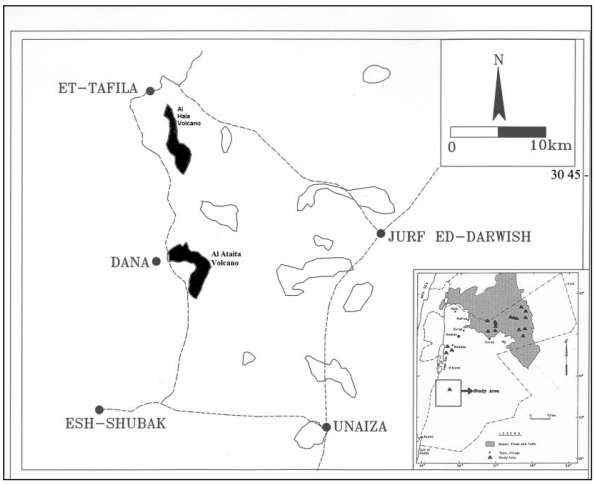

Figure 1. Volcanic tuff location map (Modified after Al Dwairi, 2007).

2.2. Material's Characterization and Preparation

Volcanic tuff from Al Hala1is highly altered to zeolite (ZT), brown and gray colored with a thickness of more than 50 m. Volcanic tuff from Al Hala2 is black fresh scoria (BT) with a thickness of 20 m. The tuff in both locations is of Paleocene and Neogene

age (Gradstien, 2012). Limestone is obtained from a local quarry in Tafila. The chemical composition and physical properties of ZT and BT were determined and characterized by Al Dwairi (2007) and (2014).

Coarse aggregates of BVT, ZVT and LS that are shown in Fig. (2-a) were used in five designed mixtures as shown in distribution in Fig. (2-b).

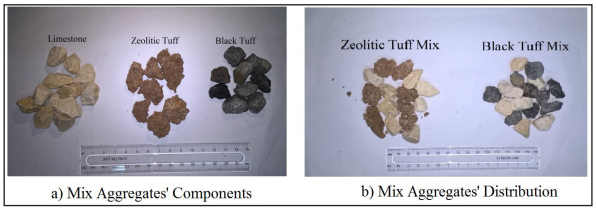

Figure 2. BVT, ZVT, and LS Aggregates Components and Distribution in Mix.

The experimental program depends on the replacement of the LS with BVT Mix and ZVT Mix in ratios from 0 to 100 % at an increments of 25 % as shown in Table (1), in addition to the normal proportion of sand stone as the fine part that is used in concrete mix. All Samples of VT were crushed using a jaw crusher with 5cm and 3cm aperture, and were sieved into aggregate size (1-4 and 4-16 mm). They were then sorted and labeled to be tested for properties.

2.3. Lightweight Aggregate (LWA) Tests

To investigate the ability of using the VT as LWA, the two bulk samples (BT and ZT) were subjected to the following laboratory tests: Specific gravity and absorption (ASTM C127-84 and ASTM C330-82a), bulk density (ASTM C 127-88 and ASTM C 128-88), porosity of LWA that was conducted according to ASTM C29 / C29M - 17a., and abrasion in the Los Angeles Machine by applying (ASTM C131 / C131M - 14). Analyses were carried out at the laboratories of the Department of Civil Engineering at Tafila Technical University in southern Jordan.

2.4. Lightweight Aggregate Concrete (LWAC) Tests

The following techniques were used to determine the most appropriate mix of VT and LS aggregate to be used as a lightweight concrete in civil engineering constructions; compressive strength, Splitting strength, Thermal conductivity, Permeability, Modulus of rupture, Shear failure and Flexural strength. Compressive strength on Concrete Cubes is determined by testing 28-days old (15x15) cm at specified rate of loading (BS 1881: Part 107: 1983 and BS 1881: Part 108: 1983). Comprehensive experimental investigations were conducted to assess the effect of volcanic tuff on concretes compressive strength. All previous techniques were conducted at the Natural Resources Authority Geotechnical Labs/ Jordan and Civil Engineering Laboratories in Tafila Technical University/ Jordan.

Table 1. Bulk samples collected from different sites in the two locations.

Concrete Type	BTC1	BTC2	BTC3	BTC4	ZTC1	ZTC2	ZTC3	ZTC4	LSC
Mixing Ratio VT:LS	100:00	75:25	50:50	25:75	100:00	75:25	50:50	25:75	00:100

3. Results

3.1. LWA Results

The obtained results of the different engineering properties for BT and ZT to be used as LWA are listed in Table (2).

Table 2. Physical properties of limestone and VT aggregates used in the experiments mixes

Type	Specific gravity	Bulk density (kg/m^3)	Porosity (%)	Water absorption (%)	Abrasion (%)
Coarse BT	1.80	1189	60	10.2	20.1
Fine BT	1.92	1812	60	11.7	19.2
Coarse ZT	1.98	2110	50	8.7	25.1
Fine ZT	2.00	2010	50	9.2	26.7
Coarse LS	2.56	2560	15	3.12	31
Fine LS	2.47	1800	15	2.51	29

Specific gravity results showed that the coarse BT has a specific gravity of 1.89 and 2.00 for the coarse ZT which conforms to the theoretical value stipulating that volcanic tuff has a specific gravity of 1.64-2. Ordinary limestone aggregate from the laboratory tests had a specific gravity of 2.51 which also conforms to the theoretical values.

Comparing specific gravities of ordinary limestone with volcanic tuff indicates that ordinary limestone is much heavier than volcanic tuff; it is, therefore, proper to categorize volcanic tuff as a light weight aggregate. Results are shown in Fig. (3).

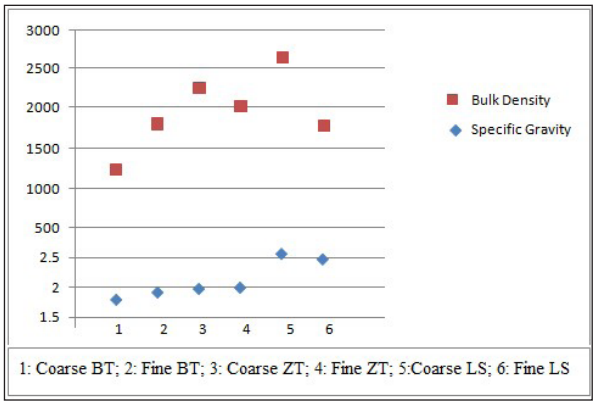

Figure 3. Specific Gravity and Bulk Density for BT, ZT, and LS

Results of bulk density (Kg/m^3) shows that coarse LS is heavier than coarse BT and ZT. Similar results are obtained regarding fine BT, ZT, and LS. The results of specific gravity and bulk density are also presented in Fig. (3). It is clear through the bulk density that fine BT is heavier than coarse BT, while the coarse ZT is heavier than the fine ZT, and coarse LS is heavier than fine LS. Also, the results of the specific gravity show that coarse and fine LS are heavier than coarse and fine ZT and BT. As for porosity, the values of BT and ZT are higher than those of LS. So, they can be used as light aggregates in the production of light concrete. The idea of using lightweight aggregates is that it acts as a water reservoir which can provide water to replenish the hydration-consumed water. The results show that porosity was about 50 % for ZT and 60 % for BT, whilst for LS it was less than 15 %. Such results indicate that a large amount of water can be stored in the pores of light weight aggregates better than ordinary limestone aggregates, providing it with more humidity which maintains the hydration of the cement and gain of strength. These results can be correlated with the water absorption results which increase more in LWA than in ordinary limestone aggregates due to the relatively high porosity. This assumption supports the use of LWA as a green and safe construction material.

As a result of porosity, absorption for BT and ZT is higher than for LS, that is, BT possesses a water absorption range of 10.2-11.7 % compared to a rate of 8.7-9.2 % for ZT. These results show that volcanic tuff can absorb 7 % more water than ordinary limestone which aborbs at a rate of 3.1 %. This rate of absorption definitely affects the workability of the mixture while producing concrete. This value is however acceptable since water absorption depends not only on the void content of volcanic tuff, but also, on the nature of volcanicity and the distance from the volcanic mountain.

As for abrasion, the values for BT and ZT were encouraging while being less for LS. The abrasion resistance of concrete is strongly influenced by the compressive strength, surface finishing techniques, curing types, aggregate properties and testing conditions, i.e. dry or wet (Topcu et al, 2009). The values of abrasion resistance for BT are ~ 20.6 %, ZT ~ 25.9 % and ~ 30 % for LS. This means that the abrasion resistance of ZT and BT as lightweight aggregate is better than the ordinary Limestone with all types of LWA. This is based upon the fact that lightweight aggregates are not as strong as the crushed stones.

3.2. BT, ZT, and LWC Results

The results of engineering properties of the lightweight aggregate concrete using different mixes are listed in Table (3).

3.2.1. Slump Test

This test is used to determine the slump of concrete. This method is applicable to plastic concrete having a coarse aggregate up to 1.5 inch in size. This method is not considered applicable to non-plastic and non-cohesive concrete. Slump test was conducted according to ASTM C143 / C143M - 15a.

3.2.2.

Modulus of rupture as determined by concentrated load. Three beams (15x15x75) cm were prepared according to (BS 1881: Part 109: 1983) and tested according to the (ASTM C78 / C78M – 18).

3.2.3.

Shear failure conducted by applying load at the midpoint of the specimen. Three beams (20x25x110) cm were tested by the (ASTM D6916 - 06c,2011).

3.2.4.

Flexural strength was conducted under a concentrated load at the midpoint of the span (D 790 – 03). Three beams (20x25x310) cm were tested. Five mixes were prepared,

namely 0 % basalt (as areference mix), 25 % basalt, 50 % basalt, 75 % basalt, and100 % basalt. The composition of each mix was 40 % fine aggregate passing sieve # 4 and 35 % passing ½" retained on sieve #4 and 25 % course aggregates passing 1" and retained on ½" sieve. In order to enhance the workability of the mix, the portion passing sieve # 4 consisted of 20 % limestone sand and 20 % basalt sand for all mixes.

3.2.5.

Splitting strength determined by the indirect tensile strength test. Three cylinders of 10 cm diameter by 20 cm height were tested. Splitting strength is determined according to the (ASTM C1006 - 07(2013).

The cube strength development curve shown in Table (3) indicates that the strength of concrete increases steadily from a minimum value of 32.5 MPa at the control point to reach its maximum strength of 29.56 KN/m^2 at an 80 % replacement and then the strength decreases again steadily to a value of 27.25 KN/m^2 at 100 %. The above value for control cubes conforms to the theoretical value of 25KN/m^2 for class 25 concrete at a twenty-eight day strength. Volcanic tuff has shown an incredible increase in strength above what was expected at twenty-eight days with all the values falling above 25 KN/m^2. The reasons behind the high strength in volcanic tuff are the process of high strength concrete first involves a balancing water demand and a paste aggregate bond potential. This was greatly achieved at an 80 % replacement due to its parking density and its corresponding particle size distribution of the combined aggregate used. In theory, this generates savings due to the reduction in the paste volume that can be used to coat the aggregates. In this study, since cement content was a constant parameter, much of the cement was used in achieving strength beyond what was anticipated in the mix design leading to the increasing strength development curve.

The optimum gradation of the fine aggregate for high strength concrete is determined more by its effect on water demand than on particle packing. High strength concrete typically contains high volumes of cementation sized materials (as in the case of volcanic tuff, it has some pozzolanic properties due to fly ash). As a result, fine sands that would be considered acceptable for use in conventional concretes may be less suited for high strength concrete due to their sticky consistency; conversely, coarse sands that may not comply with the standard specifications for concrete aggregates may be highly desirable for high strength concrete.

In regard to their impact on workability, physical grading of fine aggregates is less critical in high strength concrete mixtures compared to conventional concrete.

Water also played a very important role in achieving the strength shown above. It is important to know that mixing water includes the free water introduced during mixing and after batching and the free moisture on aggregates.

The hardened cement paste has two fundamental types of pores capillary and gel pores. Capillary pores are the spaces between the masses of cement gel grains; they make up what is called the "capillary system". Depending on the degree of hydration and the initial separation of the cement grains, capillary pores may be interconnected (percolated). The gel pores are spaces between the solid products of hydration within the cement gel.

Gel pores are normally filled with water that is strongly held to the solids. Capillary and gel pores will be filled with water if the paste is saturated. When the paste is exposed to drying conditions, these pores become empty, as the evaporable water is lost. Due to the sticky consistency of conventional concrete, the fine aggregates fill most of the pores leading to complete disconnection between the capillary and gel pores hence making internal hydration quite difficult.

Table 3. Fresh and Hardened Concrete Properties for BT, ZT, and LS Concrete.

Concrete Type	Slump (mm)	Density g/cm^3	Water Absorption %	Flexural Strength (MPa)	Splitting Strength (KN)	Compressive Strength (MPa)	Modulus of Rupture (MPa)	Shear Stress (MPa)
BT C1	27	2.128	5.6	1.2	162	33	2.40	0.82
BTC 2	24	1.931	5.3	1.31	166	35.3	2.60	0.91
BTC3	28	1.900	4.2	1.50	171	38.1	3.20	0.95
BTC 4	26	1.850	4.5	1.60	178	41.0	3.50	1.10
ZTC1	28	2.210	4.6	1.1	164	31	1.9	0.71
ZTC 2	26	2.140	4.5	1.20	169	32.3	2.20	0.73
ZTC 3	30	1.988	4.6	1.32	174	33	2.40	0.81
ZTC 4	27	1.899	4.8	1.50	178	35.50	2.70	083
LSC	42	2.400		1.10	181	30	1.50	0.72

Compressive strength was found to decrease with the increase of VPP content, and more than 25 % reduction in strength is observed at the 25 % replacement compared to 0 % VPP. This is reasonable due to the reduction of the cement content in the mix with the increase of VPP content. The finely divided silica (61%) in VPP can combine with calcium hydroxide (liberated by the hydrating Portland cement) in the presence of water (Hossain, 1999) to form stable compounds like calcium silicates, which have cementation properties. Such pozzolanic action of VPP contributes to the enhancement of strength and long-term durability (Hossain, 1999); however, the reduction of strength in the blended cement due to the cement replacement by VPP is not compensated in the current study.

The strength is reduced as a result of increasing the VPP percentage from 0.0% to 25%; 26% (one-day strength), 26.4% (three-days), 22.7% (seven-days) and 24.2% (twenty-eight - days) when VPP content varies from 0% to 25%. The strength reduction is decreased with the increase of age.

Also, The thermal conductivity test was conducted for the samples and the results are shown in Table (4). Three samples (30x30x5) cm were tested according to (ASTM D5334 - 14).

and permeability determined by the water pressure test. Three plate samples (30x30x5) cm were tested according to (CRD-C48-92).

Fig. (4) presents the values of slump (mm), density (g/cm^3), and water absorption %.

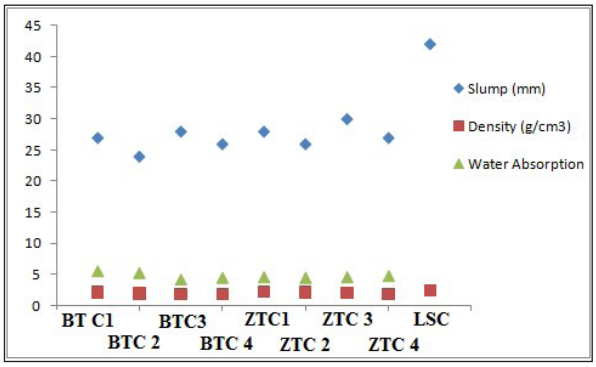

Figure 4. Values for Slump (mm), Density (g/cm3), and Water Absorption %

It is clear that in Fig. (4), the slump values are ranging from 23 to 27 mm for all samples were mixed using BTC and ZTC samples. While the slump value is the highest for LSC which is about 43 mm; it gives more workability in the concrete mix at this value and maintains compressive strength of concrete because of the water/cement ratio that it is constant for all mixes.

Fig. (5) represents values of flexural strength, splitting strength, and compressive strength of the concrete mixes for the samples of BTC 1, BTC 2, BTC 3, BTC 4, ZTC 1, ZTC 2, ZTC 3, ZTC 4, and LSC.

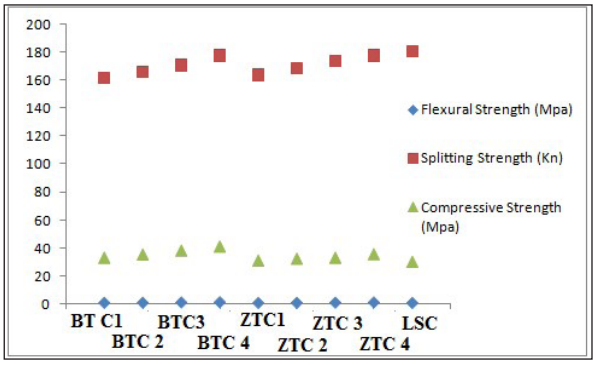

Figure 5. Values for Flexural Strength, Splitting Strength, and Compressive Strength

As is clear from Fig. (5), LSC has higher values regarding splitting strength and flexural strength than the BTZC and ZTC samples. As for compressive strength, BTC has higher values than the ZTC and LSC samples.

Table 4. Thermal Conductivity and Permeability of BT, ZT, and LS Concrete.

Concrete Type	Mixing Ratio VT:LS	Thermal Conductivity	Permeability Pressure
BTC1	100:00	0.35	30
BTC2	75:25	0.48	42
BTC3	50:50	0.67	65
BTC4	25:75	1.14	127
ZTC1	100:00	0.31	36
ZTC2	75:25	0.43	53
ZTC3	50:50	0.62	79
ZTC4	25:75	1.06	136
LSC	0:100	0.94	171

Fig. (6) presents the values of thermal conductivity and permeability pressure for the concrete mixes using BTC 1, BTC 2, BTC 3, BTC 4, ZTC 1, ZTC 2, ZTC 3, ZTC 4, and LSC.

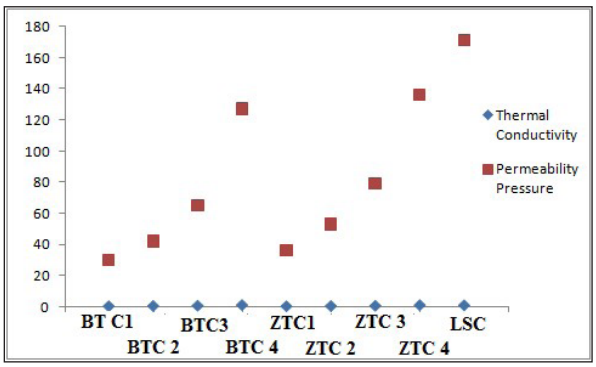

Figure 6. Values of Thermal Conductivity and Permeability Pressure

From Fig. (6), it is obvious that ZTC achieves more in permeability pressure than the BTC samples, but less than LSC samples. As for thermal conductivity, the values are relevant for BTC, ZTC, and LSC.

4. Discussion

The compressive strength is the most commonly used parameter to describe the quality of concrete in practice (Wiegrink et al., 1996). According to ASTM C 330-89, the twenty-eight-day cylinder compressive strength should not be less than 17 MPa (Neville and Brooks, 2008). Okafor (1988) reported that the maximum compressive strength of lightweight concrete produced using this agricultural shell is approximately 25 to 35 MPa. This range is within the typical compressive strength for structural lightweight concrete (20-35 MPa) (Kosmatka et al., 2002). Mannan and Ganapathy (2001) showed that by using 480 kg/m^3 cement, a free water to a cement ratio of 0.41 and mix proportion of 1:1.71:0.77 by weight of cement, sand and OPS aggregate, the twenty-eight-day compressive strength of OPS concrete is between 20 and 24 MPa depending on the curing.

The potential applications of light weight aggregate are more phenomenal in terms of the usage as new construction materials. Cost effective construction practices with alternate construction materials are most desired in terms of huge

savings in the construction cost. Fly ash is not a waste and can be effectively used in concrete either as aggregate fillers, replacement for fine aggregates, or as a fly ash brick material. The overall studies conducted by various researches showed that the fly ash aggregate produced by pelletization can be an effective aggregate in the concrete production. Also, the efficiency of pelletization depends on the speed of the pelletizer, angle of the pelletizer, and the type of binder added along with the fly ash. The cost effective and simplified production techniques for manufacturing fly ash aggregate can lead to mass production, and can be an ideal substitute for the utilization in many infrastructural projects. In the near future, the depletion of the nature resources for aggregate can be suitably compensated by the fly ash aggregate.

According to this study, using volcanic tuff as a light weight aggregate concrete material will be most successful. The authors deeply recommend JV and JVT as lightweight aggregates since the results prove that they are less expensive than normal aggregates in terms of transportation, and because the construction will be environment friendly (Green House Building) and because of the chemical characteristics of zeolite itself. Lightweight aggregates are considered to be a promising material which should be replaced by the normal aggregates in the construction projects.

Conclusion

JVT in its two forms including BT and ZT shows suitability and usage in construction as local non-expensive material. Many benefits can be gained through the use of JVT in the concrete mix production:

1. Volcanic tuff lightweight has shown incredible results on issues related to its compressive strength, as well as the tensile strength.
2. It was proven that volcanic tuff and ordinary limestone can be well blended together at different percentages in order to achieve a targeted strength without any significant effects.
3. The correct mix design of volcanic tuff in concrete to be used in modern structural problems was established.
4. Volcanic tuff deposits are well scattered out along the rift valley and in places where there are no major rivers to supply ordinary sand and gravels; hence, volcanic tuff comes out to be the best alternative as an available and cost-effective structural material.
5. Specific gravity of volcanic tuff is 1.89 compared to 2.51 for ordinary limestone/sand. Therefore, modified concrete turns out be lightweight compared to the conventional concrete.
6. The values of abrasion resistance show that the abrasion resistance of ZT and BT as lightweight aggregate is better than the ordinary Limestone with all types of LWA.

Limitations of the Study

During testing and applications in this study, the authors had the following limitations:

1. Volcanic tuff must be tested on a dry-basis for sieve analysis, abrasion, and in taking weight and volume in any season.
2. The samples should be tested for specific gravity periodically at each mixing operation in order to change on volume-basis the mix constituents.
3. A national project on the characterization of volcanic tuff throughout the country.

Acknowledgement

The authors of this research would like to direct their great thanks to their colleagues at the Department of Natural Resources and Chemical Engineering and the Department of Civil Engineering, Engineering Faculty at Tafila Technical University, also the Department of Applied Geology and Environment, Faculty of Science, at the University of Jordan for their help and support for the duration of this study. Also, thanks are extended to the presidency offices at Tafila Technical University, and the University of Jordan and to the students in the faculties of engineering as well. Many thanks and gratitude go also to their families for the time and support which enabled us to come out with this valuable work.

References

[1] Al Dwairi, R. (2007). Characterization of the Jordanian zeolitic tuff and its potential use in Khirbet esSamra wastewater treatment plant. PhD Thesis, University of Jordan, Jordan, pp204.

[2] Al Dwairi, R., Khoury, H., and Ibrahim, K. (2009). Mineralogy and Authigenesis of Zeolitic Tuff from Tall-Juhira and Tall Amir, South Jordan, Jordan Journal of Earth and Environmental Sciences, 2(2): 81- 88.

[3] Al Dwairi, R., Khoury, H., Ibrahim, K. (2010). Occurrences and Properties of Jordanian Zeolites and Zeolitic Tuff. Germany: VDM Verlag. 2010.

[4] Al Dwairi, R., Ibrahim, K., Khoury, H. (2014). Potential use of faujasite–phillipsite and phillipsite–chabazite tuff in purification of treated effluent from domestic wastewater treatment plants, Environmental Earth Sciences 71: 5071-5078

[5] Al Dwairi, R., Omar, W., Al-Harahsheh, S. (2015). Kinetic modelling for heavy metal adsorption using Jordanian low cost natural zeolite (fixed bed column study) 05.2 2015 pp 231-238.

[6] ASTM C127-84. "Test for Specific Gravity and Absorption of Coarse Aggregate."

[7] ASTM C128-84. " Test for Specific Gravity and Absorption of Fine Aggregate."

[8] ASTM C-128-88, Standard test method for specific gravity, density and absorption of fine aggregate, 1988.

[9] ASTM C-127-88, Standard test method for specific gravity and absorption of coarse aggregate, 1988.

[10] Standard Test Method for Resistance to Degradation of Small-Size Coarse Aggregate by Abrasion and Impact in the Los Angeles Machine

[11] BS 1881: Part 107: 1983. "Method for Determination of Density of Compacted Concrete."

[12] BS 1881: Part 108: 1983. "Method for Making Test Cubes from Fresh Concrete."

[13] ASTM C 330-89, "Standard Specification for Lightweight Aggregates for Structural Concrete", Annual Book of ASTM Standards, 4.02, 193- 195
[14] ASTM C29 / C29M - 17a: Standard Test Method for Bulk Density (Unit Weight) and Voids in Aggregate.
[15] ASTM C143 / C143M - 15a. Standard Test Method for Slump of Hydraulic-Cement Concrete.
[16] ASTM C1006 - 07(2013). Standard Test Method for Splitting Tensile Strength of Masonry Units.
[17] BS 1881: Part 109: 1983. "Method for Making Test Beams from Fresh Concrete."
[18] ASTM C78 / C78M – 18. Standard Test Method for Flexural Strength of Concrete (Using Simple Beam with Third-Point Loading).
[19] ASTM D6916 - 06c (2011). Standard Test Method for Determining the Shear Strength Between Segmental Concrete Units (Modular Concrete Blocks).
[20] ASTM D5334 – 14. Standard Test Method for Determination of Thermal Conductivity of Soil and Soft Rock by Thermal Needle Probe Procedure
[21] CRD-C48-92 Standard Test Method For Water Permeability of Concrete
[22] Awwad, M., Y asin, A., Hajjeh, H., Al-Sahawneh E. (2012). Flexural and Shear Capacities of Reinforced Concrete Beams with Volcanic Tuff. Innovative Systems Design and Engineering. Vol 3, No 10.
[23] CEB / FIP Manual of Design and Technology. (1977). Lightweight Aggregate Concrete. First pub. Great Britain.
[24] Colella, C., de' Gennaro, M., Aiello, R. (2001). Use of zeolitic tuff in the building industry, In: D.L. Bish and D.W. Ming, (Eds.), Reviews in Mineralogy &Geochemistry-Natural Zeolites: Occurrence, Properties, Applications. Mineralogical Society of America, Blacksburg, Va, USA. 551–587.
[25] D 790 – 03. Standard Test Methods for Flexural Properties of Unreinforced and Reinforced Plastics and Electrical Insulating Materials.
[26] Dwairi, I.M.(1987) A chemical study of the palagonitic tuffs of the Aritain area of Jordan, with special reference to nature, origin and industrial potential of the associated zeolite deposits. PhD thesis, Hull Univ., UK, 408p.
[27] Gradstein, F.M, Ogg, J.G., Schmitz, M.D. (2012). The Geologic Time Scale 2012: Boston, USA, Elsevier, DOI: 10.1016/B978-0-444-59425-9.00004-4.
[28] Ghavami K. (1995). Ultimate load behaviour of Bamboo-reinforced lightweight concrete beams, Cem. Concr.Compos. 17(4): 281– 288.
[29] Hossain K. (1999). Performance of volcanic ash concrete in marine environment, Proceedings of 24th OWICSConference, "21st Century Concrete and Structures", 25 – 26 August, Singapore, vol. XVIII: 209 – 214.
[30] Ibrahim, K. (1993). The geological framework for the Harrat Ash-Shaam Basaltic Super-group and its volcano tectonic evolution. Natural Resources Authority, Geological Mapping Division Report, Amman-Jordan, 61p.
[31] Jamal, A., Khalid, A., Haque, M., Khalid, E. (1999). Lightweight concrete in hot coastal areas, Cem. Concr. Compos. 21(5–6): 453– 458.
[32] Khoury, H., Ibrahim, K., Al Dwairi, R., Torrente, D. (2015). Widespread zeolitization of the Neogene – Quaternary volcanic tuffin Jordan, J. of African Earth Sci. 101: 420–429.
[33] Klinefelter, T.A. (1960). Aggregates - lightweight aggregates. In:Lefond, S.J. (Ed.), Industrial Minerals and Rocks, AIME, 487-495 and 5th ed., 1983.
[34] Kosmatka, S.H., Kerkhoff, B., Panarese, W.C. (2002). Design and control of concrete mixtures. 14rd ed. USA: Portland cem.assoti.
[35] Loughbrough, R. (1991). Minerals in lightweight insulation: filling the market. Ind. Miner. October, 21-35. Nappi, G., 1969. Stratigrafia e petrografiadeiVulsinisud-occidentali, Caldera di Latera. Boll. Soc. Geol. It. 88: 171-181.
[36] Mannan, MA, Ganapathy C (2001). Long-term strengths of concrete with oil palm shell as coarse aggregate. Cem. Con. Res. 31: 1319–1321.
[37] Neville AM, Brooks JJ. (2008).Concrete technology. Malaysia: Prentice Hall.
[38] Okafor, F.O. (1988). Palm Kernel Shell as a Lightweight Aggregate for Concrete. Cem. Con. Res., 18: 901-910.
[39] Polat, R., Demirboğa, R., Karakoç, M.B., Türkmen, I. (2010). The influence of lightweight aggregate on the physico-mechanical properties of concrete exposed to freeze–thaw cycles. ColdReg. Sci. Tech., 60: 51-56.
[40] Purbrick, J. (1991). Lightweight aggregates – manufacture and applications. In: Exploration, Mining & Uses of Ceramic RawMaterials, Proc. 23rd Ann. Symp. South African Ceram. Soc.,45-49.
[41] Sarireh, Mohmd (2015). Optimum Percentage of Volcanic Tuff in Concrete Production. Yanbu Journal of Engineering and Science, 11: 43-50.
[42] Topcu, I. B., Bilir, T., Uygunoğlu, T. (2009). Effect of Waste Marble Dust Content as Filler on Properties of Self-Compacting Concrete, Construction and Building Materials, 23(5): 1947 - 1953.
[43] Wiegrink, K., Marikunte, S., Shah, S.P. (1996). Shrinkage cracking of high strength concrete. ACI Mat. J., 93(5): 409 - 415.
[44] Yasin, A., Awwad, M., Hajjeh, H., Sahawneh, E. (2012). Effect of Volcanic Tuff on the Concrete Compressive Strength. Contemporary Engineering Sciences, 5(6): 295 – 306.

المملكة الأردنية الهاشمية

صندوق دعم البحث العلمي

الجامعة الهاشمية

المجلة الأردنية
لعلوم الأرض والبيئة

JJEES

مجلة علمية عالمية محكمة

المجلد (٩) العدد (٢)

http:// jjees.hu.edu.jo/

ISSN 1995-6681

المجلة الأردنية لعلوم الأرض والبيئة

مجلة علمية عالمية محكمة

المجلة الأردنية لعلوم الأرض والبيئة: مجلة علمية عالمية محكمة ومفهرسة ومصنفة، تصدر عن عمادة البحث العلمي في الجامعة الهاشمية وبدعم من صندوق البحث العلمي - وزارة التعليم العالي والبحث العلمي، الأردن.

ترسل البحوث إلكترونيا إلى البريد الإلكتروني التالي:

رئيس تحرير المجلة الأردنية لعلوم الأرض والبيئة

jjees@hu.edu.jo

لمزيد من المعلومات والأعداد السابقة يرجى زيارة موقع المجلة على شبكة الانترنت على الرابط التالي:

www.jjees.hu.edu.jo

المملكة الأردنية الهاشمية
صندوق دعم البحث العلمي
Scientific Research Support Fund
الجامعة الهاشمية
THE HASHEMITE UNIVERSITY
JORDAN

JJEES

المجلة الأردنية لعلوم الأرض والبيئة

المجلد (٩) العدد (٢)

مجلة علمية عالمية محكمة تصدر بدعم من صندوق دعم البحث العلمي

ISSN 1995-6681
jjees.hu.edu.jo
آب ٢٠١٨